Cruise Report

Atalante Cruise Leg – 2

MARSUED IV

(replacement of MSM06/3)

07.01.08 Recife - 31.01.08 Dakar

Contents

2.1 Participants 3

2.2 Research Program 5

2.3 Cruise Narrative 9

2.4 Preliminary Results 10

2.4.1 Physical Oceanography 10

2.4.1.1 Instruments and Methods 10

2.4.1.2 First results 12

2.4.2 Microbiology from low-temperature, diffuse and hot hydrothermal fluids 16

2.4.3 Temperature measurements of low-temperature, diffuse hydrothermal fluids 24

2.4.4 Fluid chemistry 28

2.4.4.1 Fluid sampling 28

2.4.4.2 Analytical procedures on-board 32

2.4.4.3 First results 34

2.4.4.4 The chemical composition of hydrothermal fluids – Perspectives 42

2.4.5 Gas Chemistry 42

2.4.6 Hydrothermal Symbioses 46

2.4.7 Paleaoceanography 50

2.4.8 Global distribution and atmospheric transport of volatile and semi-volatile polyfluorinated compounds 52

2.4.9 Volcanic rocks 52

2.4.10 Rocks from the deeper crust 58

2.4.11 ROV deployments during MAR SOUTH IV 67

2.5 Acknowledgements 68

2.6 References 69

Appendix 71

2.1 Participants

1.	Prof. Colin Devey	Chief Scientist	IFM-GEOMAR
2.	Dan Cormany	ROV Pilot	High Sierra Technologies
3.	Dr. Nicole Dubilier	Hydroth. Symbioses	MPI Bremen
4.	Gerd Fraas	Phys. Oceanography	Univ. Bremen
5.	Andy Foster	ROV-Team	Schilling Robotics
6.	Dieter Garbe-Schönberg	Fluid Chemistry	Univ. Kiel
7.	Petra Günnewig	Phys. Oceanography	Univ. Bremen
8.	Phillip Hach	Fluid Chemistry	Jacobs Univ. Bremen
9.	Almuth Harbers	Palaeoceanography	IFM-GEOMAR
10.	Claus Hinz	ROV-Team	IFM-GEOMAR
11.	Verena Klevenz	Fluid Chemistry	Jacobs Univ. Bremen
12.	Jürgen Koepcke	Petrology	Univ. Hannover
13.	Eric Labahn	ROV-Team	Fa. K.U.M.
14.	Klas Lackschewitz	ROV-Team	IFM-GEOMAR
15.	Ralf Lendt	Gas Chemistry	Univ. Hamburg^{+}
16.	Nadine Markus	Microbiology	Univ. Hamburg*
17.	Arne Meier	ROV-Team	IFM-GEOMAR
18.	Bernd Melchert	Bathymetry	IFM-GEOMAR
19.	Christian Mertens	Phys. Oceanography	Univ. Bremen
20.	Holger Paulick	Petrology	Univ. Bonn
21.	Mirjam Perner	Microbiology	Univ. Hamburg*
22.	Martin Pieper	ROV-Team	IFM-GEOMAR
23.	Katja Schmidt	Fluid Chemistry	Jacobs Univ. Bremen
24.	Jörg Schneider	ROV-Team	IFM-GEOMAR
25.	Richard Seifert	Gas Chemitry	Univ. Hamburg^{+}
26.	Harald Strauss	Fluid Chemistry	Univ. Münster
27.	Jillian Struck	Hydroth. Symbioses	MPI Bremen
28.	Günter Suhr	Petrology	Univ. Cologne
29.	Frederic von Guilleaume	Gas Chemistry	Univ. Hamburg^{+}
30.	Marco Warmuth	Gas Chemistry	Univ. Hamburg^{+}

Participating Institutions

IFM-GEOMAR
Wischhofstr. 1-3
24148 Kiel

MPI Bremen
Max-Planck-Institut for Marine Microbiology
Celsiusstr. 1
28359 Bremen

University of Kiel
Institut für Geowissenschaften
Olshausenstr. 40
24118 Kiel

University Bremen
Fachbereich 1 "Environmental physics"
Postfach 330440
28334 Bremen

Jacobs University Bremen
PO Box 750561
28725 Bremen

University Hannover
Institut für Geowissenschaften
Welfengarten 1
30167 Hannover

University of Cologne
Institut für Geologie und Mineralogie
Zülpicher Str. 49 a/b
50674 Köln

University of Hamburg*
Department of Biology, Biozentrum Klein
Flottbek
Ohnhorststr. 18
22609 Hamburg

University of Hamburg+
Institut für Biogeochemie und Meereschemie
Bundesstraße 55
20146 Hamburg

University of Münster
Geologisch-Paläontologisches Institut
Corrensstraße 24
48149 Muünster

University of Bonn
Mineralogisches und Petrologisches
Poppelsdorfer Schloss
53115 Bonn

Schilling Robotics
201 Cousteau Place
Davis, CA., 95618
U.S.A.

High Sierra Technologies
40940 Baptist Church Drive
Lebanon, Oregon, 97355
U.S.A.

2.2 Research Program

The research cruise had, in the time available, two major aims: returning to observe and sample at the 4°48´S hydrothermal site (Turtle Pits etc.) and observing and sampling the lower crust on the 5°S Inside Corner High. The following gives some details on these goals:

4°48´S (Turtle Pits, Red Lion, Wideawake Field)

Vents at Turtle Pits (location, Fig. 2.2.1) show turbulent fluid emanations with temperatures of about 400°C. This is the highest temperature measured so far in fluids at the MAR. Consequently, the system is close to the critical point of seawater on the two-phase boundary

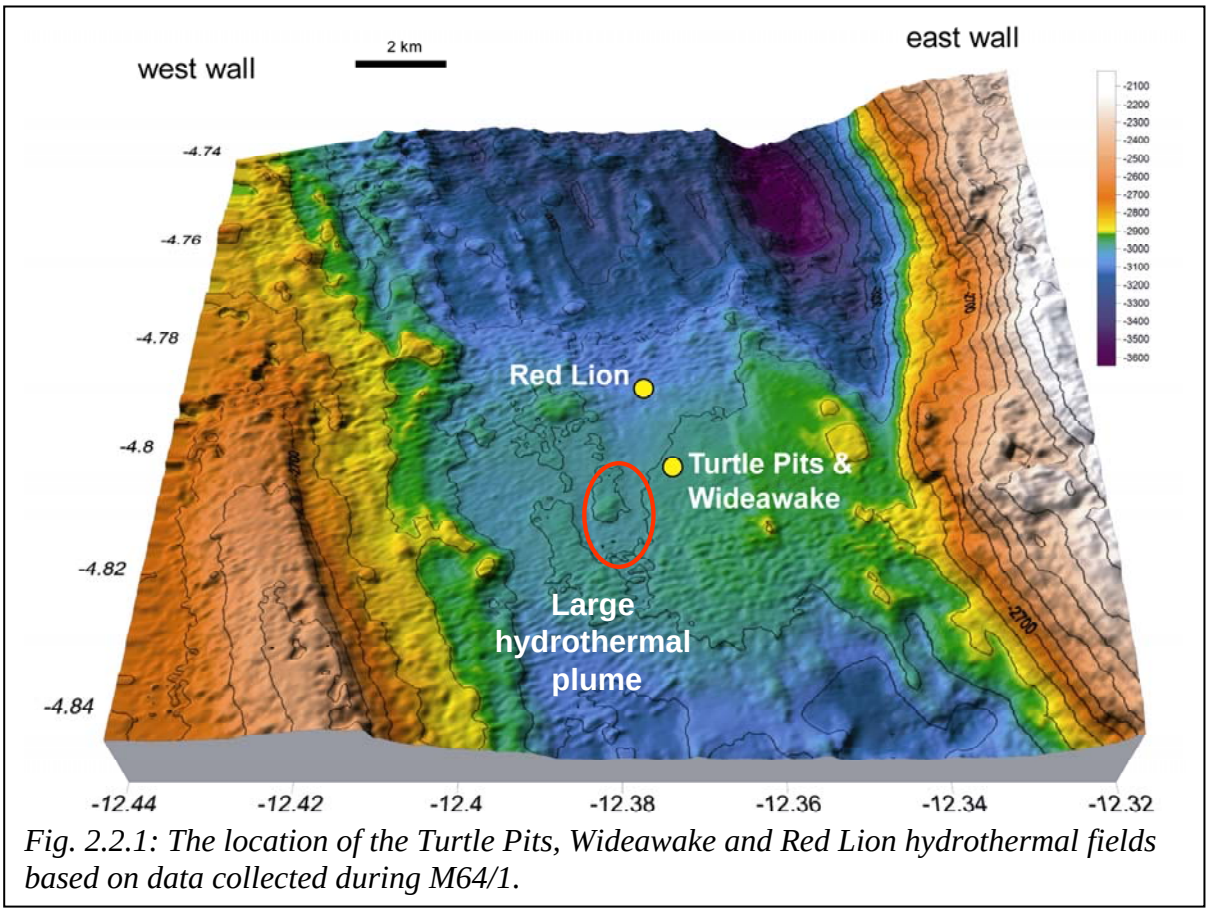

Fig. 2.2.1: The location of the Turtle Pits, Wideawake and Red Lion hydrothermal fields based on data collected during M64/1.

for a boiling system. The Turtle Pits boiling fluids have significantly reduced chloride concentrations (end member value of 254 mmol/l Cl, Fig. 2.2.2) compared to a background bottom seawater value of about 560 mmol/l Cl. This indicates that the fluids are phase-separated and that the samples collected represent the vapour-type phase in the boiling fluids. The diffuse-flow Wideawake mussel field, which is located at a distance of only a few hundred meters from Turtle Pits, is on the same mixing line of seawater and hydrothermal end member chlorinity (Fig. 2.2.2), indicating that Turtle Pits and Wideawake are supplied from the same fluid source at depth. Interestingly, the fluids from the Red Lion field apparently do not show any signs of phase separation (chlorinity end member of 563 mM undistinguishable from seawater, Fig. 2.2.2). Although we have no in-situ temperatures from the Red Lion vents, we can deduce that the Red Lion fluid source at depth has a significantly lower temperature than at Turtle Pits. The high Fe/Mn ratio of 6.8 at Turtle Pits is as high as it is documented for ultramafic systems such as Rainbow and Logatchev fields (Douville et al., 2002) and contrasts with a Fe/Mn ratio of 1 in the Red Lion fluids.

The Turtle Pits fluids have a very high H_2/CH_4 ratio of about 15, even exceeding those found in the serpentinite-hosted Logatchev and Rainbow hydrothermal vents (see data for cruise

M60/3 and from Douville et al., 2002). In contrast, the H_2/CH_4 ratio at Red Lion is only 2.7. Dissolved sulphide concentrations for the three individual hydrothermal vent sites at 5°S are quite variable, ranging from a low abundance of 3 µmol/l (measured data) in the diffuse fluids at the Wideawake Mussel Field to concentrations as high as 830 µmol/l (measured; endmember 1.3 mM) for hot fluids emanating from black smokers at the Turtle Pits site.

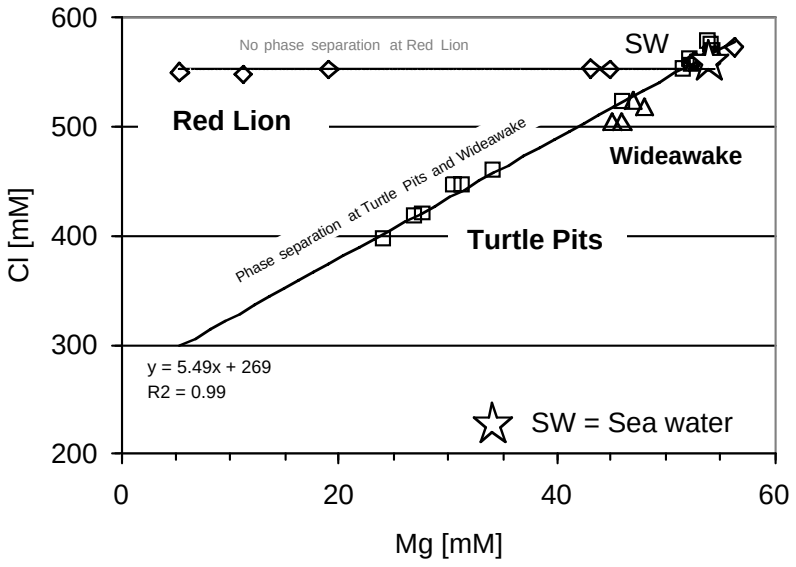

Fig. 2.2.2: Concentrations of Mg and Cl measured in vent waters from the 4°48´S hydrothermal fields.

Preliminary sulphur isotope data for sulphide particles in the hydrothermal fluids as well as for massive sulphides from different chimneys at Turtle Pits display a range between +3.5 to +6.7 ‰ (VCDT). Based on respective data for sulphide precipitates from other sites of hydrothermal activity at mid-ocean ridges, this range in $d^{34}S$ suggests that sulphur in the fluid represents a mixture of mantle sulphur and seawater sulphate sulphur.

During M64/1 the first microbiological studies at the southern hydrothermal vent sites of the MAR were initiated. Genetic analyses and cultivation experiments are in progress, microscopic observations of microorganisms from the Wideawake field revealed heterogeneous morphological assemblages in most cases. Interestingly, enough rock samples collected at the border of Bathymodiolus assemblages showed white structures (0.5-2 mm length) which covered the entire rock and could easily be recognized by eye. Morphological these cells had the typical features of Thiothrix species. In addition, some netlike cracks were observed which were dominated by a large coccoid microorganism (20 µm width) with obvious similarity to species of Achromatium. Both microorganisms contained numerous sulphur globules and represent members of the group of colorless sulphur bacteria. Both microorganisms are important primary producers and are highly abundant at these vent sites. To our knowledge, this is the first observation of these two colorless sulphur bacteria at deep sea hydrothermal vent systems.

Lower crustal and mantle rocks in the spreading axis

Decompression melting of adiabatically upwelling mantle is probably the cause of most magmatism at the mid-ocean ridges (e.g. Klein and Langmuir, 1987). At most ridges, the lower crust and upper mantle are therefore difficult to study as they are coated by and buried beneath 2+ km of dikes and lavas. At slower spreading rates, however, the adaibatic melting process can start to become heterogeneous and rocks from the lower crust and mantle start to become more accessible.

This occurs through two processes. Firstly, the mantle produces generally less melt and this melt production becomes focussed towards the spreading segment centres as a result of 3-D upwelling (Parmentier and Morgan, 1990). The „crust" is then made up of a mixture of basalt

and mantle rocks, the latter of which may contain intrusives such as gabbros (e.g. Cannat, 1996; Cannat et al., 1992; Cannat et al., 1995). Secondly, the increasing importance of tectonic processes in accommodating the spreading movement at magma-starved slower spreading ridges can lead to the formation of low-angle normal faults (Cann et al., 1997). These faults generate tectonic windows which can provide the necessary exposures of the lower crust and mantle (Tucholke et al., 1998). They can lead to the formation both of so-called „megamullions" (areas of striated seafloor close to the ridge axis reflecting the slip surface of the low-angle normal faults) and also of inside corner highs (areas of raised

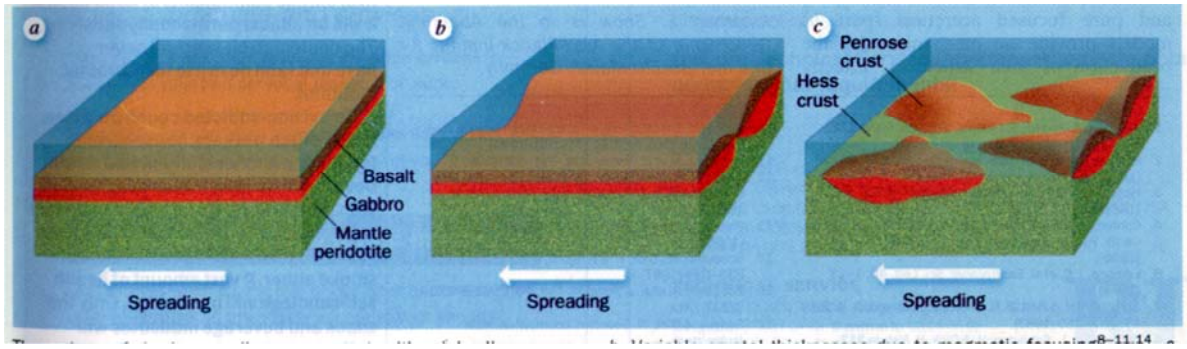

Fig. 2.2.3: Theoretical variations in seafloor structure with decreasing spreading rate (from left to right). From Snow (1995)

bathymetry on the inner side of a spreading axis – transform boundary). These low-angle detachment faults may be rooted above a shallow magma chamber, or even cut all the way into the mantle rocks. Baines et al. (2003) showed that the uplift of "inside corner highs" is partially caused by transpressional forces of large faults around them.

The seafloor generated at slow-spreading ridges (Fig. 2.2.3, c) is therefore in principle vastly different to that generated at fast-spreading ridges (Fig. 2.2.3, a).

This could have enormous implications for hydrothermal processes, as the nature of the rock in which the hydrothermal system is rooted is of paramount importance for the composition of the hydrothermal fluids. This point was made forcibly by the serendipitous discovery of a hydrothermal system situated on, and deriving all its energy from, ultramfic (mantle) rocks at the Lost City site in the Atlantic (Kelley et al., 2001).

The low-angle normal faults also bring samples from great depth up to the seafloor. This allows us almost unique access to rocks from the lower crust and upper mantle influenced by the hydrothermal circulation operating at very high temperatures at the interface between magmatic and hydrothermal processes. The geological record of this process was discovered in many gabbros from the Kane Fracture zone at the MAR, 23°N (Koepke et al., 2005b) and also from the Atlantis II core complex of the slow-spreading Southwest Indian Ridge (Koepke et al., 2005a; Koepke et al., 2004). These authors found evidence to support the hypothesis that seawater-derived water-rich fluids

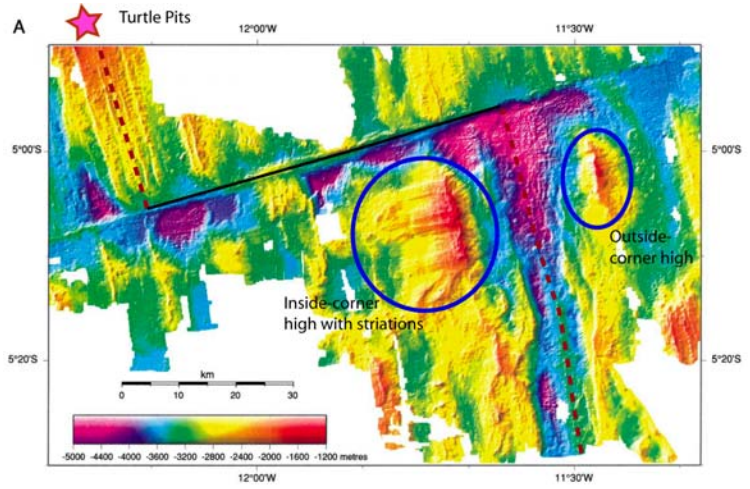

Fig. 2.2.4: Bathymetric map of the region around the 5°S Fracture Zone (from Reston et al., 2002). The present-day spreading axis is marked with a dashed line, the tranform fault with a black line. The location of the Turtle Pits hydrothermal field (see Fig. 2.2.1) is also shown.

propagate along high-temperature shear zones down into the deep oceanic crust causing locally hydrous partial melting on grain boundaries. This results in the formation of a characteristic interstitial mineral paragenesis and a SiO_2-rich melt which may separate and crystallize within cracks forming typical felsic veins or netveining matrices. With the help of a newly developed in-situ Sr isotope technique it was recently verified that the fluids triggering the partial melting are seawater-derived. Thus, the observed fluid/melt transport in the deep oceanic crust within core complexes represents a first and fundamental stage in the transfer of heat from the crust to the surface.

Two areas in which lower crustal and mantle rocks are exposed are known from previous work in the MARSUED-area. Geophysical and rudimentary sampling studies south of a small fracture zone at 5°S (Reston et al., 2002) have shown the presence of both gabbros and serpentinites on a so-called inside-corner high. This high appears to have been split in relatively recent times (0.75 Ma) by rifting, forming a new axis in the middle of the uplifted block and generating a complimentary outside-corner high (see Fig. 2.2.4).

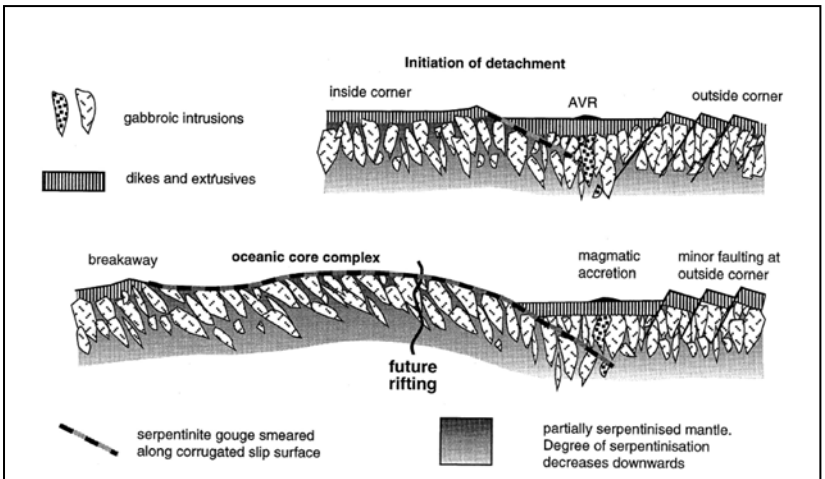

Fig. 2.2.5: Reston et al.´s (2002) model for the interplay of tectonics and magmatism south of the 5°S fracture zone. They envisage no clear distinction between periods of magmatic and tectonic accretion, instead the detachment fault which leads to the formation of an oceanic core complex initiates close to the axial volcanic zone and may at times be split by a ridge jump.

Four dredges collected by Reston during M47/2 showed that the inside-corner massif is predominantly made of gabbroic intrusive rocks, although serpentinised peridotites were found on the corrugated upper surface of the massif, probably associated with smearing along the detachment fault. These authors suggest that detachment faulting and uplift of lower crustal and mantle rocks may be occurring concurrently with magmatic rifting (see Fig. 2.2.5). This situation may be exactly the one which is needed to explain the types of hydrothermal activity seen at the other SPP site at Logatchev and perhaps even at Nibelungenfeld, where fluids with temperatures which require them to have been in close contact with magmas are vented in areas of the seafloor characterised by lower crustal or mantle rocks. One of the major aims of the cruise proposed here will be to study this uplifted massif to determine (a) its geology and the distribution of rock types and (b) to look for the distribution of alteration channels which may have been former root zones for hydrothermal systems.

Reston et al.´s (2002) observation of gabbronorite among the plutonic rocks of the inside corner high is significant, since the dominance of orthopyroxene primocrysts in primitive gabbros indicates crystallization and fractionation at depth, several km deeper than that level where the axial magma chambers under ridges are typically located. For example, high amounts of gabbronorites were recovered farther north, between 14° - 16°N by both M60/3 and the ODP (Ocean Drilling Program, Leg 209) recording cooling and partial crystallization of ascending MORB at great depth (15–25 km). Moreover, crystallization and fractionation of MORB magmas at depth is also in agreement with phase equilibria modelling in combination with experimental work based on the dredged basalts of different segments of the MARSUED area, revealing different equilibrium pressures for individual segments between 1.5 and 8

kbar. These results show also that the differentiation under distinct segments was strongly influenced by water activity.

2.3 Cruise Narrative

The N.O. "Atalante" left Recife harbour on schedule in the morning of 7th January 2008. There followed a 7 day transit to the working area, including a stop to lower the ROV cable to 5500m to remove twists in the wire. The ship arrived in the working area late in the evening of 13th January and the research program started with CTD stations to establish the strength and position of any hydrothermal plume. This was the beginning of activities which repeated each day – a night program consisting of CTD work or rock sampling with the volcanic corer interspersed with a day program of ROV dives. Whenever the ROV needed maintenance the day program consisted of mapping or longer CTD stations. The penultimate day of the working period was marked by an attempt (unfortunately unsuccessful) to recover releasers from the University of Bremen mooring which did not surface followed by the deployment of a profiling mooring from IFM-GEOMAR. The last day saw a long dive on the fracture zone wall at 5°S. Early in the morning of 26th January the ship left the working area on course for Dakar where we docked at 08:00 on 31st January 2008.

2.4 Preliminary Results

2.4.1 Physical Oceanography

(C. Mertens, G. Fraas, P. Günnewig)

2.4.1.1 Instruments and Methods

Conductivity-temperature-depth (CTD) casts were carried out using a Sea-Bird Electronics, Inc. SBE 911plus system (IFM-GEOMAR) that was equipped with double temperature, conductivity, and oxygen sensors as well as with a Wetlab C-Star transmissometer (D. Quadfasel, Univ. Hamburg). The underwater unit was attached to a SBE 32 carousel water sampler with 24 Niskin bottles. Three bottles were left out for a lowered acoustic Doppler current profiler system (LADCP), hence a maximum of 21 bottles was used. The complete system worked properly throughout the entire cruise. Salinity samples, typically three on each cast, were collected for later analysis at home. In total 20 CTD casts were carried out, including three time series (yoyo) stations, and one towed transect across the rift valley (Fig. 2.4.1.1).

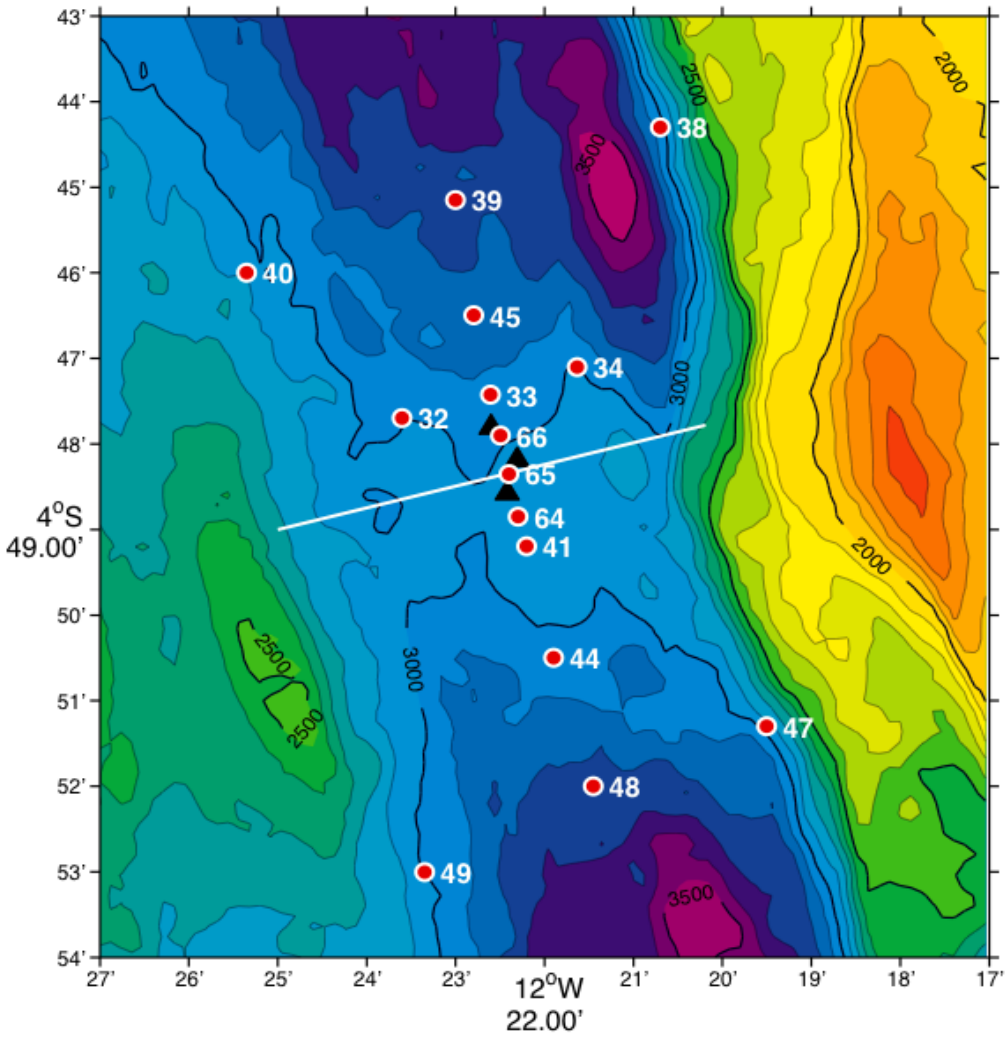

Fig. 2.4.1.1: Map of the working area showing the CTD/LADCP stations (dots). The track of a tow-yo track across the rift valley is shown as a white line. The hydrothermal vent sites Turtle Pits, Comfortless Cove, and Red Lion are depicted as black triangles. Additionally three time series stations were carried out. Two north of Red Lion (at station 33) and one north of Comfortless Cove (near station 66).

The LADCP system consisted of two RD Instruments 300 kHz Workhorse Monitor ADCPs. The instruments worked in a synchronized master-and-slave setup, where the downward looking master (S/N 630, IFM-GEOMAR) triggers the upward looking slave (S/N 7915, Univ. Bremen). The instruments were powered by an external battery supply, that consisted of 35 commercial quality 1.5 V batteries assembled in a pressure resistant Aanderaa housing. On one of the time series stations (62, CTD17) the slave instrument did not collect any data. This was presumably caused by a communication problem between master and slave.

An inverse method incorporating the bottom track velocities was used for the post processing of the raw data. The overall performance of the two instruments was very good: The range of each instrument was typically 150 m in the upper parts of the water column and 60 to 70 m at depth exceeding 1500 m. Thus, the total range of the package reached from 150 to 300 m. With lowering and heaving velocities of 1 m/s of the instrument package, this range amounted to 100 to over 200 estimates of current shear in each depth cell in the deep water, and more in the shallow layers, depending on the amount of backscatter. For the cast with the single instrument, the reduction of range lead to a decrease of shear estimates per bin, but as the water depth did not exceed 3000 m and the abundance of backscatterers was high, the resulting current data were still of good quality.

During yoyo and towyo stations three (serial numbers 33, 36, and 38) miniature autonomous plume recorders (MAPR, E. Baker, NOAA/PMEL) were used to improve the data coverage. MAPRs are self-contained instruments, that record data at pre-set time intervals from temperature (thermistor mounted in a titanium probe, resolution 0.001°C), pressure (0 - 6000 psi gauge sensor, resolution 0.2 psi), and nephelometer (Sea Tech Light Backscatter Sensor, LBSS) sensors. One MAPR (S/N 38) had an additional redox potential (Eh) probe build by K. Nakamura. During operation two of the MAPRs were clamped on the hydrgraphic wire, 100 m and 200 m above the water sampler, and the MAPR with the Eh probe was directly attached to the water sampler. The instruments were working fine throughout the cruise, with only one exception during the cross-valley towyo, were one MAPR (S/N 38) recorded only the first 70% of data. On four CTD stations near the vent sites the MAPR with Eh probe was also attached to the water sampler. In total, MAPRs were used on 9 of the 20 CTD stations.

For measurements of the Helium concentrations and isotopic signature, water samples were taken in the water column from the Niskin bottles (94 samples in total) and directly from the vents with the ROV (3 samples). The samples were sealed free of head space and gas tight in copper tubes (sample volume 40 ml). Special containers for sampling vent fluid (developed & tested in the framework of the SPP 1144) were used for the ROV samples. The sampling containers can keep a pressure of more than 3·107 Pa and avoid phase separation of vent fluids and gases. Helium isotope measurements will be carried out at the University of Bremen with a fully automated UHV mass spectrometric system. The sample preparation includes gas extraction in a controlled high vacuum system. Helium and neon are separated from permanent gases in a cryo system at 25 K. A split of the sample is analyzed for 4He, 20Ne and 22Ne with a quadrupole mass spectrometer. At 14 K He is separated from Ne and released into the sector field mass spectrometer for analysis of 3He and 4He. The facility achieves about ± 0.2% precision for 3He/4He ratios, and ± 0.5% or better for helium and neon concentrations. The primodial components of helium isotopes are ideal tracers for large-scale distribution of vent fluids in the water column. Samples collected during this cruise are supposed to provide the regional distribution of dispersing vent fluids in the water column leading to an estimate of its volume.

On January 14, an attempt was made to recover a mooring with three Aanderaa RCM11 current meters (Univ. Bremen) at 4° 48.21' S, 12° 22.50' W, that was deployed during Meteor cruise M68/1 in May 2006. However, the mooring did not leave the ground, although the release execution command was clearly confirmed during several attempts from both

releasers. Acoustic ranging revealed that the releasers were located at a depth of about 3000 m which is the seafloor depth at this location. It was therefore concluded that the mooring must have lost all buoyancy because the nominal depth of the releasers was 45 m above the seafloor. Knowing the approximate position of the releasers from the acoustic ranging measurements, a recovery dive with the ROV was undertaken in the evening of January 24 to find the two releasers and possibly one of the current meters. During the dive an area of about 150 m x 100 m was searched but (probably because of the rough terrain) the instruments could not be found.

A new mooring equipped with a CTD profiler and an acoustic current meter (IFM-GEOMAR) was deployed at nearly the same location as the previous mooring. The instrument was programmed to carry out 11 profiles between 2295 dbar and 2990 dbar every 5 days. The deployment started on January 24, 23:10 with the anchor first. The top buoy went into the water on January 25, 01:18. Afterwards the mooring was carefully lowered towards the seafloor and acoustically released as the anchor was 15 m above the ground at 02:55. The position of the anchor drop was 4° 48.20' S, 12° 22.51' W and the water depth 3004 m.

2.4.1.2 First results

Two hydrographic sections with 3 casts each (CTD/LADCP/Water sampling/48 Helium samples) were carried out north (CTD6-CTD8) and south (CTD13-CTD15) of the area. The local topography is closed to the sides below a water depth of 2700 m, hence these two sections form a box where measurements of the current field and the stratification allow to calculate fluxes of volume, heat and helium into and out of the vent field area. A third section, again with 3 casts (CTD2-CTD4, 34 Helium samples) was carried out directly north of the Red Lion vent site. Six additional CTD stations (CTD9, CTD11, CTD12, CTD18-CTD20) were used to close an along-valley section (including 13 on stations 11 and 12). Three time series stations (yoyo) were carried out; two north of Red Lion (CTD5 and CTD17) and one north of Comfortless Cove (CTD16). Finally a 5 nm long tow-yo transect completely covering the deep part of the axial valley below the maximum plume hight. During the tow-

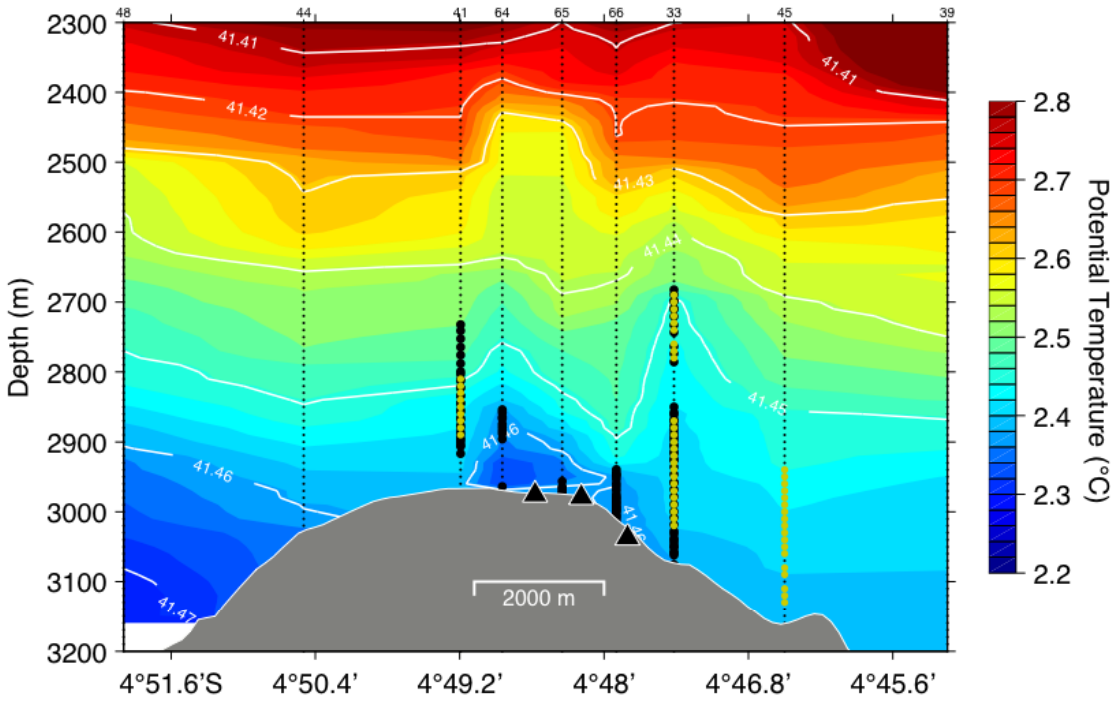

Fig. 2.4.1.2: Potential temperature section along the rift valley put together from nine non-synoptic CTD stations. Contours of potential density are shown in white. Transmission and Eh anomalies are marked with yellow and black dots (no Eh data on station 45). The locations of the vent sites are indicated by black triangles.

yow, POSIDONIA was used to navigate the CTD.

The along-valley temperature and density structure (Fig. 2.4.1.2) clearly indicates a mean northward flow, as the water below sill level is colder and denser on the southern side. Downstream of the sill, the isotherms and isopycnals (and hence the plume anomalies) deepen, showing that water spills over the sill, and the water column stretches, i.e. the vertical spacing between isopycnals increases. Plume signals, either transmission or Eh anomalies, were found at all stations close to the vent sites (33, 41, 45, 64-66) up to a depth of about 2700 m. The distance from the vent sites where plume signals are still found in the water column is larger in northward than in southward direction which indicates prevailing northward currents in the plume layer. Interestingly, Eh signals were found on three stations (64-66) rather close to the vent sites but no indications for the particle plume, neither in the transmissometer data nor in the backscatter measurements of the MAPR. Above the sill the isopycnals show large vertical excursions of up to ±100 m caused by tides and internal waves.

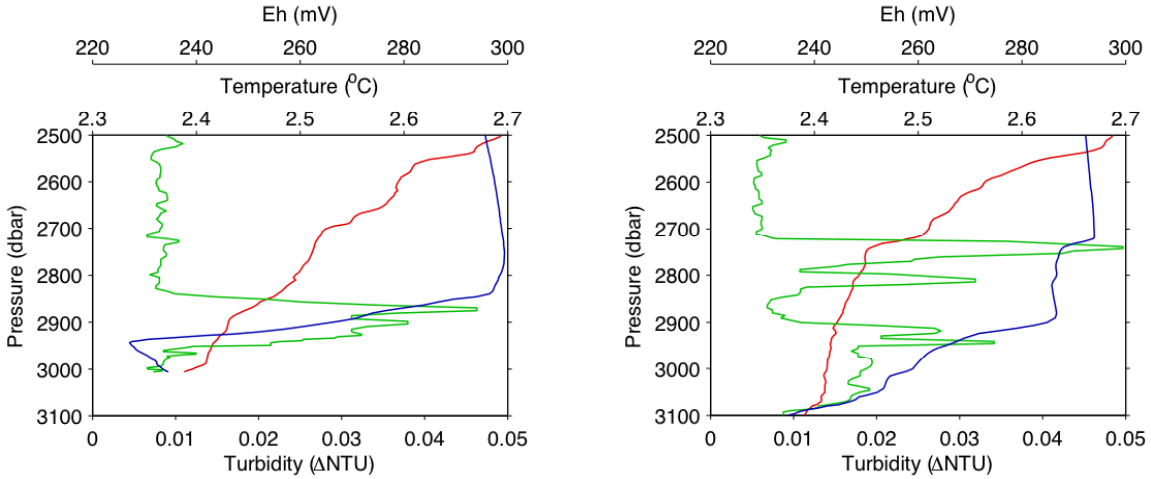

Fig. 2.4.1.3: Vertical MAPR profiles of temperature (red), turbidity (green), and Eh (blue) at two stations south (station 41, left) and north (station 33, right) of the vent sites.

The maximum rise hight of the plume corresponds roughly to the 2.5 °C isotherm, observed at the stations 33 and 41. The MAPR data at these two stations are shown in Fig. 2.4.1.3. At the southern station a single plume between 2800 and 2950 m was observed. At the northern station the vertical structure of turbidity and Eh reveal an upper plume between 2700 and 2850 m, followed by a second plume between 2900 and 3000 m. The decrease in Eh in the upper plume is smaller compared to the second plume and therefore the water in upper plume is farther away from the source and probably originating from the Turtle Pits vent site. Below 3050 m a third decrease in Eh is observed again smaller than in the second plume, suggesting comfortless cove as the source. The central plume with the strongest Eh signal should therefore be attributed to the Red Lion vent site.

Detailed measurements of the plume variability were obtained during two time series stations (yoyo) carried out about 700 m north of the Red Lion vent site. The first yoyo was on January 14/15 with a duration of 9 hours and the second was about 8 days later on January 22/23. The time series of turbidity (Fig. 2.4.1.4) show a large variability of the particle plume. During the first yoyo stations two distinct maxima were observable, although changing in depth and intensity with time. These two maxima could be attributed to Turtle Pits (upper) and Red Lion (lower). The lowest plume that originates from Comfortless Cove starts to appear after 4-5 hours between 3000 and 3050 m. The vertical excursions of the plumes can be explained by internal waves, as the plume clearly follows the isotherms.

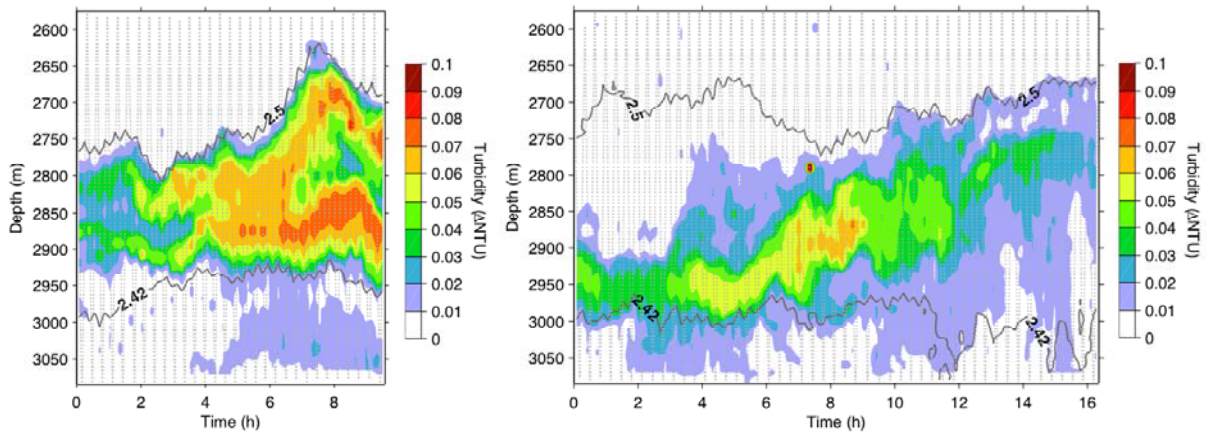

Fig. 2.4.1.4: Time series of turbidity measured during two yoyo stations carried out on January 14/15 (left) and January 22/23 (right), both at the same location about 700 m north of the Red Lion vent field (at station 33 in Fig. 2.4.1.1). Also shown are two temperature contours that depict the upper and lower boundaries of the non-buoyant plume.

During the second yoyo the turbidity measurements suggest a slowly rising single plume, which makes physically no sense in a non-buoyant plume. Instead the variability of the currents has to be taken into account which show a nearly constant northward flow and tidal fluctuations of ±4 cm/s in east-west direction (Fig. 2.4.1.5). Therefore the path of the particles from the source to the observational site is strongly bent, depending on the tidal phase. At the beginning of the time series the current is purely northward and we observe the lower plume from Red Lion not the Turtle Pits plume, because during the hours before the current had an eastward component, driving the Turtle Pits plume away from the observational site. Later on, as the currents get a westward component, the upper Turtle Pits plume appears while the lower Red Lion plume gets weaker.

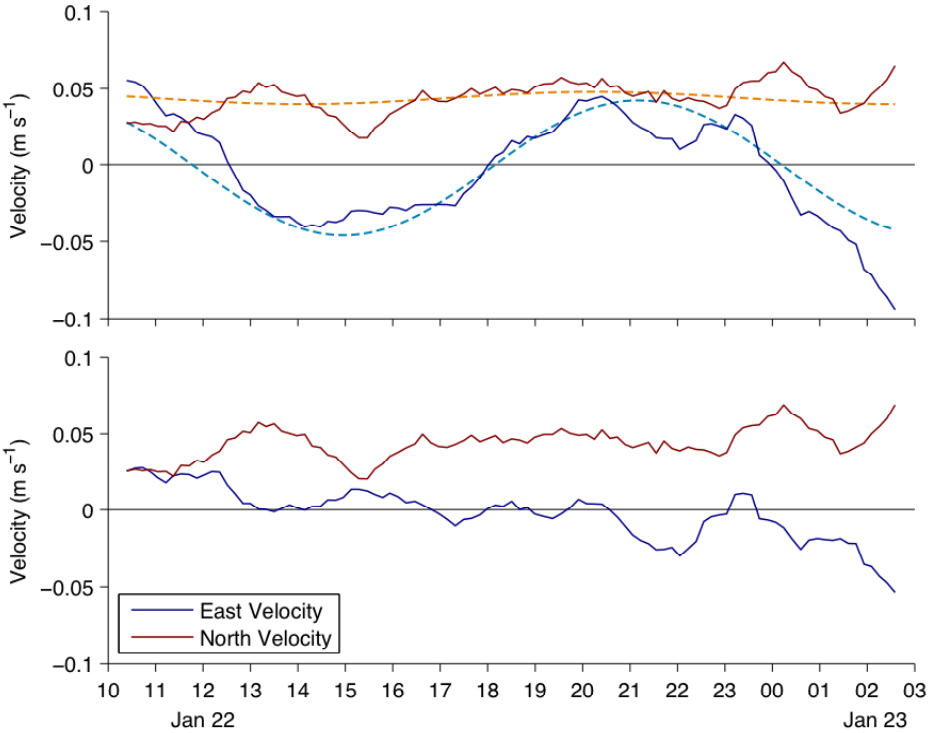

Fig. 2.4.1.5: Time series of the mean velocity in the plume layer between 2750 m and 3000 m measured on January 22/23 about 700 m north of the Red Lion vent field. The east velocity is shown in blue and north velocity in red. Harmonic fits of the semidiurnal M_2 tide are shown as dashed lines. The residual velocities after removal of the tides are shown in the lower panel

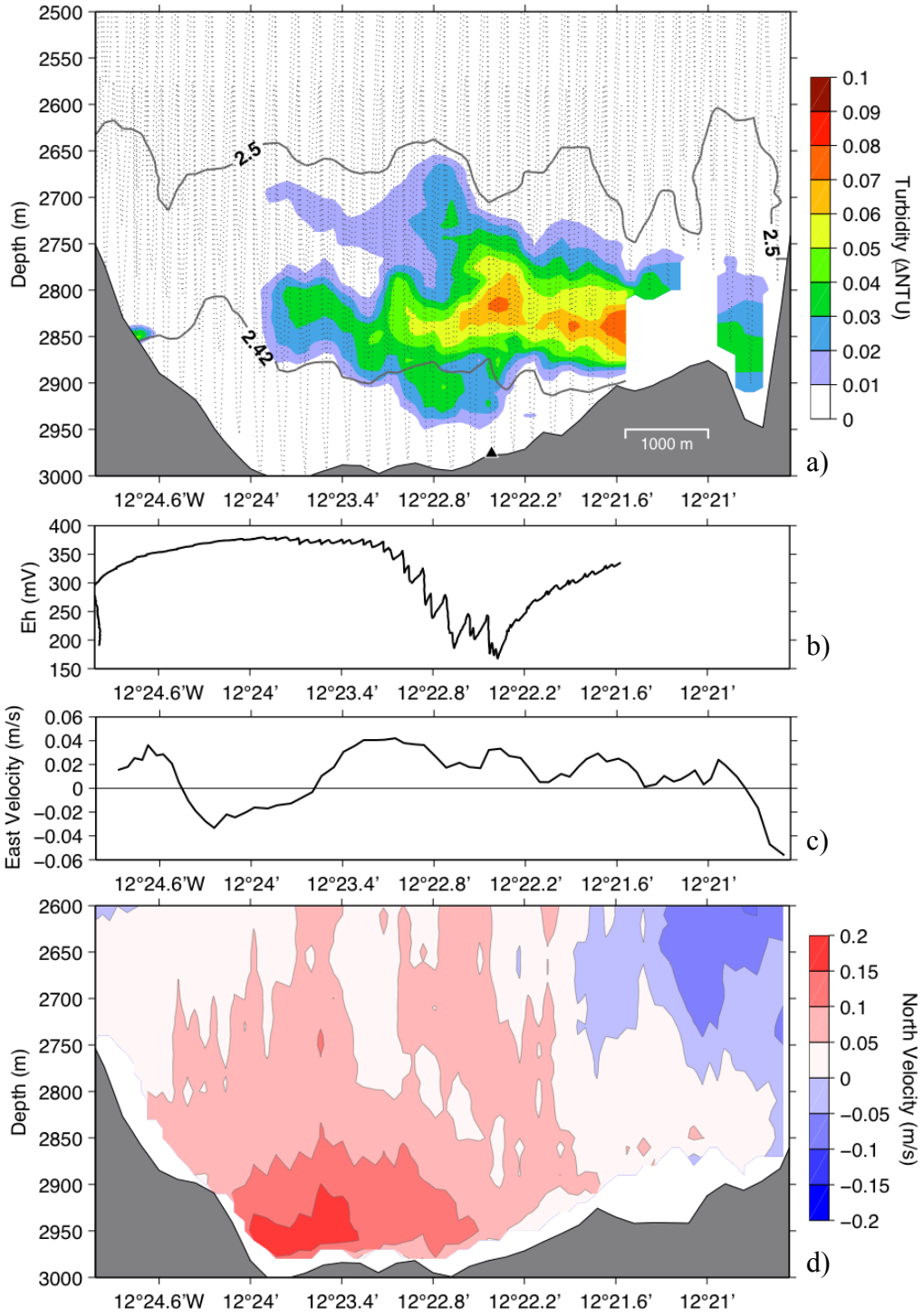

Fig. 2.4.1.6: Observations during a 5 nm long tow-yo crossing the rift valley from west to east. The CTD was navigated using POSIDONIA. (a) Turbidity from three MAPRs, one mounted on the CTD frame and two attached to the wire 100 m and 200 m above the CTD. (b) Eh from the MAPR parallel to the CTD. (c) Mean eastward current velocity below 2750 m from ADCP measurements. (d) Contours of northward velocity from ADCP measurements

The tidal phase of the currents is also of large importance to explain the structure of the particle plume that was observed during the cross-valley tow-yo. The plume appears to be extremely wide and covers about three fourth of the section (Fig. 2.4.1.6). Again we have a northward flow of about 5 cm/s and a fluctuating east-west component that is eastward at the beginning of the towyo, then westward for about two hours, and then mostly eastward for the

remaining part of the towyo. Thus we can assume that the plume is first pushed westward toward the ship for a few hours which explains the far west reaching plume. Afterwards the plume moves eastward and more or less follows the ship and instrument package.

The current measurements during the towyo show that the area was dominated by along-valley northward currents. The average current velocity is typically of about 5 cm/s, with maxima of more than 15 cm/s. The strongest currents were observed close to the bottom where the overflow across the sill takes place. The volume transport associated with the flow observed during the towyo amounts to 0.12 Sv (1 Sv = 10^6 m^3/s). For a more general determination of the background flow field that takes long term variability into account and for the precise determination of tidal amplitudes and phases, a moored profiler that measures CTD and velocity data in the lower 700 m was deployed at the sill of the valley, in the center of the vent fields at 12° 22.51' S, 4° 48.20' S.

2.4.2 Microbiology from low-temperature, diffuse and hot hydrothermal fluids

(Mirjam Perner, Nadine Markus)

The main objective of the microbiology group during this cruise was to collect low-temperature, diffuse and hot hydrothermal fluids from hydrothermal fields on the southern Mid-Atlantic Ridge to investigate:

1. the intra-field and inter-field microbial variability
2. the functioning of the microbial community, specifically focusing on microbial H_2- and H_2S-oxidation and CO_2 fixation.

Intra-field and inter-field microbial variability

To investigate the intra-field and inter-field microbial variability the following fluids were collected (see table 2.4.2.2):

3 hot hydrothermal fluids (Sisters Peak, Mephisto, Two Boats)

5 low-temperature diffuse fluids (Wideawake and Clueless, mussel patches)

To identify and quantify the local microorganisms in the fluids of different sites material was collected to construct clone libraries using the 16S rRNA gene and perform fluorescence *in situ* hybridization in the home laboratory.

Functioning of the microbial community

The functioning of the vent microbial community is studied by two approaches. The first includes cultivation of selected groups of bacteria and archaea. The second involves analysis of functional genes and parallel-performed ^{14}C-incubation experiments with the decrease of potential electron-donors and acceptors being monitored.

Cultivation experiments

To characterize at least parts of the microbial community cultivations have been started on board (and will be continued in the home laboratory) specifically selecting for H_2-oxidizing and CO_2 fixing microorganisms (e.g. *Epsilonproteobacteria*, *Aquificales*, and

Methanococcales). For this purpose, selective media for autotrophic microorganisms was supplemented with various electron donors (H_2, H_2S, S°, S_2O_3) as well as suitable electron acceptors (O_2, NO_3, S°, S_2O_3) in the presence of CO_2.

Additionally, media for aerobic and anaerobic heterotrophic microorganisms was used. Cultivations were conducted along a temperature gradient of 25-75°C.

For the cultivation experiments, material was gathered from:

1 hot hydrothermal fluid (Sisters Peak, Comfortless Cove)
3 low-temperature diffuse fluids (Wideawake and Clueless mussel patches)

^{14}C-incorporation experiments

The second approach investigates the functioning of the vent microbial community by using functional genes encoding for key enzymes of H_2-oxidation, oxidation of reduced sulfur compounds and CO_2 fixation. However, the presence of functional genes encoding key enzymes of specific metabolisms is no proof of the actual functioning of this metabolism. Therefore, additionally, ^{14}C-incorporation experiments (at 25°C) were performed with hydrothermal fluids, which were supplemented with H_2 (under oxic and anoxic conditions) or H_2S as electron donor. The decrease of the supplied electron donors (H_2 or H_2S) and electron acceptors (O_2) was monitored during the 30 hours of incubation.

For this experiment hydrothermal fluids were collected from 3 diffuse fluids (Wideawake, Clueless) and 1 hot fluid from Mephisto (Red Lion)

Four parallels with each 15 ml of the hydrothermal fluids were supplemented with

- H_2-gas under anoxic conditions
- H_2-gas under oxic conditions
- H_2S
- nothing (reference)

and injected with $^{14}CO_3^{2-}$. Three parallel controls using liquids that were microorganism-free (filtered through a 0.1 µm filter) and liquids with non-active microorganisms (sample was fixed with formaldehyde) were incubated to determine the non-biological loss of H_2, O_2 and H_2S in the incubation bottles. These values were taken into consideration when evaluating the decrease of H_2, O_2 and H_2S in the incubation experiment.

H_2, O_2 and H_2S contents were monitored at time points 0 and after 30 hours of incubation (Fig. 2.4.2.1). The amount of labeled inorganic carbon, which has been incorporated into the cells, has been measured for one of the parallels on board (Fig. 2.4.2.1) and will be determined for the other three parallels in the home laboratory.

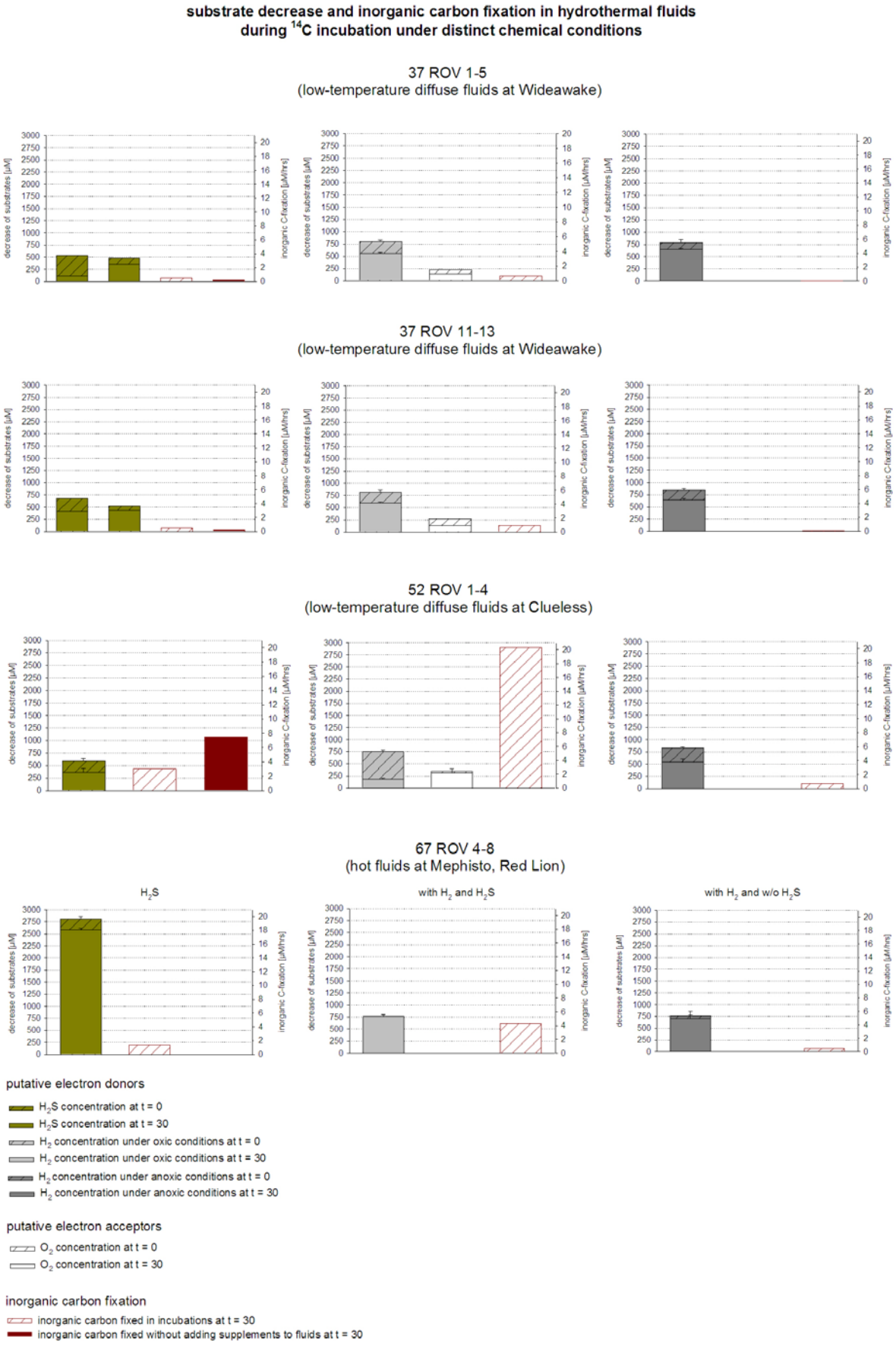

Fig. 2.4.2.1: The decrease of substrates (H_2, H_2S and O_2) under distinct conditions is shown for a 30 hour time-period in the incubation experiments at 25°C. H_2 data by Marko Warmuth and Richard Seifert (University Hamburg); H_2S data by Harald Strauss (University Münster). Fluids at Mephisto were anoxic therefore no O_2 decrease could be determined.

Table 2.4.2.1: Sample list of CTDs

station	depth [m]	niskin bottle number	DNA (-70°C)	FISH (fixed in formaldehyde)
ATA02-31CTD = ATA02-CTD01	3000	1-6	filter 2-2 (900 mL)	filter 3000 (100mL)
	2700	13	filter 2-3 (900 mL)	filter 2700 (100mL)
	2600	14	filter 2-1 (900 mL)	filter 2600 (100 mL)
	2200	17	filter 2-7 (450 mL)	filter 2200 (45 mL)
	1800	19	filter 2-5 (450 mL)	filter 1800 (45 mL)
	100	20	filter 2-4 (900 mL)	filter 100 (100mL)

Table 2.4.2.2: Sample list of hydrothermal fluids taken with the KIPS during the ROV dives

station	site	KIPS bottle number	DNA (-70°C)	FISH (fixed in formaldehyde)	culture name	target organism	t (°C)	CO_2 rates
Rocks Turtle Pits 35 ROV								
ATA02-35 ROV 16	Turtle Pits		rock	rock				
ATA02-35 ROV 16A	Turtle Pits		rock	rock				
Diffuse fluids Wideawake (4 bottles taken) 37 ROV 1-5 11:50-12:18 UTC					38	Desulfurobacterium group, Desulfurococcales & Epsilonproteobacteria	25	1H2.0-1
ATA02-37 ROV 1-5	Wideawake	C8/B6/B5	filter 2-8 (200 mL)	filter (200 mL)	39		55	1H2.0-2
			filter 2-9 (400 mL)		40		75	1H2.0-3
			filter 2-10 (200 mL)		41	Thermales + Aeropyrum	55	1H2.0-4
					42	Thermales + Aeropyrum	75	1H2.A-1
					43	Methanococcales	37	1H2.A-2
					44	Methanococcales	55	1H2.A-3
					45	Methanococcales	75	1H2.A-4
					46	Thermococcales	75	1H2S-1
					47	Aquificales + Epsilonproteobacteria	25	1H2S-2
					48	Aquificales + Epsilonproteobacteria	37	1H2S-3
					49	Aquificales + Epsilonproteobacteria	55	1H2S-4
					50	Aquificales + Epsilonproteobacteria	75	1Ref1
					51	Archaeoglobales	55	1Ref2
					52	Archaeoglobales	75	1Ref3
								1Ref4

station	site	KIPS bottle number	DNA (-70°C)	FISH (fixed in formaldehyde)	culture name	culture target organism	culture t (°C)	CO_2 rates
Diffuse fluids Wideawake (5 bottles taken) 37 ROV 10-13 15:58-16:18 UTC					55	Desulfurobacterium group, Desulfurococcales & Epsilonproteobacteria	25	2H2.0-1
ATA02-37 ROV 11-13	Wideawake	A2/A3	filter 2- 11 (500 mL)	filter (200 mL)	56		55	2H2.0-2
					57		75	2H2.0-3
					53	Thermales + Aeropyrum	55	2H2.0-4
					54	Thermales + Aeropyrum	75	2H2.A-1
					58	Methanococcales	37	2H2.A-2
					59	Methanococcales	55	2H2.A-3
					60	Methanococcales	75	2H2.A-4
					61	Thermococcales	75	2H2S-1
					62	Aquificales + Epsilonproteobacteria	25	2H2S-2
					63	Aquificales + Epsilonproteobacteria	37	2H2S-3
					64	Aquificales + Epsilonproteobacteria	55	2H2S-4
					65	Aquificales + Epsilonproteobacteria	75	2Ref1
					66	Archaeoglobales	55	2Ref2
					67	Archaeoglobales	75	2Ref3
								2Ref4
Hot fluids ATA02-42 ROV 12 (Sisters Peak, Comfortless Cove) 16:54-16:58 UTC					68	Desulfurobacterium group	75	
ATA02-42 ROV 12			filter 2-12 (100 mL)	filter (10 mL)	69	Methanococcales	75	
			filter 2-13 (100 mL)	filter (40 mL)	70	Thermococcales	75	
			filter 2-14 (100 mL)		71	Aquificales + Epsilonproteobacteria	75	
					72	Archaeoglobales	75	

station	site	KIPS bottle number	DNA (-70°C)	FISH (fixed in formaldehyde)	name	culture	t (°C)	CO_2 rates
Rocks ATA02- 46 ROV (Wideawake slurp gun)			rock					
Diffuse fluids Clueless (4 bottles taken) 52 ROV 1-4 13:59-14:17 UTC					73	Desulfurobacterium group, Desulfurococcales & Epsilonproteobacteria	37	3H2.0-1
ATA02-52 ROV 1,2, 4	Clueless	C9/C8/B6	filter 2-21 (100 mL)		74		55	3H2.0-2
			filter 2-22 (100 mL)		75		75	3H2.0-3
			filter 2-23 (100 mL)		76	Methanococcales	37	3H2.0-4
			filter 2-24 (100 mL)		77	Methanococcales	55	3H2.A-1
					78	Methanococcales	75	3H2.A-2
					79	Thermococcales	37	3H2.A-3
					80	Thermococcales	55	3H2.A-4
					81	Thermococcales	75	3H2S-1
					82	Aquificales + Epsilonproteobacteria	37	3H2S-2
					83	Aquificales + Epsilonproteobacteria	55	3H2S-3
					84	Aquificales + Epsilonproteobacteria	75	3H2S-4
					85	Archaeoglobales	37	3Ref1
					86	Archaeoglobales	55	3Ref2
					87	Archaeoglobales	75	3Ref3
ATA02-52 ROV 5,6,7	Clueless	B4/B5/A3	filter 2-20 (400 mL)					3Ref4
ATA02-52 ROV 8,9	Clueless	A2/A1	filter 2-15 (150 mL)					
			filter 2-16 (55 mL)					
			filter 2-17 (55 mL)					
			filter 2-18 (55 mL)					
			filter 2-19 (55 mL)					
Hot fluids 57 ROV 2 (Turtle Pits) (4 bottles) 15:35-15:39 UTC								
ATA02-57 ROV 2	Turtle Pits		filter 2-25 (3 x 66 mL) filter 2-26 (3 x 66 mL)	filter (1 mL) filter (45 mL)				

station	site	KIPS bottle number	DNA (-70°C)	FISH (fixed in formaldehyde)	culture name	culture t (°C)	CO_2 rates
Hot fluids Mephisto (Red Lion) (5 bottles taken) 67 ROV 4-8 14:48-15:03 UTC							
ATA02-67 ROV 4-8	Mephisto	C9/C8/B6	filter 2-27 (50 ml)	filter (1 mL)			4H2.0-1
			filter 2-28 (50 ml)	filter (45 mL)			4H2.0-2
							4H2.0-3
							4H2.0-4
							4H2.A-1
							4H2.A-2
							4H2.A-3
							4H2.A-4
							4H2S-1
							4H2S-2
							4H2S-3
							4H2S-4
							4Ref1
							4Ref2
							4Ref3
							4Ref4

2.4.3 Temperature measurements of low-temperature, diffuse hydrothermal fluids

(Mirjam Perner, Dieter Garbe-Schönberg)

During the sampling of the low-temperature hydrothermal fluids with the KIPS at Wideawake and Clueless the temperature was monitored (Fig. 2.4.3.1 A-C).

A

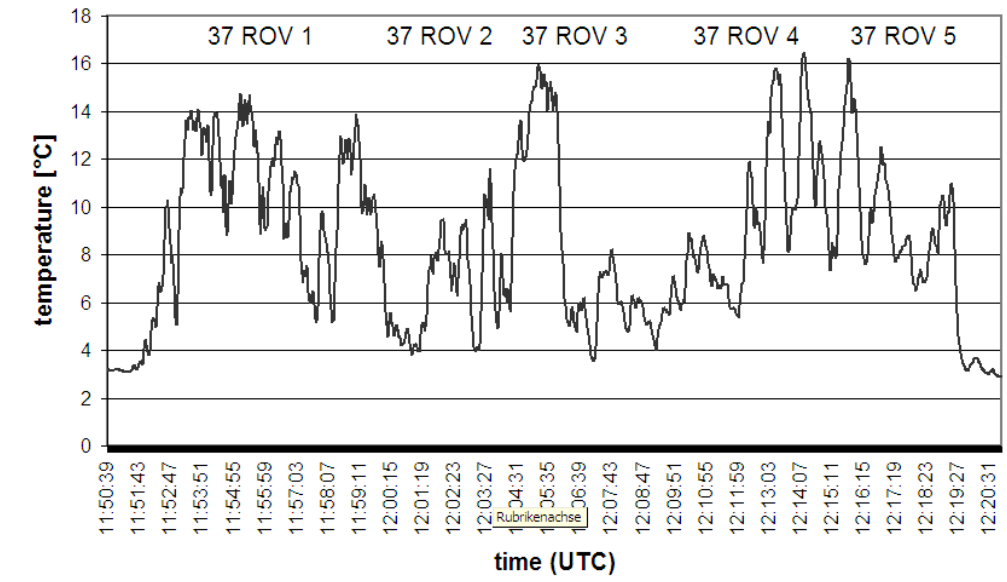

B

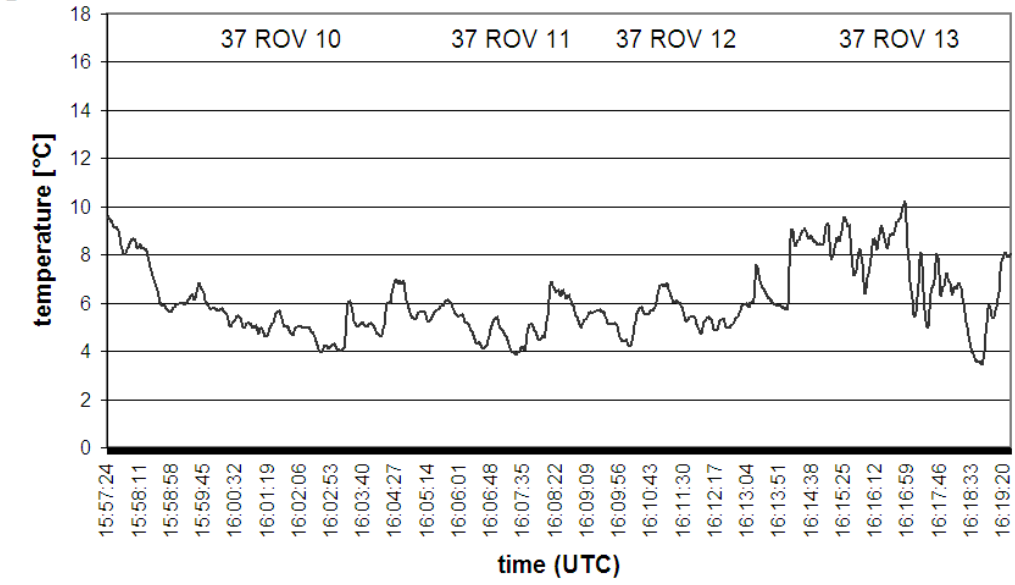

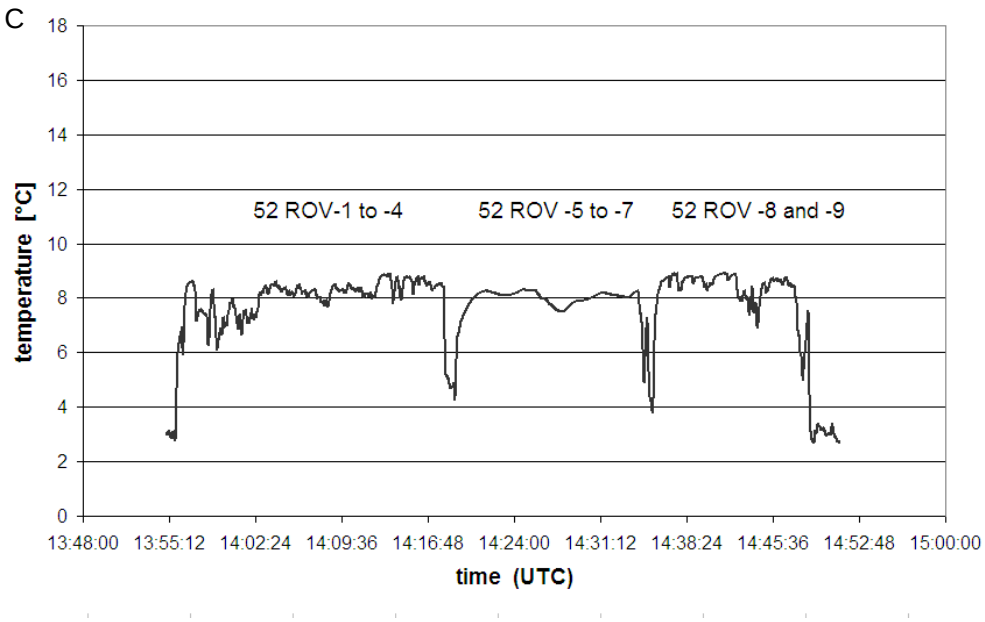

Fig. 2.4.3.1: Temperature measured during sampling of low-temperature diffuse fluids at Wideawake (A, B) and at Clueless (C).

Following the fluid sampling the 8-chanel temperature logger was inserted into the spot of sampling and measured temperatures along a vertical gradient for 20-30 minutes (Figs. 2.4.3.3, 2.4.3.5, 2.4.3.7).

Fig. 2.4.3.2: Measurment of temperature with the 8-channel temperature logger at the low-temperature diffuse outlet at Wideawake (37 ROV6).

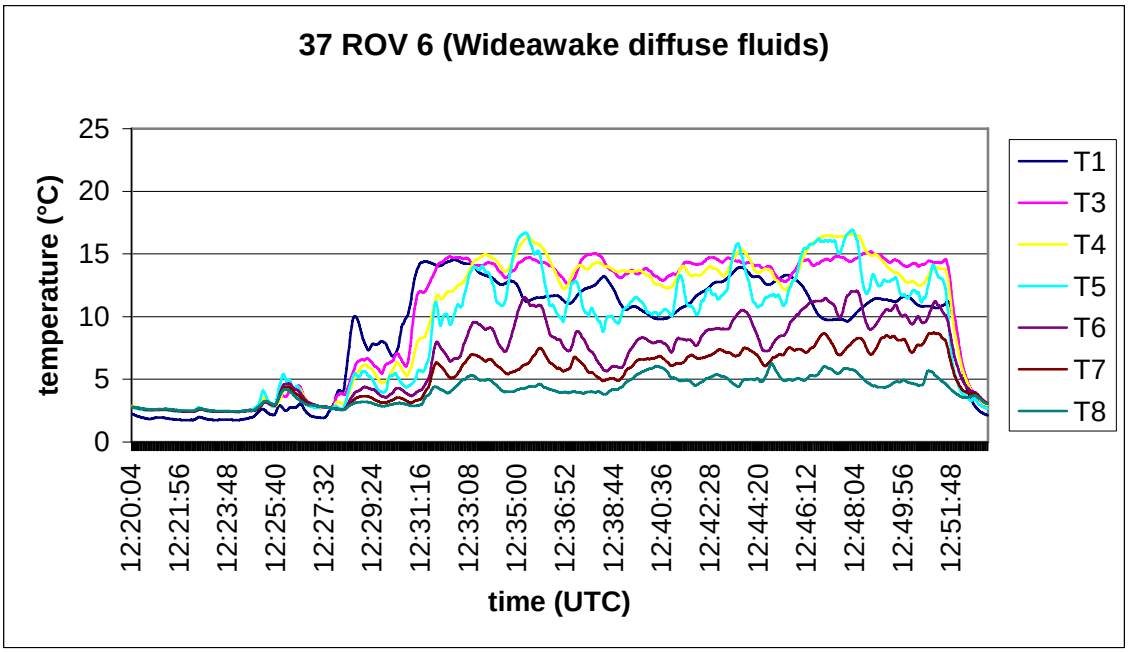

Fig. 2.4.3.3: Measurment of temperature with the 8-channel temperature logger at the low-temperature diffuse outlet at Wideawake (37 ROV6). T1 = 28 cm depth, T3 = 24 cm, T4 = 20 cm, T5 = 16 cm, T6 = 12 cm and T7 = 8 cm.

Fig. 2.4.3.4: Measurment of temperature with the 8-channel temperature logger at the low-temperature diffuse outlet at Wideawake (37 ROV13).

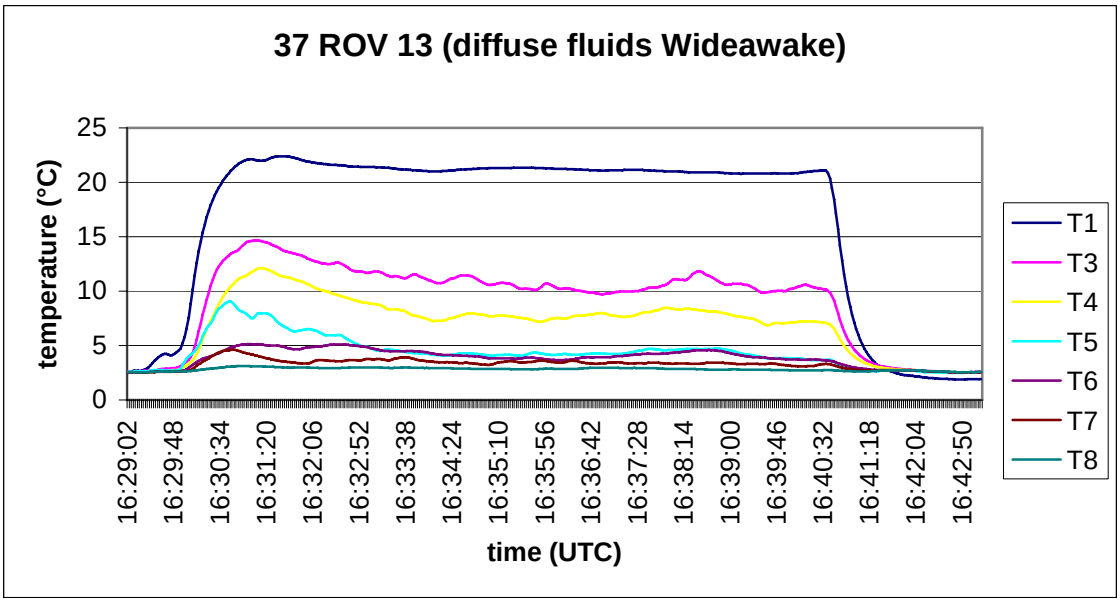

Fig. 2.4.3.5: Measurment of temperature with the 8-channel temperature logger at the low-temperature diffuse outlet at Wideawake (37 ROV13). T1 = 28 cm depth, T3 = 24 cm, T4 = 20 cm, T5 = 16 cm, T6 = 12 cm and T7 = 8 cm.

Fig. 2.4.3.6: Measurment of temperature with the 8-channel temperature logger at the low-temperature diffuse outlet at Clueless (52 ROV10).

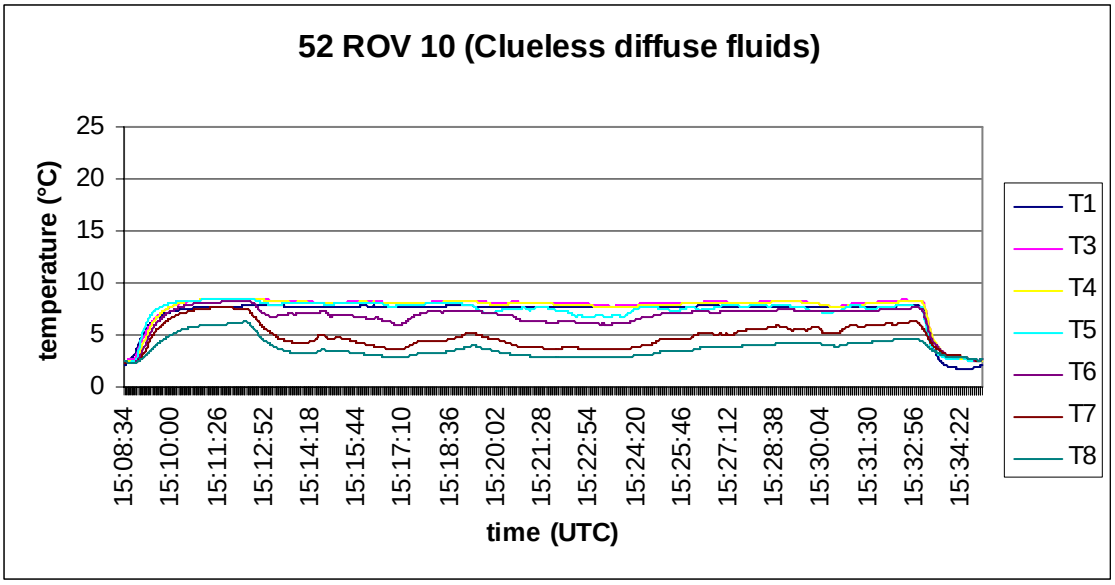

Fig. 2.4.3.7: Measurment of temperature with the 8-channel temperature logger at the low-temperature diffuse outlet at Clueless (52 ROV10). T1 = 28 cm depth, T3 = 24 cm, T4 = 20 cm, T5 = 16 cm, T6 = 12 cm and T7 = 8 cm.

2.4.4 Fluid chemistry

(Dieter Garbe-Schönberg, Katja Schmidt, Harald Strauss, Verena Klevenz, and Phillip Hach)

2.4.4.1 Fluid sampling

Kiel Pumping System (KIPS)

One pre-requisite for an accurate estimate of the composition of hydrothermal fluids venting at high-temperature Black Smokers or from diffuse mussel-field sites is sampling of the hydrothermal fluids without entrainment of ambient seawater which would cause immediate precipitation of sulphides and barite and, hence, loss of these compounds from solution. One measure of the purity of the sampled hydrothermal fluid is temperature. Consequently, real-time *in-situ* measurement of the temperature helps to guide the tip of the sampling nozzle to the hottest region within the vent orifice where the purity of the venting fluid is highest and least diluted with seawater. Another pre-requisite is that all materials coming into contact with the sampled fluid are inert and have lowest adsorption coefficients preventing systematic errors introduced by either contamination or losses due to adsorption. Precipitation during cooling of the sampled fluid, however, cannot completely be avoided.

A remotely controlled flow-through system – the Kiel Pumping System (KIPS-3) - mounted on the ROV's starboard tool sled was used for this purpose (Garbe-Schönberg et al., 2006). The parts of the system getting into contact with the sample are entirely made of inert materials and are stable up to temperatures of 260 °C (short-term 305 °C): perfluoralkoxy (PFA), polyetherethyleneketone (PEEK), polytetrafluorethylene (PTFE, Teflon®), and a short tube of high-purity titanium (99.9 % Ti). Fluid enters via this titanium tube (40 cm length, 6 mm I.D., bent to 90°) - the nozzle - mounted to a T-handle which is guided by the

ROV's ORION manipulator arm (Fig 2.4.4.1). Parallel to the titanium nozzle is a high-temperature sensor (see below) delivering real-time temperature data for the tip of the nozzle. Coiled PFA tubing (3/8" O.D., 3 m length) connects the nozzle to a remotely controlled multi-port valve (PEEK/ PTFE) delivering the fluid to the respective sampling flask. The valve is driven by a stepper motor (electric actuator, Schilling Robotics, U.S.A.) and controlled from a separate laptop via RS232 tunneling through the ROV control system (Kiel 6000 ROV: Node 6, port #14). The software package used was FluidCtrl V. 3.0.0 by Jens Renken @ Marum Soft, Bremen.

The multiport valve has 9 ports connected to 9 single PFA flasks with 675 ml volume each (Nalgene, USA). Each bottle is equipped with a check valve at the outlet. The flasks are mounted in three racks A-C, with every rack containing three horizontally positioned bottles (A1-A3, B4-B6, C7-C9), allowing an easy transfer of the racks to the laboratory where sub-sampling was done. Flasks were pre-filled with ambient bottom seawater (North Atlantic Deep Water, NADW) obtained from previous CTD hydrocasts. A 24 V deep sea mechanical gear-pump is mounted downstream to the sample flasks, thus avoiding contamination of the samples. The pumping rate was approx. 1 L/min at 24 VDC. The standard pumping time per sample was set to 4 min. making sure that the flask volume was exchanged at least 5 times. The outlet of the KIPS system is located on the porch at the front-side of the ROV, where video control allows the observation of warm shimmering fluids leaving the system. In addition, a flow mobile was attached to the outlet tube at diffuse vent sites.

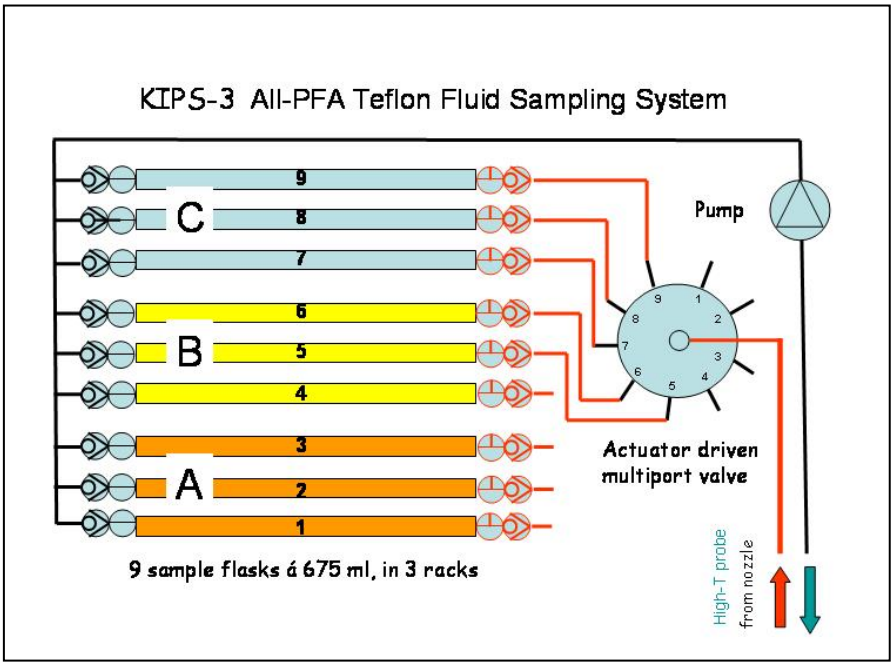

Fig. 2.4.4.1: Schematic configuration of the inert KIPS fluid sampling system (only tubing connections to flasks # 5 - # 9 are shown for clarity). Fluid entering the nozzle is distributed by a motorized multiport-valve to 9 PFA sample flasks á 675 ml, each with check valves and stopcocks. The pump is positioned downstream. Racks A, B, C with 3 flasks each can be quickly removed and sub-sampled in the lab.

A high-precision thermistor temperature sensor (manufactured by H.-H. Gennerich, Bremen) inside a stainless steel pressure housing was attached parallel to the nozzle. The 90% time constant of the sensor in water was better than 10 s. The sensor is connected to a RBR logger TR-1050R (Serial# 12644, RBR Brancker, Canada) for real time data conversion to

calibrated temperatures and data storage. A Y-splice cable connection accomplished real time data transfer through the ROV's RS232 data line and the display on a ROV control van monitor. Two individual sensors were used during this cruise: temperature probe #5 during stations ATA 35 ROV through ATA 42 ROV, and T probe #4 for all subsequent dives. Calibration coefficients used during the cruise are tabulated in Table 2.4.4.1. Prior to the cruise a 23-points high-precision calibration covering 0-450 °C was performed at an ISO-certified calibration lab (TESTO, Germany) for each of the sensors.

Table 2.4.4.1: Calibration coefficients for resistance data-to-temperature conversion of T probes #5 and #4 at RBR logger TR-1050.

T probe #5 (NTC No 193729)		T probe #4 (NTC No 193731)	
A0	0.003516129399127	A0	0.00347114037326
A1	-0.000256163403706	A1	-0.000255203453916
A2	0.000002731961606	A2	0.000002719519579
A3	-0.000000081982648	A3	-0.000000080192994

Major water samplers

In addition to the KIPS, we used two titanium syringes ("Major" after von Damm et al., 1985; manufactured by IFREMER/ BREST-MECA) to collect hot hydrothermal fluids at Turtle Pits, Comfortless Cove and Red Lion. The total sample volume for one major is 750 ml (Fig 2.4.4.2). The samplers were constructed primarily of titanium with seals made of teflon and viton. The syringes are not gas-tight: a simple lab test showed that bubbling from the samplers started at 1.5 bars overpressure. They are constructed to be self-flushing and are sent to the seafloor in chocked mode. To take a fluid sample, the snorkel is placed into the vent orifice. First, only the snorkel gets flushed by the fluid; a control for a good position in the undiluted part of the fluid outflow is allowed by observing the small flushing outlet opening. Undiluted hydrothermal fluid without seawater mixing is indicated by a clear solution leaving the outlet. Triggering the sampler is accomplished by pushing the releaser with a hydraulic cylinder mounted on the ROV manipulator arm. This releaser 1) closes the flushing valve, 2) opens the valve to the sample chamber, and 3) releases the pin holding the piston rod so that the large spring can pull the piston back soaking hydrothermal fluid into the sample chamber. To recover the sample on board tubing is connected to the small outlet valve of the sample chamber. For gas sampling, vacuum extraction was applied (see section on Dissolved Gas Chemistry). Thin black coatings in the sample chamber were observed in most cases, caused by precipitation of sulfides.

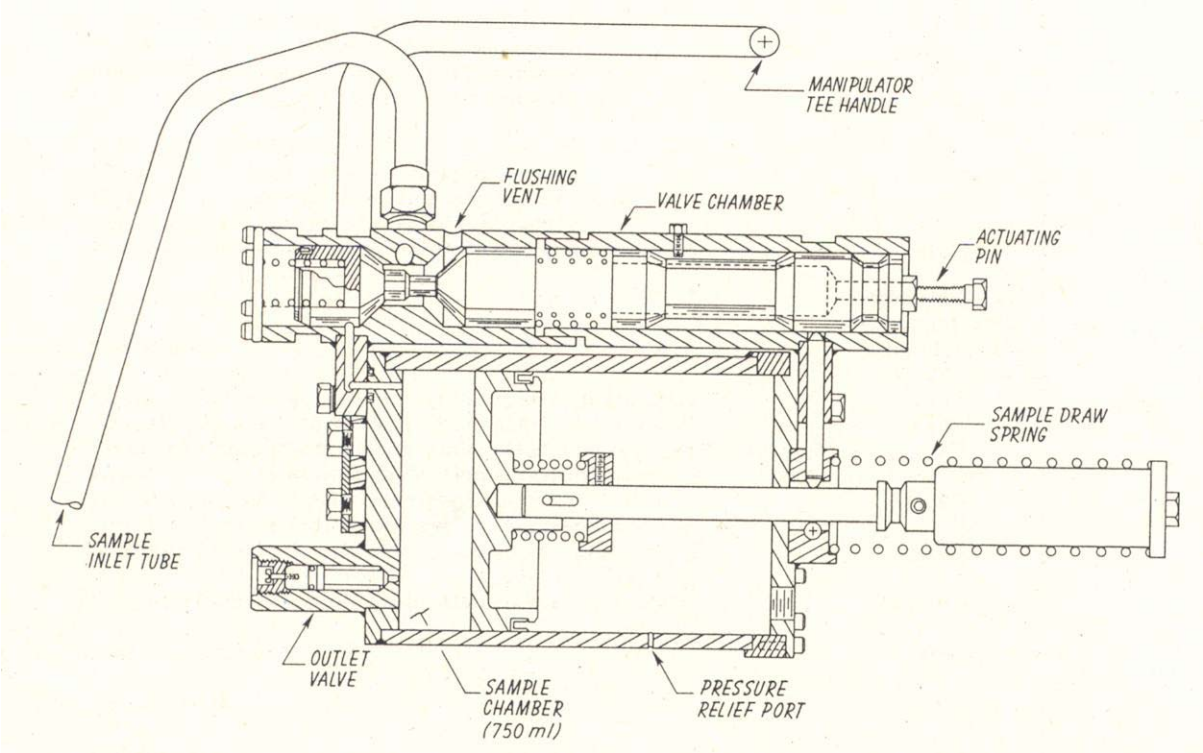

Fig. 2.4.4.2: Schematic drawing of "Major" titanium syringe sampler after von Damm, 1985 (Geochimica et Cosmochimica Acta 49, 2197–2220).

In total, 22 hot fluid samples were collected utilizing KIPS and Majors: seven from Turtle Pits (Two Boats), nine from Comfortless Cove (Sisters Peak) and six from Red Lion (Mephisto). Diffuse fluids were collected at two different locations at Wideawake (9 samples) and Comfortless Cove (Golden Valley – 9 samples).

Buoyant hydrothermal plumes were sampled by means of the CTD/Rosette, equipped with 24 bottles à 10 l volume and operated as tow-yos (see section oceanography for details). In total, 16 water column profiles were sampled and immediately acidified in order to determine Fe and Mn in these samples.

Sub-sampling and sample preparation for on-board analyses and subsequent measurements in the home laboratories

Immediately after recovery of the ROV on deck KIPS sample racks and Ti majors were transferred to the laboratory for subsampling following a standardized protocol (see appendix). In addition to the onboard analyses, further fluid sample aliquotes were taken for measuring fluid chemical composition and selected isotopes.

In order to fullfill the requirement for trace metal analyses to work on indentical sample aliquots, the rest of each sample was first transferred to one PFA bottle, homogenized by shaking and further distributed to the respective bottles. Furthermore, hot hydrothermal fluids emanating from black smokers contain precipitates formed during cooling and mixing with seawater. On board, aliquots were not filtered but acidified with 1-5 ml subboiled HNO_3 per 100 ml fluid and stored in PFA bottles. A second set of aliquots were pressure filtrated (99.9990 nitrogen) through 0.2 µm Nuclepore PC membrane filters in a Sartorius filtration unit, acidified with 0.2 ml subboiled concentrated nitric acid per 100 ml and also stored in

100 ml PFA bottles until analyses. Procedural blanks were processed in regular intervals. All work was done in a class 100 clean bench (Slee, Germany) using all-plastic labware (HDPE, PC, FEP, PFA). Rinse water was ultrapure (>18.2 MOhm) dispensed from a Millipore Milli-Q system.

After return to the home labs in Kiel and Bremen samples will be analysed for major and minor elemental composition (Na, K, Ca, Mg, Sr, Ba, B, Fe, Mn, Cu, Zn) by means of ICP-optical emission spectrometry (Ciros SOP; Spectro) and trace elements (e.g., I, Br, B, Li, Al, Ti, Cs, Ba, Sr, Y-REE, Fe, Mn, Cr, V, Cu, Co, Ni, Pb, U, Mo, As, Sb, W) by ICP-mass spectrometry using both collision-cell quadrupole (U-Kiel: 7500 cs, Agilent, JU-Bremen: Elan DRC-e, Perkin Elmer) and high resolution sector-field instrumentation (U-Kiel: PlasmaTrace 2, Micromass). At JUB in Bremen, complementary analyses on the speciation of metals will be carried out using voltammetry (computrace VA 757, Metrohm). For anion analyses (e.g., Cl^-, Br^-, I^-, SO_4^{2-}), aliquots of hot hydrothermal fluids with precipitate were pressure-filtrated through 0.2 µm PC membrane filters (Nuclepore). For amino acids and other organic compounds, respective measurements will be carried out in collaboration with Dr. Ostertag-Henning at Bundesanstalt für Geowissenschaften und Rohstoffe (BGR, Hannover, Germany). Onboard, non-filtered sub-samples for organic analyses were immediately frozen (-20°C) as 50 ml aliquots in glas bottles. Filters from filtration of the KIPS fluid samples of the ROV were kept in plastic containers. Samples for the detection of dissolved inorganic silica were diluted 1:50 from the concentrated fluid (filtered and acidified) with DI water.

Further subsamples were collected for stable isotope analyses. Filtered aliquotes of hot hydrothermal fluids (2x2 ml) were stored with no headspace in crimp-sealed glass vials for hydrogen (δ^2H) and oxygen isotope measurements ($\delta^{18}O$). Hydrogen sulfide disolved in the hydrothermal fluids was precipitated as zinc sulfide with a 3% zinc-acetate solution, filtered and dried for measuring the four stable sulfur isotopes (^{32}S, ^{33}S, ^{34}S, ^{36}S). For determining the carbon isotopic composition of inorganic carbon ($\delta^{13}C$) dissolved in hot and diffuse hydrothermal fluids, 20 ml aliquotes were poisened with two drops of $HgCl_2$ and stored in the dark. Stable isotope measurements will be carried out at the Geologisch-Paläontologisches Institut, Universität Münster, Germany. For Ca, Sr, and Cl isotope measurements, 50 ml of non-filtered hydrothermal fluid were stored in HDPE bottles.

2.4.4.2 Analytical procedures on-board

In general, on-board measurements were performed immediately after sample recovery on deck. Sampling followed a standardized protocol in order to avoid oxidation of highly redox-sensitive dissolved constituents in the hydrothermal fluids.

pH and Eh

Non-filtered aliquots of each sample were subjected to immediate pH and Eh measurements (Ag/AgCl reference electrode).

Dissolved oxygen

Dissolved oxygen was determined for diffuse hydrothermal fluids following the classical Winkler method as outlined in Grasshoff (1999). The method was slightly modified in order to utilize 10 ml volumetric flasks. The detection limit is approx. 0.5 ml/l O_2, precision is in the range of ± 0.1 ml/l O_2. The samples were analysed by Mirjam Perner and Nadine Markus (see section on Microbiological Diversity).

Iron speciation

Determination of iron speciation was performed spectrophotometrically. The method is based on determining the orange-red ferroin complex, which is formed by Fe(II) ions in the fluid sample complexed with 1% (w/v) 1,10-phenantroline in a pH range of 3-5. In addition to the quantification of Fe(II), the total Fe content is measured by reducing all Fe with a 1% (w/v) ascorbic acid solution. Fe(III) concentration is calculated as the difference between total Fe and Fe(II). Analyses were carried out with a Biochrom Libra S12 spectrophotometer at a wavelength of 511 nm.

Dissolved sulfide

For onboard analysis of dissolved sulfide concentrations, initially two different methods were applied: voltammetry and spectrophotometry.

All voltammetric measurements were performed on a 757 VA Computrace with a standard PC (Metrohm, Herisau, Switzerland). The three-electrode configuration consisted of the static mercury drop electrode (SMDE) as the working electrode, an Ag/AgCl reference electrode (3M KCl), and a platinum wire as the auxiliary electrode. Sulfide concentrations were determined by using a NaOH 0.1M oxygen-free solution (Application Bulletin No. 199/3, Metrohm, Herisau, Switzerland).

Spectrophotometry of dissolved sulfide is based on the light absorption of methylene blue at a wave length of 660 nm. Dissolved sulfide is stabilized in a colloidal form as zinc sulfide using zinc acetate gelatine solution (100 µl for 1 ml of hydrothermal fluid). The sulfide reacts with N,N_dimethyl-1,4-phenylene-diamine-dihydrochloride to colourless leucomethylene and – through oxidation by Fe(III) supplied by an $FeCl_3$-solution – further to methylene blue. Photometric measurements were performed using a Biochrom Libra S12 spectrophotometer. Concentrations of the freshly prepared stock solution utilized for calibration were determined by titration with a 0,02N sodium-thiosulfate solution.

Further measurements of sulfur speciation (i.e., intermediate sulfur species like sulfite or thiosulfate) will be performed at the home laboratory, following the monobromobimane method (Fahey and Newton, 1987). On board, 50µl volume of the hydrothermal fluid was added to 110µl of previously prepared derivatization mixture, composed as follows: 50µl of HEPES buffer, 50µl acetonitrile and 10µl monobromobimane (48mmol/L). Derivatization was performed in the dark and was stopped after 30 min by adding 100µl of methanesulfonic acid (Rethmeier et al., 1997). Several advantages derive from this approach: the opportunity to quantify additional metastable sulfur phases, to separate these for isotopic measurements (method currently being developed in cooperation with Dr. Ostertag-Henning, BGR Hannover), and to perform respective measurements on substantially smaller sample volumes.

Chloride

Phase separation in hydrothermal fluids is reflected in chlorinities substantially different from seawater. Accordingly, chloride concentrations were quantified by titration with 0.1M $AgNO_3$ using fluoresceine-sodium as indicator (after FAJANS). For reference, seawater was measured at 560 mM.

2.4.4.3 First results

In situ-temperatures and chemistry of Black Smoker hydrothermal fluids

A dedicated high-precision thermistor-based temperature sensor integrated within the KIPS fluid sampling system and mounted parallel to the sampling nozzle was used for our temperature measurements of hydrothermal fluids. It has to be kept in mind that fluids emerging e.g., at the top of a 12 m tall chimney may have already cooled or mixed with seawater inside the chimney structure. Moreover, vigorous venting involves turbulent mixing of hydrothermal fluids with seawater leading to a highly chaotic temperature distribution within the orifice. It becomes evident that temperature measurements under these conditions and with a ROV difficult to hold in position within a few millimetre for some tens of seconds are only a rough estimate of the real temperature of the hydrothermal fluid. However, quite constant temperature readings could be obtained for some high-temperature vents including the Two Boats vent at Turtle Pits where we measured a stable temperature of 451 ± 1.6 °C and a maximum temperature of 529 °C. These are the highest temperatures ever obtained for a black smoker fluid on the seafloor. This suggests that the phase-separated hydrothermal system at Turtle Pits and Comfortless Cove (T_{max} = 429 °C (529 °C) might react above the critical curve of the NaCl-H_2O system. In contrast, non-phase-separated fluids emerging at the Mephisto vent in the Red Lion hydrothermal system - in only 1 km distance to Two Boats - have temperatures of 366 °C (Table 2.4.4.2). The following Figs. 2.4.4.3 through 2.4.4.9 illustrate the temperature conditions during our fluid sampling of the high-temperature black smoker chimneys.

Table 2.4.4.2: Measured temperatures of venting hydrothermal fluids

Area	*Site*	*2006 T_{max} (°C)*	*2008 Station*	*2008 T_{max} (°C)*	*2008 T_{avg} (°C)*	*Fluid sample No.*
Hot venting						
Turtle Pits	Two Boats-Top	409	35 ROV	429	416 ± 2.3	No sample
	Two Boats-Bottom		35 ROV	529	451 ± 1.6	35 ROV-7
	Two Boats-Bottom		46 ROV	412	./.	46 ROV-7
	Two Boats-Bottom		57 ROV	371	./.	57 ROV-2/ -5
Comfortless Cove	Sisters Peak	400	42 ROV	379	367 ± 4.9	42 ROV-2 /-7
Red Lion	Mephisto	346	67 ROV	366	364 ± 0.6	67 ROV-3/ -8
Diffuse venting						
Wideawake	Wideawake mussel field	19	37 ROV	16	8	37 ROV-1/ -5 37 ROV-10/ -13
Comfortless Cove	Golden Valley/ Clueless Site	4	52 ROV	9	9	52 ROV-1 /-9

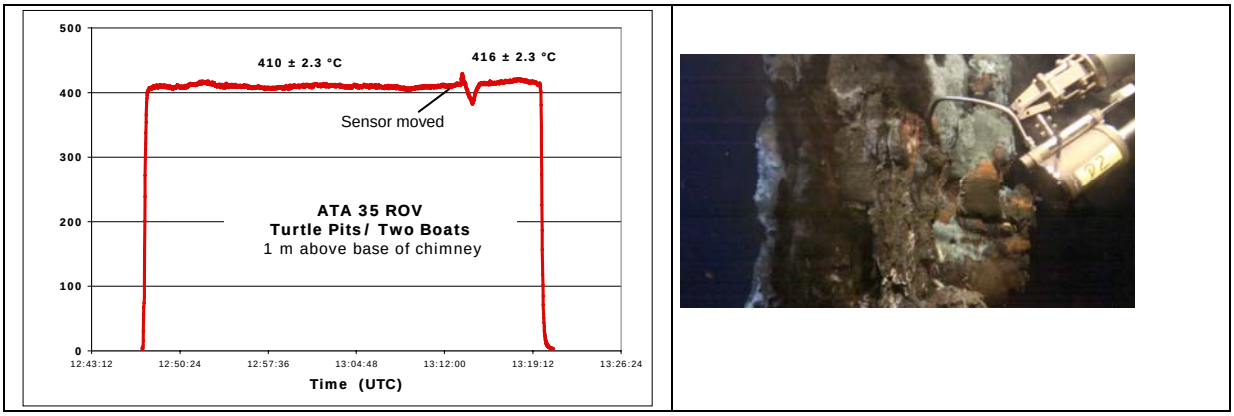

Fig. 2.4.4.3: Station ATA 35 ROV, Turtle Pits. Temperature readings and fluid sampling was at a small outlet approx. 1m above the base of Two Boats. Average over 20 minutes: ***410 ± 2.3 °C.*** *After the sensor had been repositioned temperature readings were* ***416 ± 2.3 °C*** *over 5 minutes. The maximum temperature recorded was* $\boldsymbol{T_{max}}$ ***= 429 °C****. KIPS fluid sampling failed. Ti Major D2 filled, 35 ROV-7.*

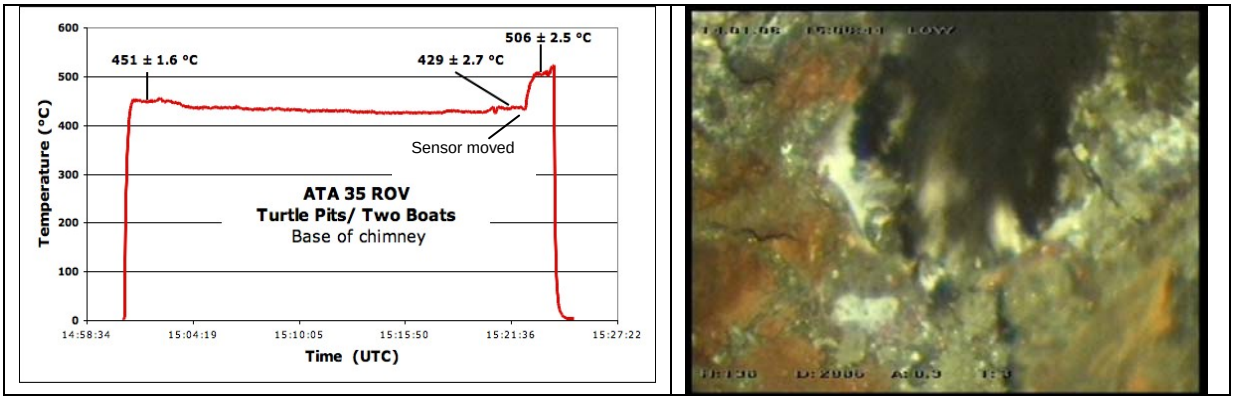

Fig. 2.4.4.4: Station ATA 35 ROV, Turtle Pits. Temperature readings were from a newly opened orifice at the base of the Two Boats black smoker. Initially, temperature was at ***451 ± 1.6 °C*** *but faded to 428 °C. Repositioning of the nozzle resulted in temperatures of* ***429 ± 2.7 °C*** *. After fluid sampling was finished an attempt was made to relocate the hottest spot by careful scanning the orifice opening. Temperature readings increased to* ***506 ± 2.5 °C****, and topped at* ***529 °C****. After opening the orifice vigorous venting with schlieren of clear hydrothermal fluid leaving the orifice could be observed. Fluid sampling failed ☹.*

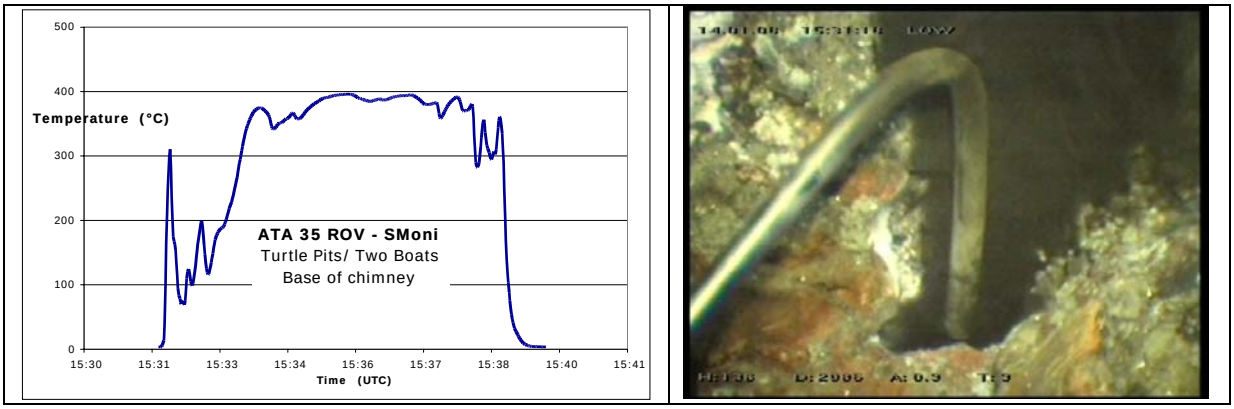

*Fig. 2.4.4.5: Station ATA 35 ROV, Turtle Pits. Temperature readings were taken in the same orifice at the base of the Two Boats black smoker, but with the SMoni offline sensor+logger combination. SMoni uses different thermistor technology than that used in the KIPS sensors. Maximum temperature obtained was **396 °C**. However, the offline design of the probe makes a systematic search for the tiny spot with the hottest temperature in the orifice impossible. (Note: The SMoni logger was unfortunately flooded during the next use at station ATA 42 ROV.)*

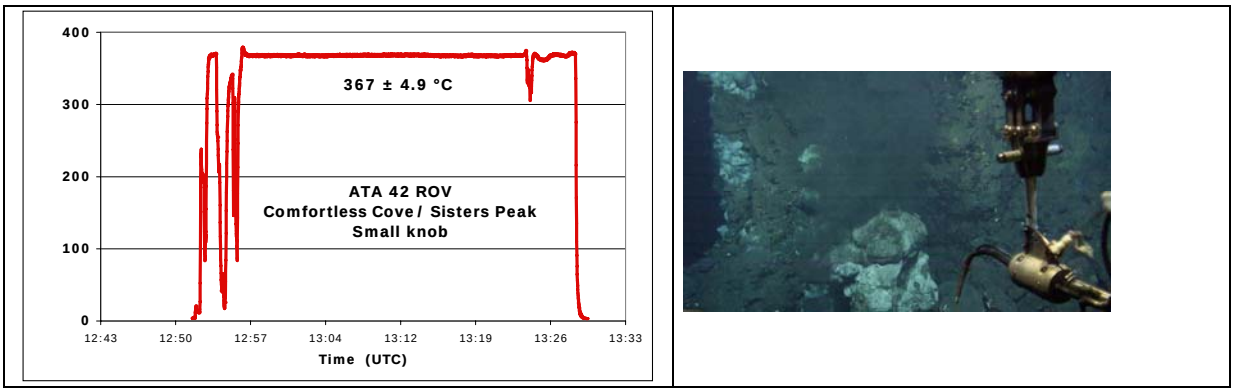

*Fig. 2.4.4.6: Station ATA 42 ROV, Comfortless Cove. Temperature readings and fluid sampling were at a small knob in the top region of the Sisters Peak chimney. Average over 20 minutes: **367 ± 4.9 °C, T_{max} = 379 °C**, KIPS fluid samples 42 ROV-2 to -5 taken and Ti-Major D1 42-ROV-7 filled. KIPS fluid samples 42 ROV-11 to -14 were taken without temperature reading because the cable had been cut during handling.*

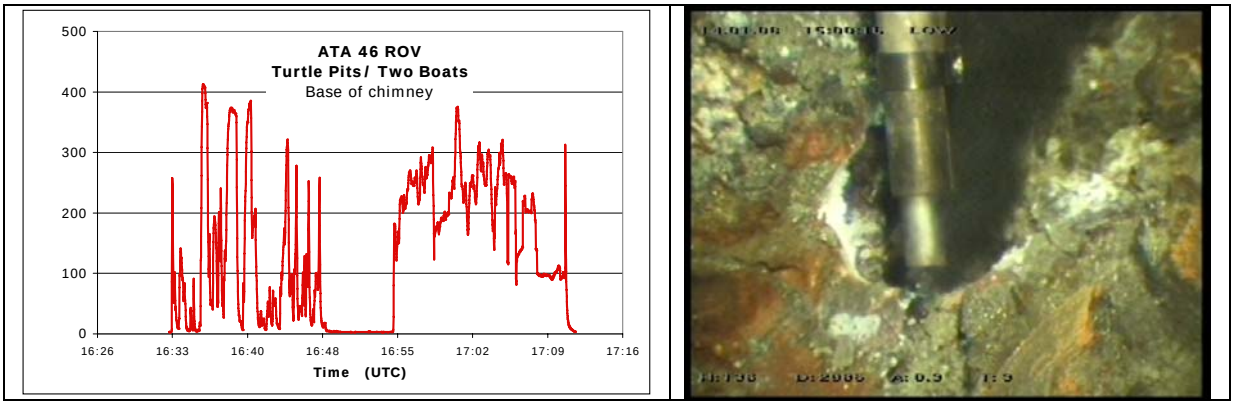

Fig. 2.4.4.7: Station ATA 46 ROV, Turtle Pits. KIPS fluid samples 46 ROV-7 and -8 were taken from the same orifice at the base of the black smoker as three days before (35 ROV). Meanwhile, a 20 cm tall chimney was re-grown over this period. After collapse of the new small chimney the venting from the orifice was found to be significantly less vigorous than during the previous visit. The feeding outlets must have plumbed by fresh precipitates. There was no accurate temperature control during fluid sampling because the T sensor had been displaced from the tip of the sampling nozzle. A maximum temperature of ***412 °C*** *was recorded.*

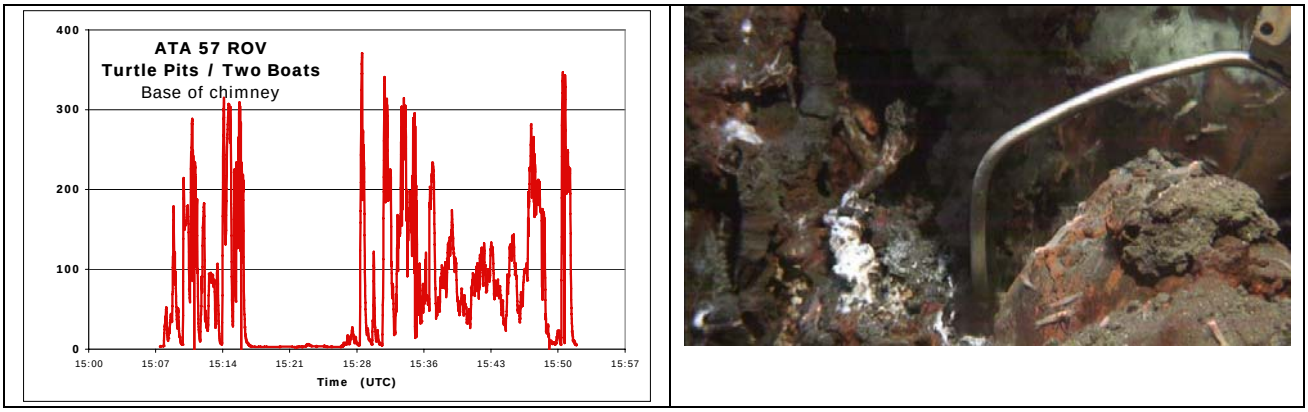

Fig. 2.4.4.8: Station ATA 57 ROV, Turtle Pits. KIPS fluid samples 57 ROV-2 to -5 collected again at base of chimney Two Boats. The orifice was now even more plumbed, and fluid flow was significantly reduced. Every attempt to reopen the orifice failed. The maximum temperature reading was 371 °C.

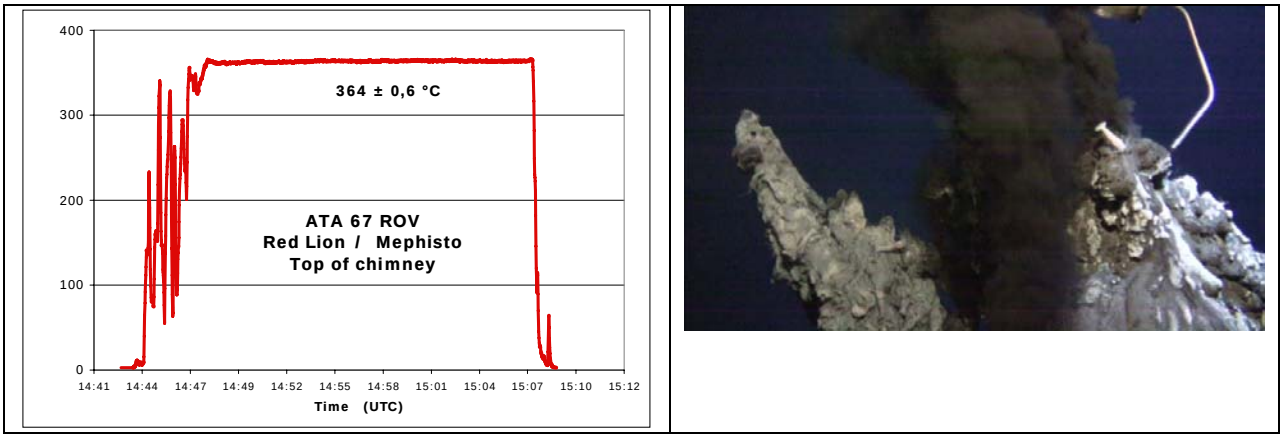

Fig. 2.4.4.9: Station ATA 67 ROV, Red Lion. A newly opened orifice in the summit region of the Mephisto chimney was sampled with Ti Major D2, 67 ROV-3, and KIPS fluid samples 67 ROV-4 to -8. Clear fluid was leaving the outlet of KIPS. Temperatures were 364 ± 0.6 °C with a maximum of 366 °C.

Chemical composition

On-board measurements comprised pH, Eh, concentrations of oxygen, sulfide, chloride and Fe speciation. For selected samples, the concentrations of dissolved H_2, CH_4, CO_2 and CO were also quantified (see chapter on Gas Chemistry). Analyses were performed in order to ascertain the quality of sampled hydrothermal fluids (i.e., the degree of admixed seawater) and to provide an initial characterization of fluid composition and characteristics, particularly with respect to phase separation. Results are presented in Figures 2.4.4.10 to 2.4.4.13 and Tables A1 and A2 (Appendix).

Turtle Pits (Two Boats)

Sampling the Two Boats chimney with the Kiel ROV 6000 turned out to be extremely difficult. Orifices with vigorous venting at the top of the smoker were inaccessible for the ROV. In addition, fluid sampling failed during the first attempt in 35 ROV. However, hydrothermal fluids were collected 1 m above, and at the base of the Two Boats chimney. However, the temperature probe was displaced from the sampling nozzle such that sampling was not guided by the temperature maximum in the orifice and more diluted fluids were sampled. Consequently, the pH range is wide between 2.8 and 6.6 in these samples. The sample with the lowest pH (57 ROV-4) displays the highest Fe concentration of 3.9 mM, and maximum sulfide concentrations of 4.8 mM were measured. Chlorinity in these Turtle Pits fluid samples is significantly reduced compared to seawater, ranging between 300 mM and 550 mM. This can only be caused by phase separation of the fluid in the subseafloor, at P/T conditions above the critical point of seawater (<3000 m, >405 °C) and the emanation of the low-salinity vapor phase.

This year's results are in good agreement with the chemical signature of fluids sampled at the same chimney in 2005 and 2006 (endmember chloride concentration: 270 mM; endmember Fe concentration: 4 mM, endmember H_2S concentration: 4.2 mM). It may be suggested from these results that the Two Boats chimney is constantly emanating a vapor phase since 2005, and, probably, the general chemical composition will be found to be as constant. Quantification of the relative percentage of hydrothermal fluid in the collected samples will be performed in the home laboratory, allowing the calculation of endmember compositions.

Comfortless Cove (Sisters Peak)

Fluids at the chimney structure Sisters Peak have been collected at 3 different orifices: one at the base of the chimney (42 ROV-2 to 42 ROV-7) and two others at the top (42 ROV-11 to 42 ROV-14). Due to difficulties in accessing the small orifices at the top, those samples contain a high amount of admixed seawater, expressed in pH values >5.6. The pH values for samples from the bottom orifice range between 3.4 and 6.8, corresponding to total Fe concentrations between 3.7 mM and 0.07 mM. The best quality sample contains 9.7 mM H_2S and 310 mM Cl; phase separation with the emanation of a low-Cl vapor phase is evident. As Two Boats, the Sisters Peak chimney has been sampled before, in 2006. Recent results for the concentrations of Fe, H_2S, and Cl are in reasonable agreement with data obtained in 2006 (endmember Fe concentration: 3.8 mM; endmember H_2S concentration: 8 mM; endmember Cl concentration: 220 mM). Again, this confirms stability in fluid composition as already observed in Turtle Pits. The chlorinity seems to be somewhat higher when compared to 2006, which could result from slight changes in P/T conditions of phase separation. However, measured data are not yet endmember-corrected.

Red Lion (Mephisto)

In the Red Lion field, six fluid samples were collected from a collapsed beehive on top of the Mephisto structure. Temperature measurements during KIPS sampling (15 minutes) recorded stable 363 °C. Fluid pH ranges between 2.8 and 5.1. A chloride concentration of 540 mM (median of 5 samples) indicates that phase separation is not a process currently taking place. Total Fe concentrations vary between 0.25 and 0.93 mM. H_2S concentrations display a maximum value of 7.6 mM. Again, concentrations of Fe, Cl, and H_2S measured during this cruise are comparable to samples from 2005 and 2006, attesting to an overall stability in fluid composition.

Compositional differences between hot hydrothermal fluids emanating at Red Lion and those emanating at Turtle Pits and Comfortless Cove are a clear function of temperature and phase separation.

Wideawake

At Wideawake, diffuse fluids emanate in an area of intense mussel inhabitation. Fluids were collected at two different locations (37 ROV-1 to 37 ROV-5; 37 ROV-10 to 37 ROV-13). Measured temperatures (KIPS) were 4 and 16 °C. The pH ranges between 7.05 and 7.5. Fe concentrations are as high as 25 µM. Concentrations of H_2S range between 1.2 and 76 µM. There is no clear correlation between H_2S and Fe concentrations. The measured chlorinity is seawater-like, with a median value of 550 mM.

Comfortless Cove (Golden Valley)

Diffuse fluids sampled at a mussel field (locality "Clueless") in the Golden Valley area seep at constant temperatures between 8 and 9°C. The pH ranges between 6.8 and 7.6. Fluids contain up to 43 µM Fe and up to 56 µM H_2S. Similar to diffuse fluids from the Wideawake mussel field, the H_2S concentrations do not correlate with respective Fe concentrations, but with pH.

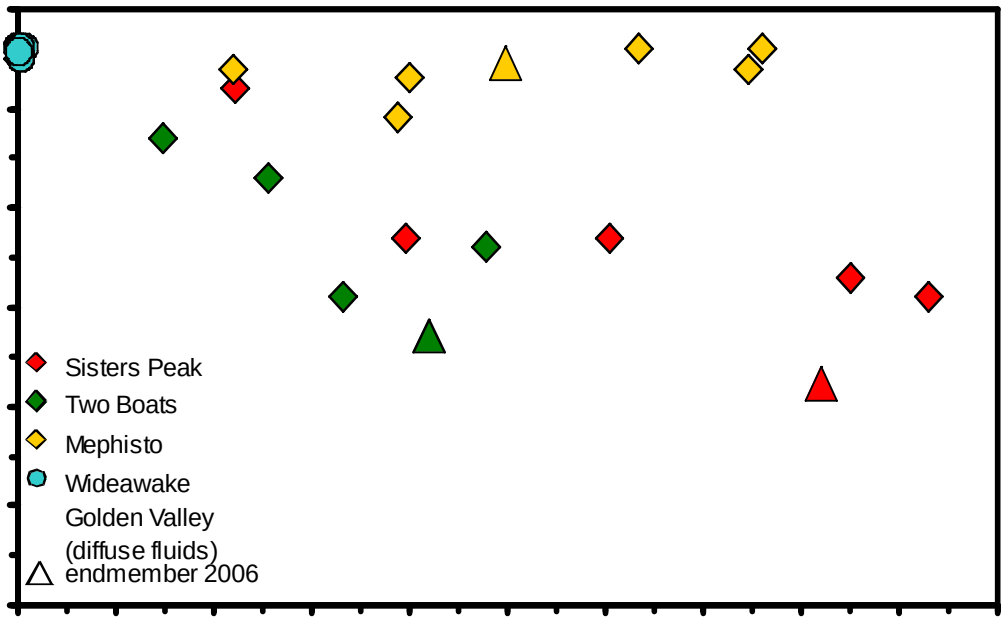

Fig. 2.4.4.10: Crossplot of H_2S and Cl concentrations for hot and diffuse hydrothermal fluids.

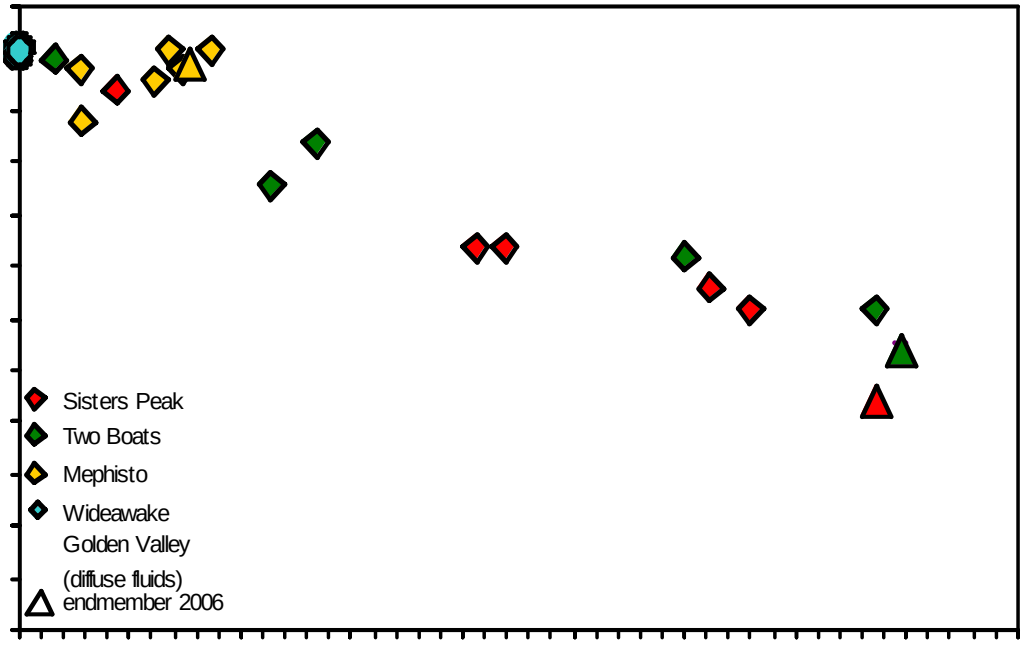

Fig. 2.4.4.11: Crossplot of Fe(II) and Cl concentrations for hot and diffuse hydrothermal fluids.

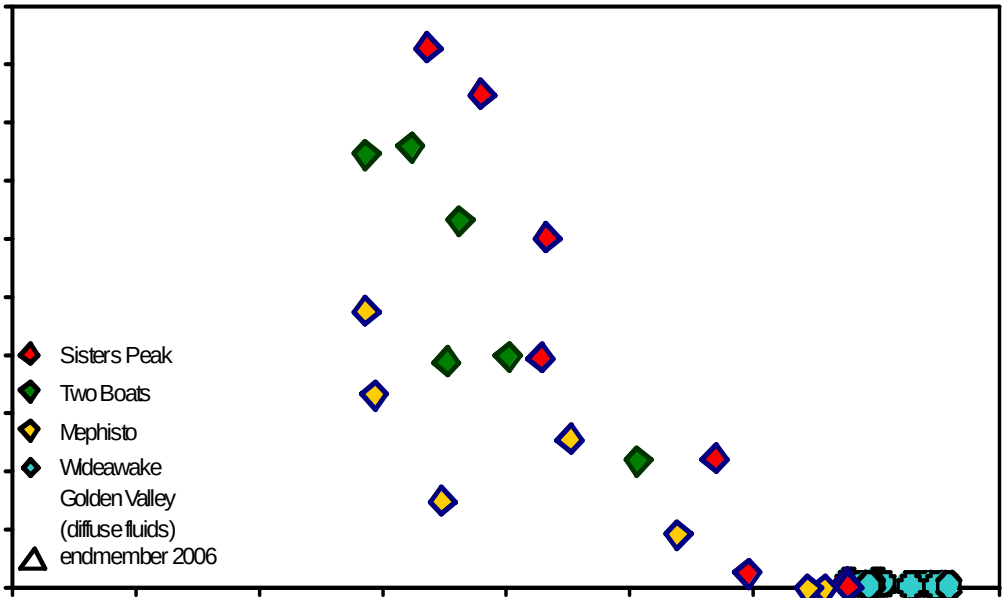

Fig. 2.4.4.12: Crossplot of pH and H_2S concentrations for hot and diffuse hydrothermal fluids.

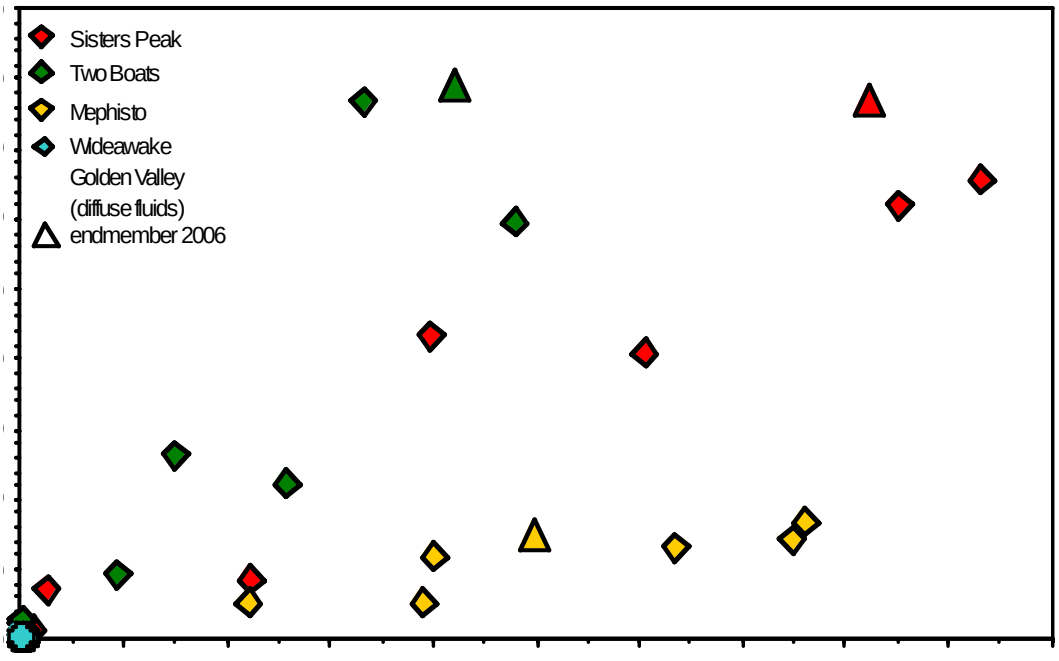

Fig. 2.4.4.13: Crossplot of H_2S and Fe(II) concentrations for hot and diffuse hydrothermal fluids.

2.4.4.4 The chemical composition of hydrothermal fluids – Perspectives

The chemical and isotopic composition of hydrothermal fluids is largely governed by the interaction of rocks and heated seawater percolating through the oceanic crust. Additional effects derive from phase separation of the hydrothermal fluid into a low-chlorinity, gas-rich vapour phase and a high-chlorinity brine phase. This process is accompanied by a strong partitioning of certain elements into either one phase. The latter aspect, i.e. phase separation, is most relevant for the two hydrothermal vent fields at Turtle Pits (Two Boats) and Comfortless Cove (Sisters Peak), as evident from respective chlorinity data measured on-board. In contrast, the Red Lion hydrothermal system shows no indication of phase separation serving as a reference site hosted in the same geological setting. This provides the unique opportunity to study partitioning effects induced by phase separation.

Resulting from these general characteristics, subsequent measurements in the home laboratories will aim to discriminate compositional effects derived from water-rock interaction from those caused by phase separation. The analytical approach comprises a wide array of analytical techniques for measuring the concentrations of major, minor and trace elements and the isotopic compositions for selected elements (Ca, Sr, Cl, Hf, S, C, H, O) in the hydrothermal fluid. **The ultimate goal is a quantitative characterization of fluid composition that will represent the base for balancing the mass flux from mantle to ocean.**

2.4.5 Gas Chemistry

(Ralf Lendt, Marco Warmuth, Frederic von Guilleaume, and Richard Seifert)

CH_4, H_2, CO, and CO_2 were measured on board by gas chromatography. Focus was given to hot fluids to obtain information on the sub-surface hydrothermal processes and on diffuse vents emphasizing on the energy and food supply of vent organisms. In addition, the stable carbon and hydrogen isotope ratio of methane from the fluid samples will be measured in the isotope laboratory at the IfBM.

The water samples for these analyses were collected from 11 CTD stations and 6 ROV dives. For ROV dives, samples were obtained by three different advices namely the KIPS, titanium in situ gas samplers (MAJORS) and an isobaric sampler.

In addition, hydrogen was monitored within incubation experiments conducted by M. Perner on the metabolism of microorganisms present in hydrothermal fluids (Section 2.4.2).

Methods

In order to analyze dissolved CH_4, H_2, CO and CO_2, the fluid samples were degassed using a vacuum degassing technique modified from the method described by Rehder et al. (1999). In brief, water sample is drawn directly into a pre-evacuated flask which is then filled to only about half of the total flask volume. During this sampling, most of the dissolved gas exsolves into the remaining headspace. The amount of water taken was measured with a flow meter (Engolit Flow Control 100S/Typ DMK). The extracted gas phase is subsequently recompressed to atmospheric pressure and transferred to a gas burette. The mole fraction of the analysts are determined by gas chromatography on aliquots of this gas.

For the determination of dissolved CH_4 a CARLO ERBA (GC 4000) gas chromatograph equipped with a flame ionization detector was used in connection with an integration software. Helium was used as carrier gas, and separation was performed using a 4m Al_2O_3 column run isothermally at 130 °C.

CO, CO_2, and CH_4 concentrations of extracted gas were determined using a gas chromatograph (CARLO ERBA, 8000 top). 0.1 to 1 ml of gas was injected on and separated by a 10m long packed column, passed a thermal conductivity detector to a methanizer transforming all oxidized carbon species into CH_4 which then is quantified by a flame ionization detector. Data are recorded for both detectors by a PC based commercial integration software. Carrier gas was helium, oven temperature was 3 min isotherm 60°C, 40°/min to 120° kept for 10 min.

A TRACE Ultra gas chromatograph (Thermo Electron) equipped with HaySep Q, and Molecular Sieve 5 A columns was used to determine the H_2 and CH_4 concentrations of the extracted gas. The run was performed isothermally at 40 °C, helium was used as carrier gas. The eluted gas was detected via a PDD (pulsed discharge detector, VICI).

After transferring the remainder of the gas into a 20 ml glass vial, the septum is sealed with silicone on the outside and with degassed saturated salt solution on the inside. ROV samples are listed in Table 2.4.5.1; CTD samples are listed in Table 2.4.5.2.

Table 2.4.5.1: ROV samples studied for gas content of fluids

Station	KIPS	Ti-MAJOR	IB
ATA 35 ROV	1	2	
ATA 37 ROV	2		
ATA 42 ROV	1		1
ATA 46 ROV			1
ATA 52 ROV	3		
ATA 67 ROV		1	

Table 2.4.5.2: Samples obtained by CTD-Rosette studied for gas content

Station	samples	H_2	CH_4	CO
ATA 31 CTD	6	6	6	
ATA 32 CTD	6	6	6	5
ATA 33 CTD	5	4	5	5
ATA 38 CTD	8	8	8	
ATA 39 CTD	8	8	8	
ATA 40 CTD	7		7	
ATA 44 CTD	6		6	6
ATA 45 CTD	8		8	8
ATA 47 CTD	7		7	
ATA 48 CTD	9	5	9	
ATA 49 CTD	4		4	
ATA 64 CTD	6		6	6

Preliminary results

CTD/Rosette samples were mainly obtained from the Turtle Pits area. Highest concentrations H_2 were found at 2740m depth with 4.4 nM, while CH_4 where up to 1.72 nM. CO was found in concentrations of about 20 nM showing no positive correlation with CH_4 or H_2. An overview on the content of CH_4 and H_2 in water samples studied is given in Fig. 2.4.5.1

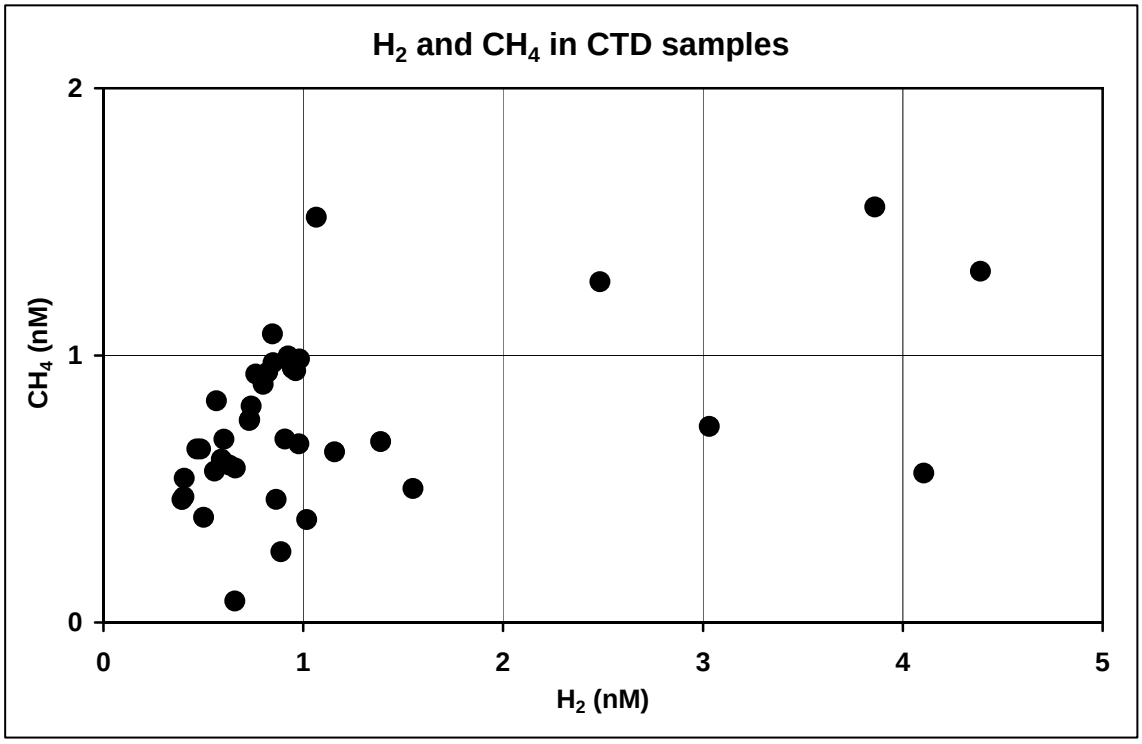

Fig. 2.4.5.1: Concentrations of CH_4 and H_2 in water samples obtained by CTD/Rosette.

A main objective of the cruise was to take samples of black smoker fluids by avoiding degassing of the sample prior to on board analysis. For this purpose, a newly built isobaric sampler (IB) was used for the first time. Figure 2.4.5.2 shows the IB brought into position by the Rick Master of the ROV Kiel 6000 during dive ATA 42 ROV at the black smoker Sisters Peak located in the area Comfortless cove (see Table 2.4.5.3). Comparison between the data obtained from the fluid taken by IB and those obtained from a sample taken by KIPS at the same location illustrates sampling of hot hydrothermal fluids by KIPS to be not suitable for studies of gas chemistry. Though from its design, the KIPS allows much better gaining samples of pure fluid when compared to the IB. Samples of high quality could also be retrieved using titanium samplers (MAJOR). Especially for the smoker Two Boats of the Turtle Pits hydrothermal field (figure 2.4.5.3), samples obtained this way showed the expected high gas concentrations (Table 2.4.5.3) exceeding those determined on KIPS samples during earlier cruises by far. The concentration of H_2 was close to 0.5 mM, exceptionally high for a fluid of

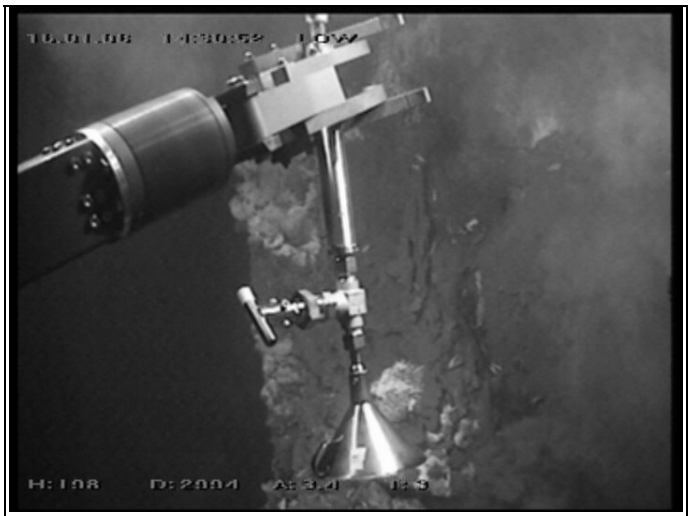

Fig. 2.4.5.2: Sampling of Sisters Peak with the IB-sampler

a system hosted by basaltic rocks, with a H_2/CH_4 ratio of 25.5. In view on the high temperatures of well above 400°C measured for the fluids during dive ATA 42 ROV, and the visual observations, we assume to have investigated an hypercritical fluid. New data on the gas content were also obtained for the fluid of the smoker Mephisto with 270 µM of H_2, 14 µM of CH4, and 8 µM of CO.

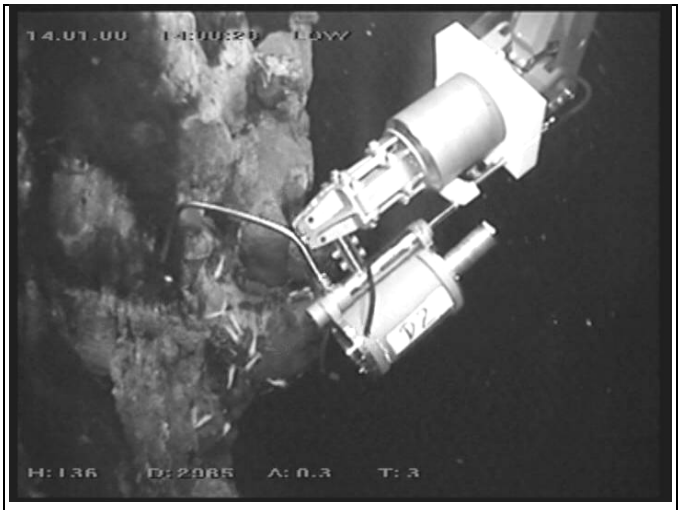

Fig. 2.4.5.3: Sampling of Two Boats with the Ti-Major sampler

Table 2.4.5.3: Gas content of selected hot black smoker fluids

Area / sample	H_2 (µM)	CH_4 (µM)	CO_2 (µM)	CO (µM)
Turtle Pits, Two Boats				
ATA 35 ROV, Major D2	406	16	12956	4
Comfortless Cove, Sisters Peak				
ATA 42 ROV, IB	204	6.8	6745	1.5
ATA 42 ROV, KIPS C9	8.5	0.3	221	0.05
Red Lion, Mephisto				
ATA 67 ROV, Major DS	270	14	n.d.	8

Investigations of fluids from diffuse vents were accomplished for samples of the Wideawake field at Turtle Pits and the Golden Valley at Comfortless Cove (Table 2.4.5.4). These data are of high relevance for the biological studies of vent faunas.

Table 2.4.5.4: Gas content of selected diffuse fluids

Area / sample	H_2 (nM)	CH_4 (nM)	CO_2 (µM)	CO (nM)
Turtle Pits, Wideawake				
ATA 37 ROV, KIPS C7	197	15	65	113
ATA 37 ROV, KIPS A1	194	22		105
Comfortless Cove, Golden Valley				
ATA 42 ROV, KIPS A1	355	36	138	992

2.4.6 Hydrothermal Symbioses

(Jillian Struck and Nicole Dubilier)

1) Genomic analyses: Our main goal for this cruise was to collect and prepare *Bathymodiolus* mussels for genomic analyses of their symbionts. Knowledge of the genomes of chemosynthetic symbionts provides us with an invaluable catalogue of their potential metabolic pathways and can show us how the symbionts gain energy from hydrothermal fluids and pass these on to their hosts. These genomic analyses can then provide the basis for examining which pathways are actually used by the symbionts under different environmental conditions through transcriptomic and proteomic analyses.

As yet, no one has been able to cultivate the symbionts of animals from hydrothermal vents and cold seeps, making direct sequencing of their genomes from cultured cells impossible. Metagenomics, the sequencing of genomes of organisms from the environment, provides an ideal tool for gaining metabolic and genomic information about uncultivable bacteria. In 2007, we were successful in obtaining a grant from the French sequencing facility Genoscope to sequence the metagenome of the bacteria in *Bathymodiolus* gill tissues. These include the methane- and sulfur-oxidizing symbionts as well as a novel bacterial parasite that lives in the nuclei of bathymodiolin mussels. Since the host genome is so much larger than the bacterial genomes (estimated sizes of 200-300 megabases (MB) for the host and 3 - 5 MB each for the bacteria), we can not simply provide Genoscope with *Bathymodiolus* gill tissues. Our sequencing allotment of 300 MB would be "wasted" on sequencing of the host instead of the bacterial genes. It is therefore essential to physically separate the bacteria from the gill tissues, and such separations or enrichments of the bacterial fraction are best done on fresh material.

To separate the *Bathymodiolus* bacteria from host gill tissues we used density gradient centrifugation. In this method, a density gradient is created by carefully layering decreasing concentrations of a sugar compound called Histodenz (here 70 – 5%) on each other. Centrifugation of particles with different sizes and weights causes them to migrate to different density gradient layers. When a mixture of host tissue and bacteria is centrifuged in such a gradient, layers enriched in bacterial cells can thus be separated from host tissues.

To prepare tissues for density gradient centrifugation, we dissected the gills out of 6 freshly collected mussels from Wideawake and Clueless (see Sampling List). Care was taken to use only a single mussel individual for each gradient, to ensure that bacterial strain variability between host individuals does not complicate the genomic analyses. One of the two gills of each mussel was fixed for morphological and molecular analyses of the bacteria in the home laboratory (transmission electron microscopy, fluorescence in situ hybridization, PCR analyses of phylogenetic and functional genes) while the other gill was prepared for genomic analyses by homogenization on ice in 1X phosphate buffered saline (PBS). For some gradients, the homogenate was filtered through 12 and 5 µm filters before centrifugation, in others unfiltered homogenate was placed directly on the gradients. Gradients were centrifuged in the cold room (ca. 10°C) for 1.5 – 2 h at 5000 RPM. In all gradients a similar layering pattern was observed: 1) at the top of the gradient (5 – 10% Histodenz) lay a thin white fraction, followed by a light brown fraction with 2 sublayers, the top one light brown (~20% Histodenz), the bottom one milky brown (~30% Histodenz). The next fraction (~40% Histodenz) was thick and dark brown, followed by a light brown fraction with a crystalline appearance (~50% Histodenz). The bottom layers (~60 - 70% Histodenz) were all clear.

Fractions were removed from the gradient in 500 µl steps and a subsample from each fraction was fixed for fluorescence in situ analyses (FISH) with probes specific to the bacteria in *Bathymodiolus puteoserpentis* from Logatchev. Analysis of the gradients with specific probes on board was difficult because the probes for the sulfur- and methane-oxidizing symbionts did not show a signal, presumably because these probes had too many mismatches to the symbionts from the Wideawake mussels. Using a probe for the intranuclear parasite, we only saw these bacteria in a single fraction (thick, dark-brown layer) from a single individual (46ROV1-1) in very low abundance. This layer was characterized by high abundances of bacteria presumed to be the sulfur- and methane-oxidizing symbionts based on DAPI-staining and their hybridization signal using the general bacterial probe EUB338. Contaminating host tissue concentrations were very low in this fraction. DAPI and EUB338 analyses of the top white layer of the gradients indicated that these were highly enriched in sulfur-oxidizing symbionts. Further analyses of these gradients in the home laboratory with probes specific to the Wideawake symbionts will allow us to decide which gradients we will use for our metagenomic analyses.

2) In situ fixation chamber DieFast: One of our main goals within the SPP 1144 is to understand the interactions between hydrothermalism and biology. To date, all animals from hydrothermal vents and other deep-sea environments are brought up to the surface and dissected and fixed on board. Most of the sites we are studying within the SPP 1144 are at 3000 m water depth. It thus can take up to 3 hours after the animals have left their environment before we can prepare them, often even longer if animal collection is not the last station for the ROV work of that day. This is a problem for analyzing the metabolic pathways the animals use in their environment. Changes in the transcription of genes to messenger RNA (mRNA) can occur within minutes, changes at the protein level within hours. We therefore designed an in situ fixation chamber, called DieFast, for fixing mussels or other biological samples directly on the seafloor within minutes of their collection (Fig. 2.4.6.1). DieFast consists of a fixation chamber with a rubber sealed lid (volume: 3 liters) that is connected through tubing to 3 syringes (each 100 ml). The chamber weighs 17 kg in air and easily fits on the ROV porch. Before deployment, the chamber and the tubing are filled with seawater. The syringes are filled with 40% formalin with stoppers placed in the syringes to prevent the formalin from running through the tubing into the fixation chambers. During deployment, the organisms are placed in the chamber, and the lid is closed and the stoppers released mechanically by the ROV arm. The 300 ml of 40% formalin are diluted to 4% in the fixation chamber, which is an ideal concentration for fixing biological samples for morphological analyses of their mRNA (mRNA FISH) and proteins (immunohistochemistry).

Our first (and only) deployment of DieFast at the Wideawake site (ATA 37 ROV 9) was highly successful. Mussels were collected singly or in clumps of 3-5 individuals and placed in the chamber using the ROV Orion arm. Closing of the chamber lid and release of the stoppers using the appropriate monkey fists was easily and quickly performed by the ROV pilots with the Orion arm. The entire time for deployment including the collection of mussels was less than 30 minutes. After recovery of the ROV, we examined the mussels: they were almost all intact and had clearly all been fixed by the formalin. Analyses of these specimens in the home laboratory and comparison with mussels fixed on board will reveal the importance of fixing animals in-situ.

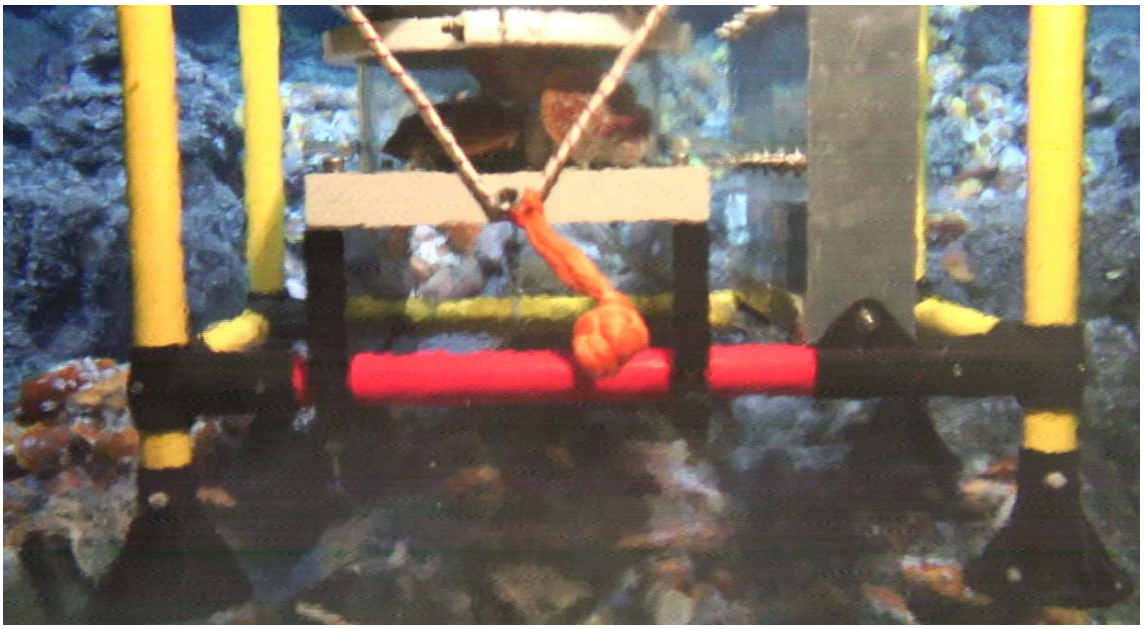

Fig. 2.4.6.1: DieFast during deployment at Wideawake. The mussels have already been placed in the fixation chamber and its lid has been closed using the elastic strap and the orange monkey fist attached to it. The syringes with formalin are on the right of the chamber behind the metal casing.

3) Collection of animals for biogeography

Our final goal for this cruise was to collect as many animals as possible for biogeography analyses (Table 2.4.6.1). One of the goals within the SPP 1144 is to better understand how ridge morphology and ocean currents influence the dispersal of vent organisms along the ridge. To do this, we compare the phylogenetic relationships of animals from different vent sites using genes as indicators of their relatedness. For example, if animals from Logatchev on the northern Mid-Atlantic Ridge were more closely related to animals from other northern MAR vents than to those from the southern MAR vents, this would suggest that geological barriers at the equator including the large offset of the ridge-axis prevented gene flow between southern and northern MAR vents. In addition to collecting mussels, we also collected at least two species of shrimp (*Rimicaris exoculata* and *Mirocaris fortuna*), and possibly a third species (*Opaepele* sp.), first found and described during the 2007 Meteor M68/1 cruise to the southern MAR. We were extremely fortunate to find a clam individual (*Calyptogena* sp.) at Clueless (ATA 52 ROV 11). This is only the second specimen that we have found at 5°S. These clams are extremely rare on the MAR and are only known from Logatchev and 5°S. We have only found dead clam shells at Logatchev but were recently given 5 alcohol-fixed *Calyptogena* sp. individuals from Logatchev by Dr. Andrey Gebruk (Shirshov Institute of Oceanology, Moscow). Phylogenetic analyses of the Logatchev and the 5°S individuals will show how these clams are related to other clams from vents and seeps around the world and may reveal their geographic origin for colonizing the MAR.

Table 1: Animals collected during L'Atalante cruise MSM06/3 to 5°S

Station number	Site	Sample	Sample treatments	Gradient centrifugation
ATA 35 ROV 18	Turtle Pits	Slurp	*R. exoculata* samples for FISH and DNA *Mirocaris fortuna* samples for FISH and DNA possibly 3 *Opaepele* sp. individuals for FISH and DNA	
ATA 37 ROV 7	Wideawake	Mussel net	*Bathymodiolus* sp. samples for FISH, DNA, RNA, electron microscopy whole *B.* sp. frozen for DNA	2 Individuals
ATA 37 ROV 8	Wideawake	Slurp	*R. exoculata* samples for FISH and DNA	
ATA 37 ROV 9	Wideawake	Die Fast	Whole *B* sp. fixed in situ for FISH	
ATA 46 ROV 1	Wideawake	Mussel net	*B* sp. samples for FISH, DNA, and electron microscopy	1 Individual
ATA 46 ROV 4	Wideawake	Slurp	Whole frozen *B.* sp.	
ATA 46 ROV 5	Wideawake	Slurp	Small *B.* sp. frozen whole for DNA	
ATA 52 ROV 11	Clueless (near Golden Valley)	Mussel net	*B.* sp. for FISH, DNA, RNA, electron microscopy *Calyptogena* sp. for FISH, DNA, RNA, electron microscopy Whole *B.* sp. frozen for DNA	2 Individuals
ATA 57 ROV 7	Wideawake	Mussel net	*B.* sp for FISH, DNA, RNA, electron microscopy *B.* sp. for cultivation experiments Whole *B.* sp. frozen for DNA	1 Individual
ATA 67 ROV 1	Red Lion - Mephisto	Slurp	Crab - *Segonzacia*, for DNA	
ATA 67 ROV 2	Red Lion - Mephisto	Slurp	*R. exoculata* samples for FISH and DNA	

2.4.7 Paleaoceanography

(Almuth Harbers)

Goals

During Leg 2 paleoceanographical investigations were focused on collecting planktonic foraminifera and pteropods. Refering to the project **Future Ocean** - "Changing habitats of calcareous plankton in the Green House World" planktonic foraminifera and their response to climate change is going to be studied. For the next hundred years a surface ocean warming of 3°-5°C is expected (Mitchell, 2005). An estimated pH drop of 0.7 units in surface waters is the effect of absorption of 50% of fossil fuel CO_2 emissions (Caldeira and Wickett, 2003).

One goal is to show the impact of acidification and surface ocean warming on planktonic foraminifera with reference to former investigations.

Investigations will include faunal inventory, assemblage composition, size distribution and shell weights, and chemical and isotopic composition regarding to $\delta^{13}C$, $\delta^{18}O$, Mg/Ca and Sr/Ca.

Methods

Samples were taken two times a day. With a, in the ship´s sytem integrated pump, $3m^3$ seawater were filtered over a 63µm sieve. The water was pumped from below the vessel, in a depth of 4-5m. The samples were washed with fresh water and put into a vial with nearly 120ml ethanol. 32 samples were taken between 09.01.2008 and 29.01.2008. The first two samples RD 1 and RD 2 have only a volume of $1m^3$. Because of low inventory volume was then increased to $3m^3$.

Other 18 samples were taken on several days with an Apstein net (100µm). Samples were taken in depth sections of 0-10m, 10-20m, 20-30m, 30-40m and 40-50m. The net with an aperture of 17cm was deployed and lifted five times in each section, so nearly $1m^3$ got filtered in each section. The samples were washed with fresh water and stored with nearly 120ml ethanol in vials. Only three depth sections were done at sampling station TP 2 because the assisting Crew had to work on other stations.

Taking water samples for isotopic analyses took place once a day between 14.01.2008 and 29.01.2008. Seawater was collected with the water pump right before or right after the other samplings (pump and/or Apstein) took place. They got stored in a 100ml vial. Because of missing Mercury Chloride ($HgCl_2$) solution in the first days of cruise, only few samples were intoxicated to stop bacterial activity.

Any analyses will be done onshore at the IFM-GEOMAR, Kiel.

Sampling stations

Pump

Sample	Date	UTM/start	UTM/end	local time	Latitude/start	Longitude/start	Latitude/end	Longitude/end
RD 1	09.01.2008	11:36	12:30	-3	07°03.443S	27°45.880W	07°02.250S	27°37.700 W
RD 2	09.01.2008	16:00	17:13	-3	07°02.144S	27°28.445W	07°02.440S	27°27.723W
RD 3	10.01.2008	9:46	12:02	-2	06°42.355S	25°07.930W	06°39.245S	24°46.878W
RD 4	10.01.2008	15:50	18:06	-2	06°34.055S	24°11.740W	06°31.088S	23°51.278W
RD 5	11.01.2008	9:50	12:22	-2	06°09.079S	21°22.808W	06°05.390S	20°57.900W
RD 6	11.01.2008	15:54	18:39	-2	06°00.368S	20°23.920W	05°56.585S	19°57.322W
RD 7	12.01.2008	9:45	11:40	-1	05°34.876S	17°30.957W	05°32.145S	17°12.581W
RD 8	12.01.2008	14:33	17:28	-1	05°27.412S	16°45.324W	05°22.640S	16°22.940W
RD 9	13.01.2008	9:01	11:39	-1	05°05.019S	14°17.077W	05°01.616S	13°52.626W
RD 10	13.01.2008	14:48	17:32	-1	04°57.474S	13°22.850W	04°53.745S	12°57.190W
RD 11	14.01.2008	9:18	11:40	-1	04°48.379S	12°22.632W	04°48.583S	12°22.427W
RD 12	14.01.2008	14:50	17:27	-1	04°48.594S	12°22.412W	04°48.590S	12°22.416W
RD 13	17.01.2008	10:55	13:45	-1	04°48.857S	12°22.332W	05°00.285S	11°59.704W
RD 14	17.01.2008	15:49	18:43	-1	05°09.764S	11°45.261W	05°06.959S	11°42.113W
RD 15	18.01.2008	9:24	12:28	-1	04°48.442S	12°22.314W	04°48.610S	12°22.346W
RD 16	18.01.2008	15:50	18:51	-1	04°48.588S	12°22.359W	04°48.586S	12°22.364W
RD 17	20.01.2008	10:11	12:57	-1	04°48.121S	12°22.282W	04°48.198S	12°22.268W
RD 18	20.01.2008	15:53	18:13	-1	04°48.193S	12°22.275W	04°48.200S	12°22.267W
RD 19	22.01.2008	11:36	13:44	-1	04°47.395S	12°22.604W	04°47.389S	12°22.599W
RD 20	22.01.2008	17:05	19:45	-1	04°47.391S	12°22.600W	04°47.398S	12°22.600W
RD 21	24.01.2008	9:11	11:36	-1	04°48.626S	12°22.721W	04°48.852S	12°22.297W
RD 22	24.01.2008	16:50	19:46	-1	04°48.044S	12°22.425W	04°48.114S	12°22.347W
RD 23	25.01.2008	9:36	12:02	-1	04°56.021S	11°39.493W	04°56.506S	11°36.996W
RD 24	25.01.2008	14:57	17:37	-1	04°56.501S	11°37.002W	04°56.339S	11°37.002W
RD 25	26.01.2008	10:32	12:32	-1	03°14.099S	12°13.800W	02°53.613S	12°21.219W
RD 26	26.01.2008	15:50	18:43	-1	02°20.826S	12°33.066W	01°52.050S	12°43.476W
RD 27	27.01.2008	9:07	11:10	-1	00°34.227N	13°36.325W	00°55.074N	13°43.866W
RD 28	27.01.2008	15:26	17:17	-1	01°39.038N	13°59.752W	01°58.295N	14°06.715W
RD 29	28.01.2008	10:03	12:12	0	04°53.398N	15°10.118W	05°14.830N	15°17.890W
RD 30	28.01.2008	15:36	17:32	0	05°48.503N	15°30.120W	05°59.988N	15°34.293W
RD 31	29.01.2008	9:25	11:33	0	08°24.125N	16°26.805W	08°44.798N	16°34.351W
RD 32	29.01.2008	15:27	17:30	0	09°20.454N	16°47.439W	09°21.026N	16°48.481W

Apstein

Sample	Date	UTM/start	UTM/end	local time	Latitude	Longitude	Depth
TP 1	15.01.2008	10:31	11:37	-1	04°48.632S	12°22.354W	0-50m
TP 2	19.01.2008	15:04	15:48	-1	05°05.697S	11°39.961W	0-30m
TP 3	21.01.2008	11:00	12:20	-1	04°48.572S	12°22.450W	0-50m
TP 4	24.01.2008	15:04	16:29	-1	04°48.832S	12°22.611W	0-50m

Water samples

Sample	Date	UTM	local time	Latitude	Longitude
RDO1	14.01.2008	17:28	-1	04°48.590S	12°22.416W
RDO2	15.01.2008	16:42	-1	04°48.637S	12°22.349W
RDO3	16.01.2008	18:22	-1	04°48.117S	12°22.270W
RDO4	18.01.2008	15:50	-1	04°48.588S	12°22.359W
RDO5	19.01.2008	11:16	-1	05°05.467S	11°39.238W
RDO6	20.01.2008	13:00	-1	04°48.175S	12°22.271W
RDO7	21.01.2008	18:32	-1	04°48.617S	12°22.411W
RDO8	22.01.2008	17:05	-1	04°47.391S	12°22.600W
RDO9	23.01.2008	13:39	-1	05°05.952S	11°40.582W
RDO10 + $HgCl_2$	24.01.2008	16:49	-1	04°48.044S	12°22.425W
RDO11 + $HgCl_2$	25.01.2008	09:35	-1	04°56.021S	11°39.493W
RDO12 + $HgCl_2$	26.01.2008	10:31	-1	03°14.099S	12°13.800W
RDO13 + $HgCl_2$	27.01.2008	09:01	-1	00°33.126N	13°35.930W
RDO14 + $HgCl_2$	28.01.2008	9:55	0	04°52.091N	15°09.647W
RDO15 + $HgCl_2$	29.01.2008	9:23	0	08°23.714N	16°26.805W

2.4.8 Global distribution and atmospheric transport of volatile and semi-volatile polyfluorinated compounds

(Annekatrin Dreyer[1], Petra Günnewig)
[1] GKSS Research Center, Institute of Environmetal Chemistry, Gesthacht, Germany

Persistent and toxic perfluorinated organic acids have been detected in high concentrations in polar biota. As these perfluorinated acids are not volatile and only partly water soluble, the mode of transport of these compounds to remote regions is not yet satisfactorily explained. Two transport modes are being thought of: directly via the water phase and indirectly by the degradation of precursors via the atmosphere. To further elucidate this problem air samples were collected at the cruise L'Atalante Recife-Dakar and analysed for organic poly- and perfluoarinated compounds. These measurements will improve understanding of the long-range transport of this emerging class of organic contaminants to remote regions and lead to a better predictability.

2.4.9 Volcanic rocks

(B. Melchert, H. Paulick)

The volcanological investigations during ROV deployments focussed on mapping individual lava flow units and taking samples from flow units with stratigraphically defined age relationships. Furthermore, we used the „Vulkanitstossrohr (VSR)" („wax corer") in oder to obtain geochemical samples from the areas immediately to the north and south of the

regional topographic high on which the hydrothermally active region at 4°48'S is located. Sample descriptions are provided in the Appendix.

Regional-scale sampling of basalt lava

The existing basalt sample set, obtained during previous visits to the area in 2005 (M64-1) and 2006 (M68-1), is restricted to an aera of approximately 2 km x 2 km representing lava units from the immediate vecinities of the hydrothermally active sites. These are located on a topographically elevated portion of the ridge axis valley rising to around 2990 m below sea level [mbsl] whereas water depths increase to 3300 m at ~8 to 10 km to the north and the south (Fig. 2.4.9.1). The geochemical and isotopic compositions of this densely sampled area has been investigated as part of research projects at Kiel and Bonn and the data show that the magmas from this area are fairly homogenous in composition (unpublished data from Karsten Haase, Thomas Kokfeld and Holger Paulick). In order to determine whether the apparently increased volcanic activity in this area, generates a locallized ridge with an elevation in the order of 300 m, samples from the surrounding axial valley are required.

We obtained 6 VSR samples from the north and south of the Turtle Pits area returning sufficient volcanic glass for geochemical analyses (Fig. 2.4.9.1). These data will be used to determine whether there are compositional gradients in the lavas which may provide contraints of the sublithospheric controlling parameters on volcanism in the area.

Turtle Pits and Wideawake hydrothermal sites and the 2002 (?) lava flow

The volcanology of the Turtle Pits and Wideawake hydrothermal sites has been investigated during previous cruises and documented in Haase et al. (2007). In addition, deployment of the AUV ABE during the Cruise M68-1 (2006) provided detailed sea floor images of the geological situation at the Wideawake mussle bed site. Here, a young, lobate lava flow with a black, glassy luster has partly covered pre- exsisting mussle beds located on top of an older lava flow with a jumbled flow top morphology. Based on the intense hydrothermal activity at Turtle Pits and the occurrence of this young lavaflow in the immediate vicinity (ca. 200 m to the east, Fig. 2.4.9.2) it has been inferred by Haase et al. (2007) that this eruption may conincide with the record of a major seismic crisis in the area from 25 to 26 June 2002. Hence, this lava flow may represent one of the few occasion in submarine volcanological studies where the age of formation for a particular lava unit is actually known. Therefore, one half of a ROV dive (station ATA-46ROV) was devoted to the task of determining the dimensions and structures of the lava flow and to define its eastern and southern borders. This information shall be used in order to guide future deployments of an AUV (potentially during the next scheduled visit of the area in 2009) for locating the eruptive vent and areal extend of this flow unit.

Dive ATA-46ROV was successful in locating the eastern, strongly serrated contact of the 2002 (?) flow and to the south. Samples from older lava units have been obtained at two locations (ATA-46ROV-2 und -3). In the south, the older sheet lava flow is characterized by the construction of up to 3 m high lava tunnels which are locally collapsed providing evidence that most of these structures are hollow (Fig. 2.4.9.3; collapse structure).

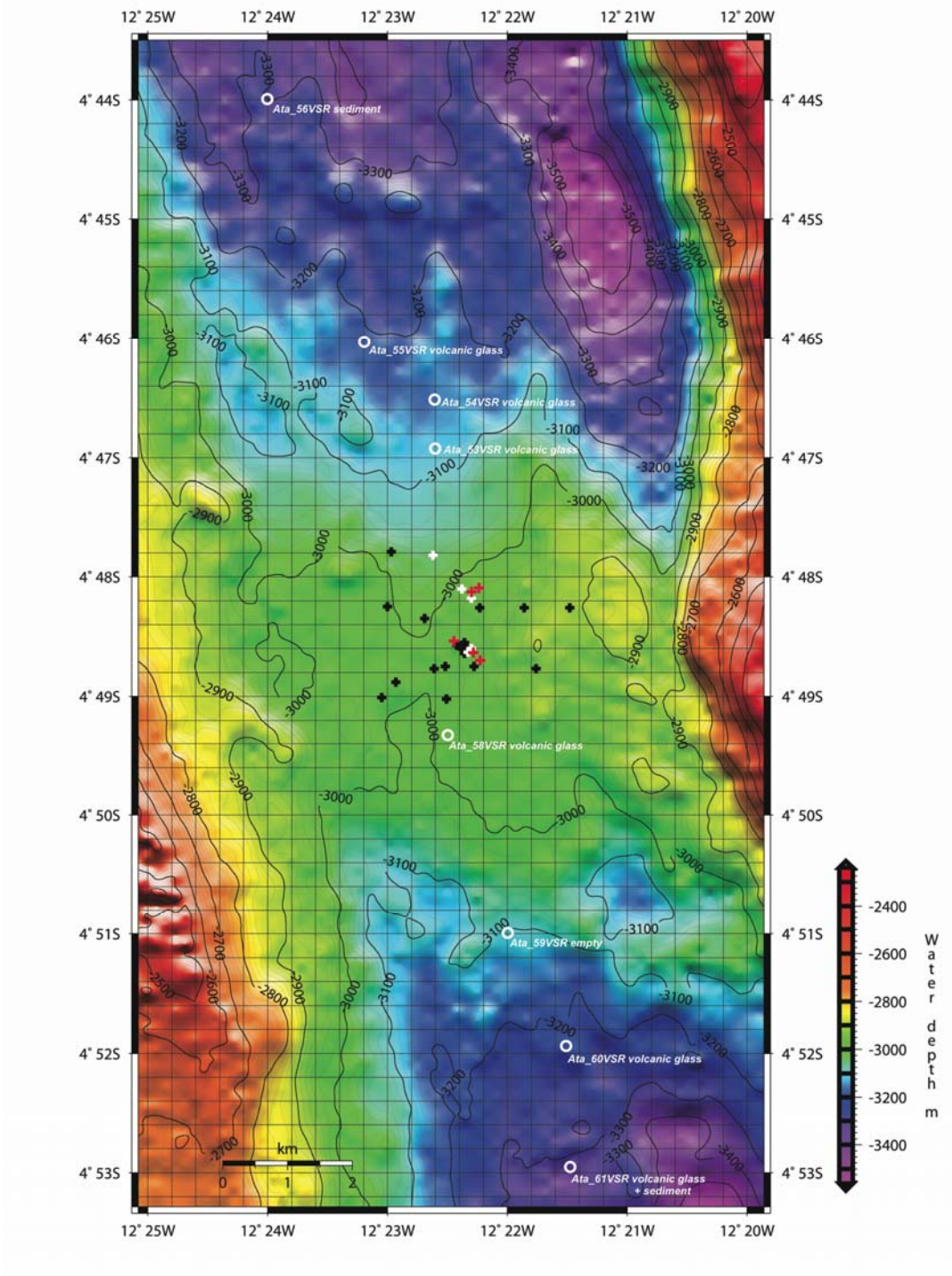

Fig. 2.4.9.1: Lava samples from the Turtle Pits area – samples collected during this cruise shown in white circles with sample numbers marked. Red crosses mark locations of basalt samples collected during ROV dives.

The lava flowing through these systems was apparently well insulated from cooling and discharged at the flow front when magma supply ceased. Such eruption processes are a common phenomenon at subaerial lava fields with high eruption rates of low viscosity-high

temperature basalt lavas such as Hawaii. Clearly, recognition of such processes is important if erupted volumes are to be determined.

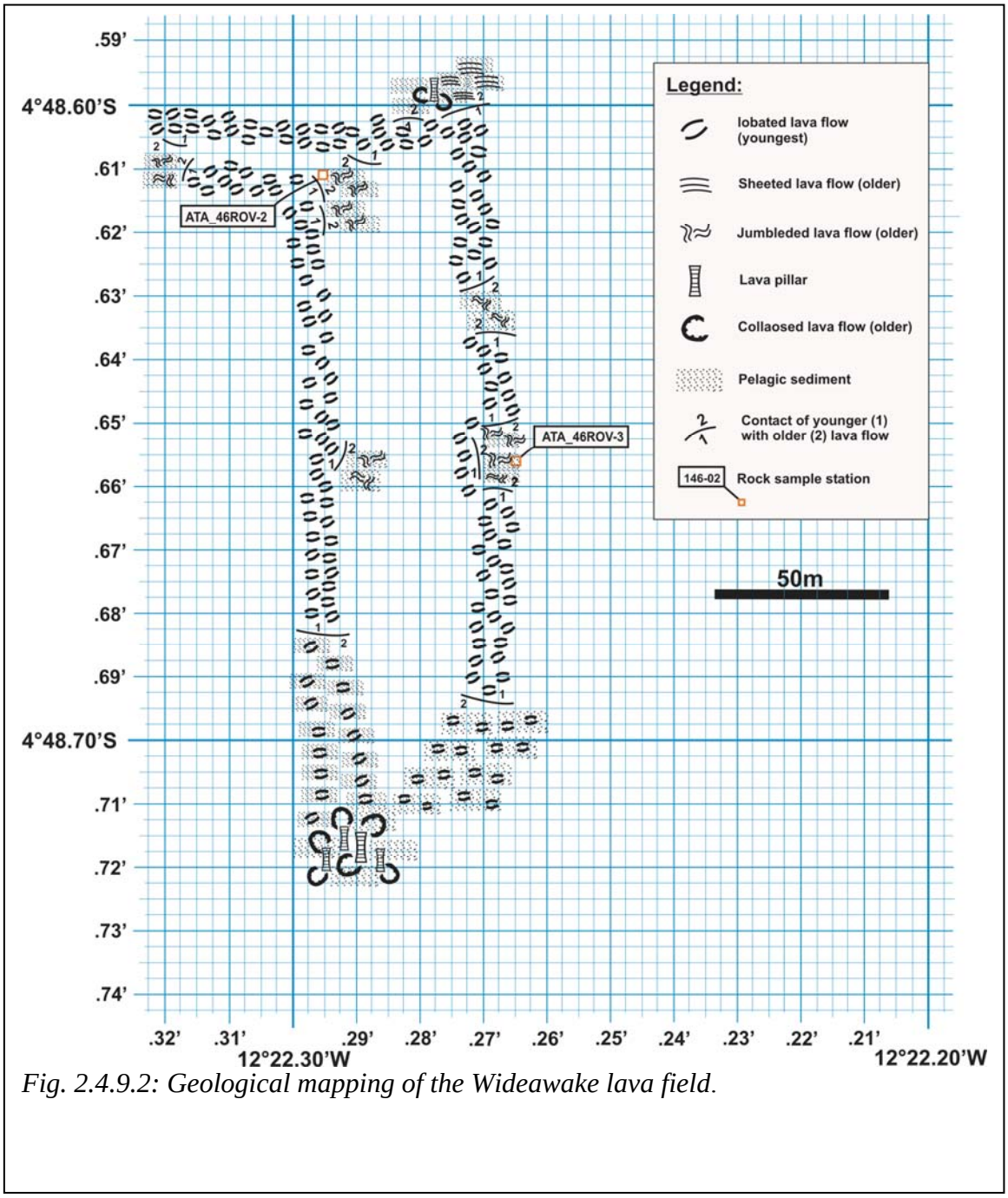

Fig. 2.4.9.2: Geological mapping of the Wideawake lava field.

As an additional complication, we recognized that the young, 2002 (?) flow is locally channelled into the pre-exsisting lava drainage system prodived by the sheet flow lava tubes. Hence, some portion of that eruption may have been emplaced below the seafloor, escaping seafloor mapping efforts.

Fig. 2.4.9.3: Young lava flow (left) in old collapsed "hall"

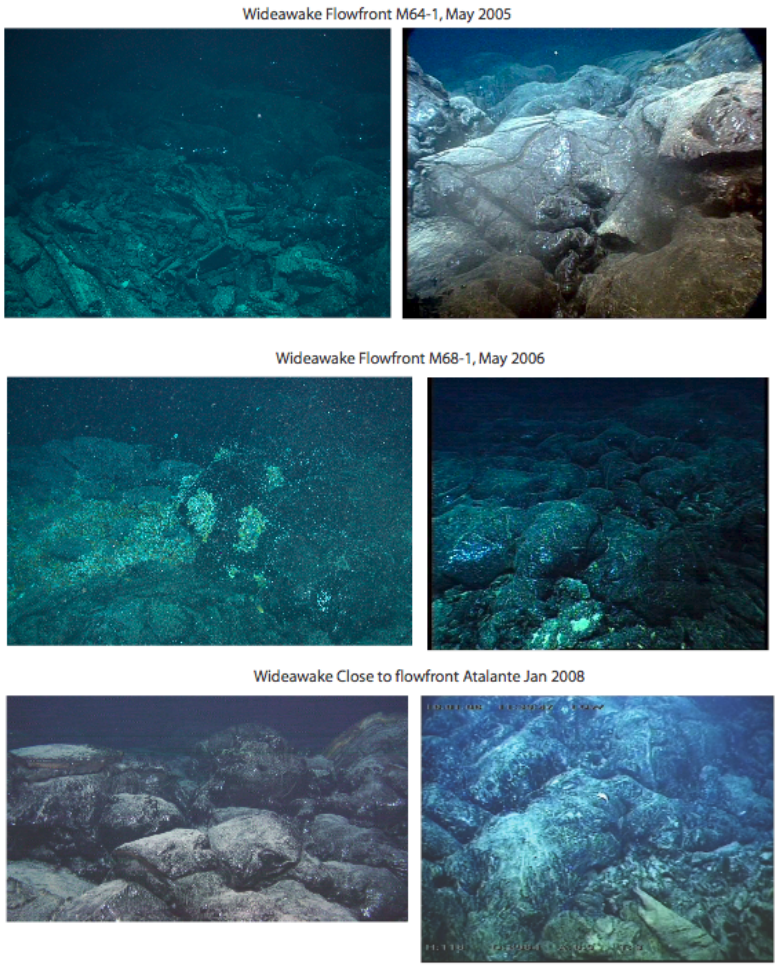

Fig. 2.4.9.4: The ageing of the Wideawake flow

Furthermore, we recognized some signs of „aging" of the 2002 (?) lava flow. Comparing the seafloor images obtained in 2005, 2006 and during this cruise, we observed that the „glassy luster" of the flow surface (described by Haase et al., 2007) is apparently waning (Fig. 2.4.9.4). This could be inferred to be due to progressive incipient alteration of the upper surface of the quenched basalt glass covering the lava lobes. Also, we encountered a site of low T (up to 10 °C) fluid discharge on the 2002 (?) lava flow itself. Fluid discharge (shimmering water) is concentrated in lava lobe intersticies and the site is colonized by abundant small mussles colonizing cracks of the lava surface. These observational similarities to the Lilliput hydrothermal site (located at ~9°30'S), discovered during cruise M64-1, are astonishing. For both sites, recent initiation of hydrothermal discharge and colonization by mussles may be inferred. Potentially, the 2002 (?) lava flow may have covered a pre-exsisitng hydrothermal discharge site and hydrothermal fluid ascent through this flow has now been established.

Comfortless Cove hydrothermal area

The ROV dives to this hydrothermally active area, located approximately 2 km to the NNE of Turtle Pits were mainly focussed on obtaining fluid and biological samples. However, it has been possible to add observational data and basalt samples to the material collected during cruise M68-1. The basalt pillow mound located to the north of the Sisters Peak black smoker chimney was sampled (ATA-42ROV-16). This pillow flow overlies the older sheet flow that the Sisters Peak smoker is situated on (sample of this sheet flow was obtained during the previous cruise: M68-1_20ROV-3B). In addition, a following dive (station 52ROV) provided spectacular insight into an eruptive fissure located on top of the pillow mound (to the east of sampling site ATA-42ROV-16). The walls of this fissure show remarkable lava flow features in cross section such as sheet flow tops and elongated tubes. In this zone, shells of dead mussles were abundant. At the southern margin of the fissure, patches of living mussels were located and sampled. From this area a basalt sample was also obtained (ATA-52ROV-12).

2.4.10 Rocks from the deeper crust

(Günter Suhr, Jürgen Koepcke)

Three ROV dives were devoted to map and sample the deeper oceanic crust around 5°S. Two dives investigated the "Inside Corner High" at 5°06'S and 11°40'W, one dive was spent at the transform wall opposing the nodal deep at 4°56'S and 11°37W (Fig. 2.4.10.1). Each dive required about 1000 m of ROV climbing.

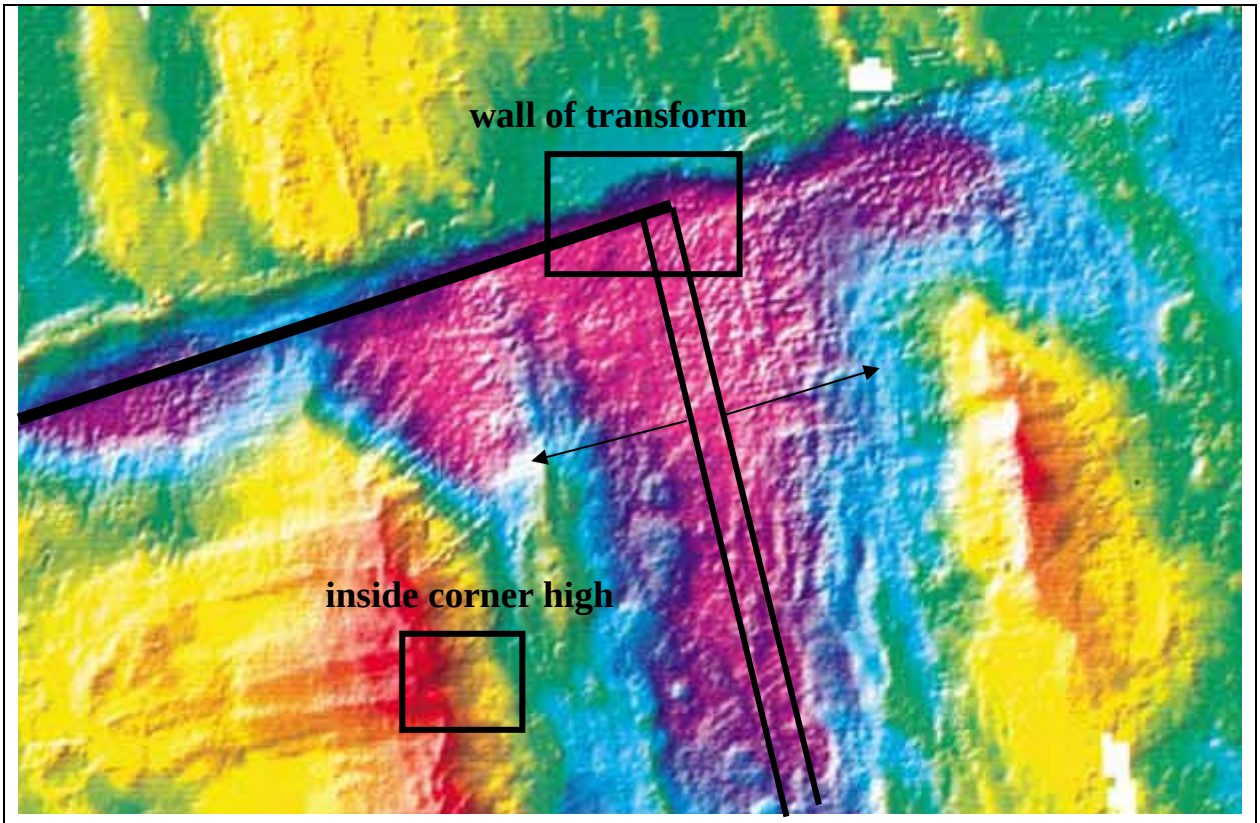

Fig. 2.4.10.1: Shaded relief map of seafloor topography in the 5°S region (Reston et al., 2002). The two areas of interest are marked by rectangles, the (new) ridge axis by a double line, and the transform fault by a thick black line. Massif to east of the ridge axis is the eastern part of the inside corner high, rifted away by the new ridge axis.

Inside corner highs are elevated plateaus with a curved surface at the intersection of a transform fault and an ocean ridge. Experience has shown that they preferentially expose unfaulted lower crustal rocks (Dick et al., 2000; Ildefonse et al., 2007), thus the common term "core complex". Our current understanding of how these rocks are exhumed is by long-term focusing of strain into a single normal fault associated with internal rotation of the block of up to 90° degrees (Lavier et al., 1999, Fig. 2.4.10.2).

The strain focusing is favored by the occurrence of volumentrically minor, rheologically weak, serpentinized mantle rocks between an otherwise gabbroic crust (Reston et al., 2002; Escartin et al., 2003; Ildefonse et al., 2007). As a result, the inside corner highs tend to have a thin cover of altered and sheared mantle rocks around a gabbroic core. Normally, the rocks inside the core would only be accessible by drilling. However, in case of the occurrence at 5°S, a westward-directed ridge-jump of the eastern ridge axis of the ridge-transform system has rifted apart the core complex, giving access to its internal setup.

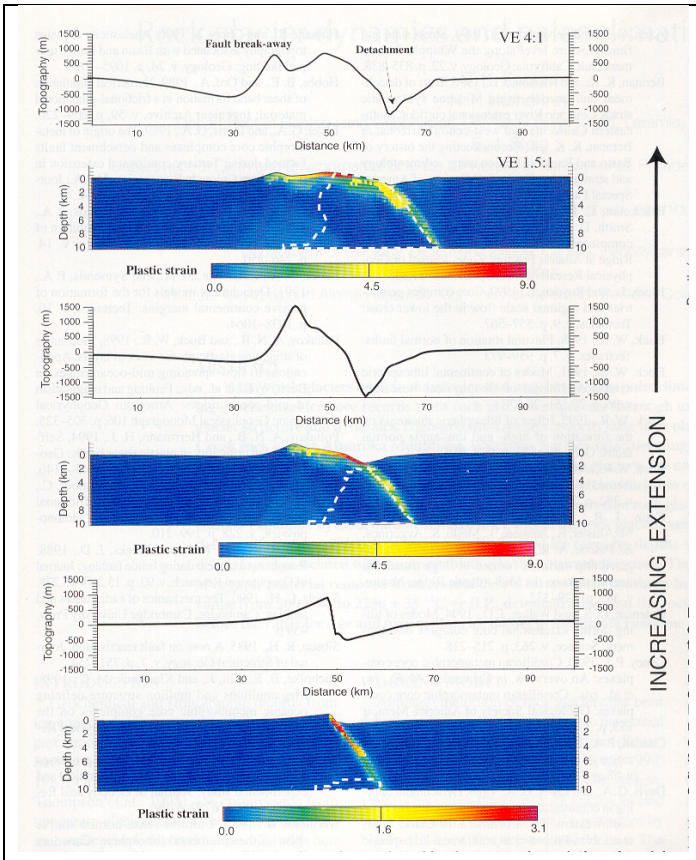

Fig. 2.4.10.2: Numerical model simulating the formation of inside corner highs. Note how an original horizontal marker rotates in an anti-clockwise fashion during exhumation (Lavier et al., 1999).

We decided to explore the western rift flank of the disected core complex with the ROV, since the eastern flank would perhaps expose a cross-section parallel to igneous units (Fig. 2.4.10.3). The targets for the dives were thus: (1) is the lithology along the rift flank as expected, i.e. deep rift volcanics, followed by gabbros, capped by sheared peridotite? And (2), can we see expressions of the rift tectonics?

The plan to investigate the northern wall of the transform was a consequence of the requirement to undertake a deep dive to test the ability of the ROV in the 5-6000 mbsf range. This was feasible in the basin forming at the intersection of the ridge axis with the transform fault ("nodal basin", the origin of which is actually poorly understood). The transform wall to the north of it was expected to expose rocks formed at the inside corner of the intersection of the northwestern ridge axis with the transform. This lithosphere has drifted with a half-spreading rate of 1.6 cm/year to the east and the rocks located at the northern extension of the south-eastern ridge axis should be ca. 5 Ma old. Since magmatism is thought to decrease (Cannat 1996) near the terminations of first-order segments as defined by transform faults (MacDonald et al., 1988), the questions for this day of the dive were (1) would the transform wall expose mantle rocks reflecting a low magmatic budget or volcanics reflecting abundant magmatism and (2) what is the expression of the transform tectonics?

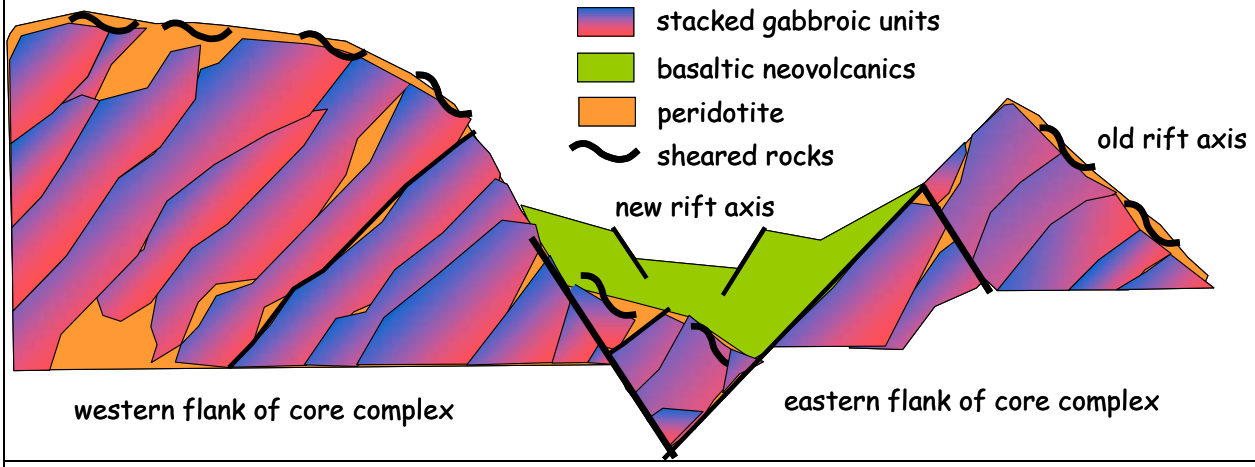

Fig. 2.4.10.3: Pre-dive model of the core-complex at 5°S. Note how the rift of the new ridge is thought to disect the core complex which would presumably be enveloped by a thin veneer of sheared mantle rocks.

Practical experience gained during the dives

The first two days of diving went without technical problems though conditions must be considered challenging. Lateral traversing meant that the ship had to follow the ROV with an equivalent speed, the covered vertical distance implied an on-going operation of the winch to haul in cable. Cliffs, corners, and huge boulders presented a danger for the cable to get caught. The group agreed that alternative sampling of this slope by dredging methods would be extremely hazardous since the dredge-container could easily be caught and ripped off. On the deep-dive test, the Orion arm behaved erratic.

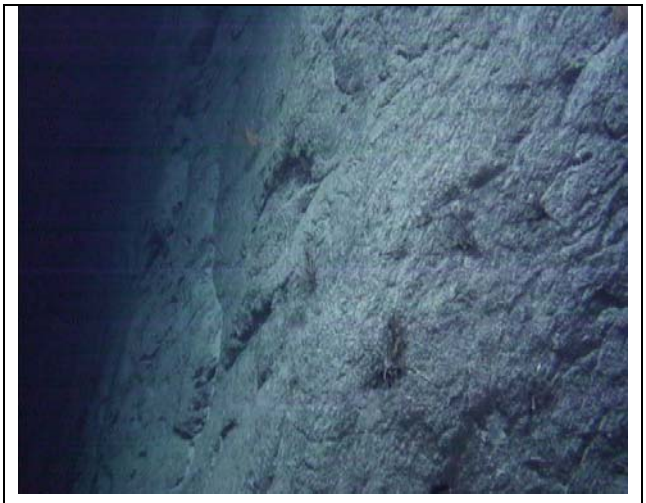

Fig. 2.4.10.4: Cliff face in gabbro with true dip of ~75° on Inside-Corner High traverse. Visible height estimated 2, in, distance 10 m. Parking the ROV and take a sample? No easy task!

On the first day we took seven, on the second day fifteen, on the third day fourteen samples, usually using the Orion-arm, but exceptionally also the Rigmaster arm. Dislodging in-situ samples turned out to be nearly impossible, so we mostly collected samples which were already loose. In most cases, we could convince ourselves that they were locally derived. Parking the ROV at the often near-vertical cliff-faces was extremely challenging and in several cases our pilots had to grab samples "on the fly". Samples were stored away in any of the four drawer compartment or – in the case of big samples – on the "porch" at the front of the ROV. Untangling some fifteen similar-looking samples required a strict book keeping during sampling and more smaller instead of few larger compartment might have been preferable for our purposes.

Fig. 2.4.10.5: The ROV drawer, configured for – and filled with – rocks. Bookkeeping required! Additional tools from left: IB sampler, shovel, bionet.

It turned out nearly impossible to discriminate different lithologies by direct observations during our dives, since nearly all rocks were covered by Mn-crusts. We thus had to use morphological features and later calibrate our mapping with the samples taken. Here, the monitoring of the dive by video and HD cameras turned out to be very useful. Measuring the orientation of the structural elements like cliffs, joints, faults, laminations, corrugations on surfaces and suspected dyke contacts was feasible thanks to the known heading of the ROV. The on-bord sonar was of great help in finding and measuring the orientation of interesting elements. It showed reliably boulders in sediments and cliffs with their orientation at distances far beyond the area illuminated by the search lights. The available topographic seafloor maps were not accurate enough for planing the route during our dives though we always used them as a rough guide. Some features of the maps turned out to be relevant, others were only artifacts. In the end, we agreed that the visual information and geographic

coordinates (for us, mainly depth) associated with our samples will be of invaluable help in interpreting the data.

Geological Results of the Inside Corner High Dives

The two-day traverse covered the depths from 3400 to 1500 mbsf. The base of western rift flank was heavily sediment (Fig. 2.4.10.6). We could only collect one boulder sample which turned out to be a peridotite breccia, ultimately perhaps derived from the very top of the plateau.

As we headed westward, the slope steepened and cliffs appeared which strike between 300 and 340° and typically dip 70° to the E to NE. The major wall of the rift is a shear cliff of some 200m vertical distance, starting at 2500 mbsf (Fig. 2.4.10.4).

We could identify downdip slickensides, consistent with rift-related faulting (Fig. 2.4.10.7).

The orientation of the major cliff face, interpretated as the master rift fault, was repeatedly measured and is not quite understood since it is at an angle of some 10°-50° to the current ridge axis (trending 350°). In more detail, the rift-flank consists of ridges and valleys, the latter ones probably originating in transverse faults. The valleys tended to be full of tallus in a matrix of foraminiferous ooze so that we preferred to ascend along the ridges. A single, doubtful observation of igneous banding on a E-W trending cliff face showed the banding dipping 30° to the west, i.e. towards the core complex.

Fig. 2.4.10.8: View in plane polarized light of an entire thin section (3 cm long) showing olivine gabbronorite. Sample D2-S12 from the 5°S core complex.

Samples taken along the rift flank are mainly gabbros with a subordinate group of microgabbros and dolerite in the upper part (63ROV-9 to 63ROV-11 at 1767 m, 1674 m, and 1636 m). The gabbros range from melanocratic to leucogabbroic. Noritic gabbros are strongly suspected by inspection of hand-specimens. Olivine was not positively identified but is present in one of the samples taking from the *Meteor* cruise M47/2 during dredging

Fig. 2.4.10.6 (top): View of seafloor at the base of the rift flank: large boulders (~ 1 m) in carbonaceous ooze.

Fig. 2.4.10.7 (right):. Slickensides on fault plane indicating down-thrown frontal block.

(Fig. 2.4.10.8). The gabbros are usually medium-grained, one sample is coarse-grained. Felsic netveining is relatively widespread, a vague argument for a closed system evolution (see rock sample photos in Appendix). Oxide gabbros, on the other hand, also representing advanced stages of differentation only reached in nearly closed systems, were not recovered. Magmatic strain was not observed, suggesting that the gabbro body cooled in the lithosphere. Plastic strain, probably mylonitic, was observed in two samples (50ROV-3 and 63ROV-14). Both appear peridotitic.

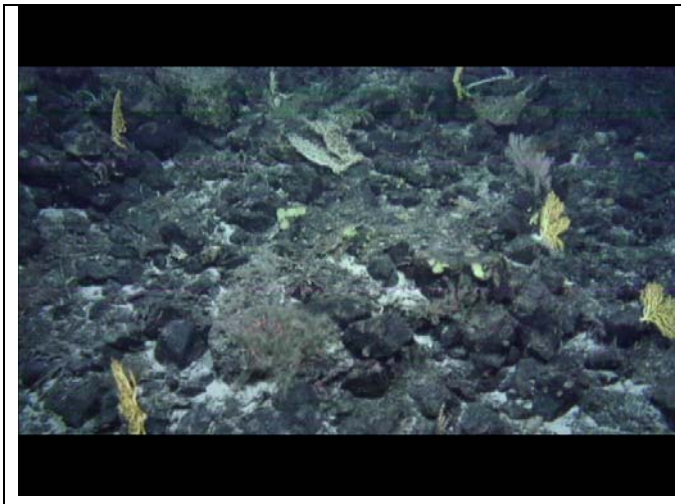

Fig. 2.4.10.9: Top of the Inside Corner High. Sampling confirmed that this is a coral-grown peridotite breccia horizon (ATA-63ROV-13 and -15).

Fig. 2.4.10.10: Highly sheared block of (ultramylonitic?) peridotite (?) 50 m beneath the plateau (ATA 63ROV-14)

Our impression is that the samples show a certain degree of greenschist-grade alteration. This is somewhat surprising, since the usually internally unfaulted nature of core complexes would make the penetration of water difficult.

The transition from the rift flank to the top of the plateau was abrupt. We traversed this edge twice to confirm the observation. Two samples taken at the top very near the edge turned out to be peridotite breccias (Fig. 2.4.10.9) whereas this breccia is absent all along the rift flank. A highly interesting, in-situ sample was recovered just beneath the plateau (ATA-63ROV-14): the dense, laminated rock appears to be ultramylonitic, probably peridotitic and may represent an early, higher temperature stage of the detachment fault (Fig. 2.4.10.10). Its orientation is moderately dipping to the NE. In total, all deformed samples (breccias and mylonites) are probably peridotitic. This strongly supports the current model of peridotite-related strain softening of the master normal fault. A cross-section and map of the traversed terrane is shown in Figs. 2.4.10.11 and 2.4.10.12, respectively.

About 32 hours video material taken with three cameras were cut to a condensed version of 20 minutes showing the main geological and morphological features.

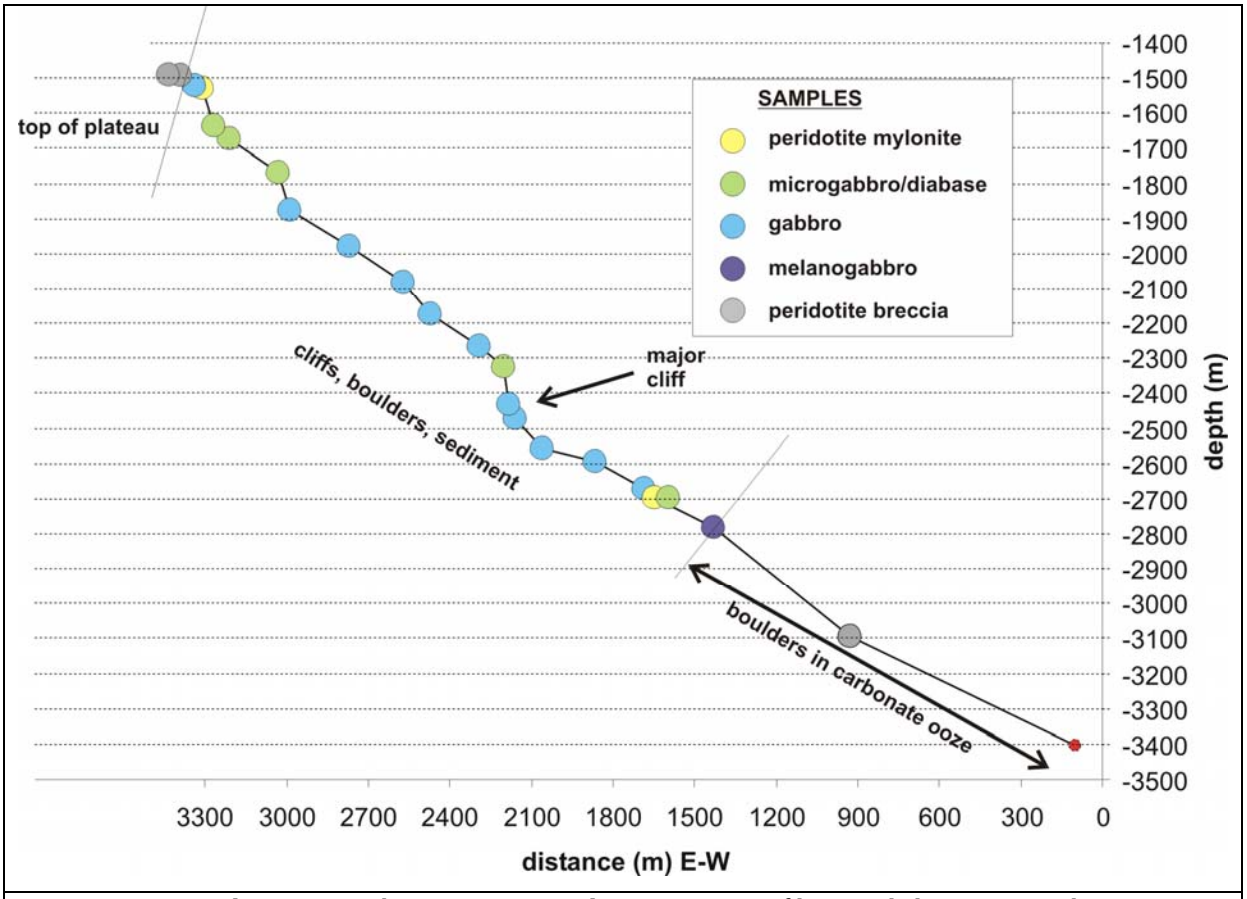

Fig. 2.4.10.11: Inside Corner High traverse projected onto an E-W profile. Sample locations are shown.

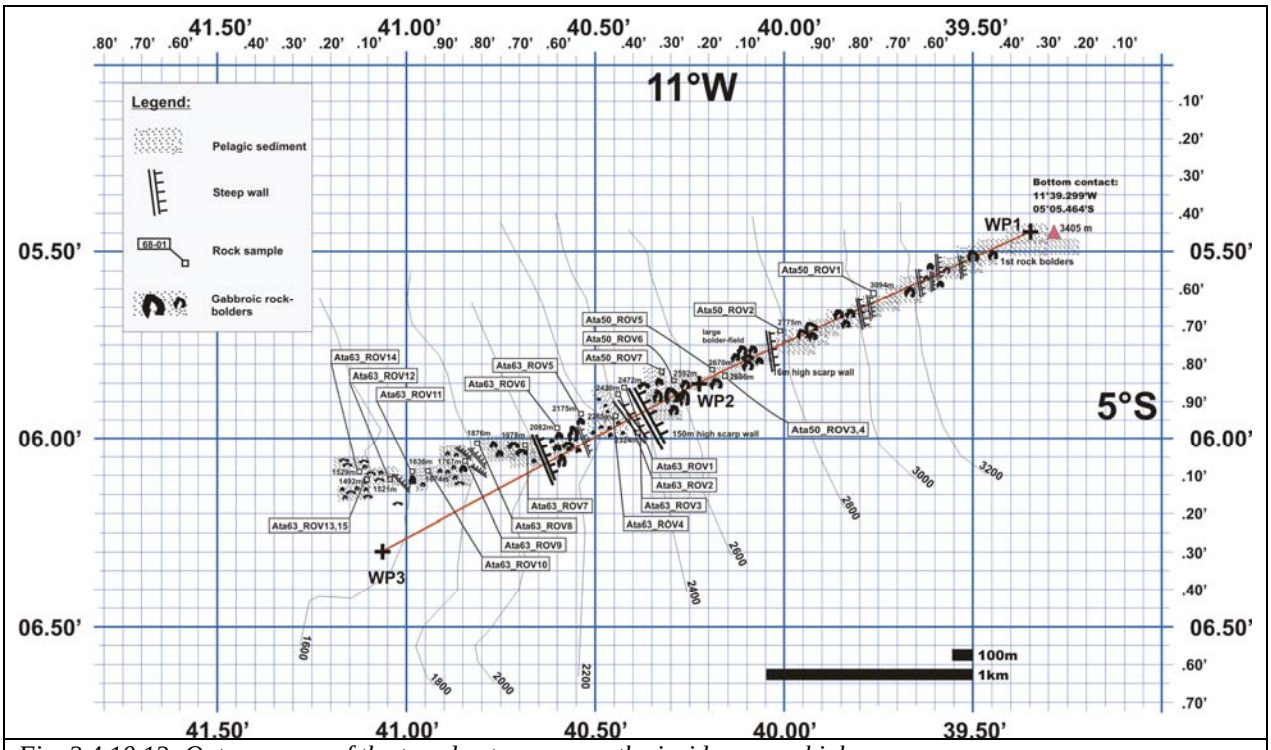

Fig. 2.4.10.12: Outcrop map of the two day traverse up the inside corner high.

Geological Results of the Transform Fault Dive

The topographic overview Fig. 2.4.10.1 shows that the new south-eastern ridge axis has also affected the opposing transform wall, since the latter shows a marked topographic depression where the continuation of the ridge axis intersects the transform wall. During our dive, however, there was a clear predominance of E-W trending cliff faces in the transform wall which we logically attribute to strike slip faulting associated with transform tectonics.

An impression of both the inside corner high and transform traverses are the striking similarity of continental and submarine landscapes. Near vertical cliff faces, talus slopes, *Felsenmeere* (Fig. 2.4.10.13) and slopes with rugged ridges and sediment-filled valleys were all recurring views familiar from land. Particularly the transform transect showed abundant evidence for mass-wasting. Perhaps the major difference to continental landscapes are the valley floors filled smoothly with sedimented, hosting groups of sticking out, large boulders as well as slopes which appeared generally to be somewhat steeper than on land (because of the reducted gravitational force available for collapse?).

Fig. 2.4.10.13: Felsenmeer, presumably collecting rocks from the dyke complex.

During the dive itself, we were convinced that in the lower part, serpentinite and gabbro is exposed. However, ground truthing via sampling showed that the entire traverse was within diabase and microgabbro which we crossed in east-west trending ridges with intervening shallower, more sedimented parts perhaps related to faulting. We thus covered about 1000 vertical meters of upper oceanic crust with the likely addition of another 300 m above the point where we had to abandon the traverse due to time constraints. Thus, the upper crust in this region is likely to be fully developed with some 1.5 km of volcanics and subvolcancis. A so-called "transform effect" with a reduced or even absent crust seems very unlikely. Our contrasting traverses up the inside corner high and the transform wall emphasized the uniqueness of core complexes in giving easy access to lower crustal rocks.

In several locations, there is strong evidence for an exposure of sheeted dykes (Fig. 2.4.10.14). Consistently, the locally sampled rocks are diabases, representing rapid cooling but no contact to seawater. We may even have collected one chilled margin sample (70ROV-7). Joints developed in the sheeted dyke complex during cooling give a characteristic, facetted outcrop picture but a dominating joints system represents the dyke contacts. Based on our observations, it seems likely that the entire cliff between 4380 and 4050 m is mainly made out of sheeted dykes. The dykes appear to have a predominant jointing dipping 70° to the west, interpreted as dyke-dyke contacts. This would translate to an inward rotation of an assumed original vertically oriented dyke swarm at the western ridge. There was no evidence for felsic veining as would be typical for the sheeted dyke – gabbro transition. Nor did we see pillow lavas which would represent the near sea-floor environment.

The degree of hydrothermal alteration can only be safely determined petrographically but hand-specimen inspection suggests that it is pervasively present. An excellent opportunity will offer itself by comparing our section to IODP Hole 1256D which recently covered 1.5 km of upper oceanic, fast-spreading crust by drilling (Koepke et al., submitted) as well as to the famous ODP Hole 504B.

Fig. 2.4.10.14. View of sheeted dykes with dominant joint-system dipping 75° to the left (west). Looking north at 4300 mbsf.

The trend of the dykes appears to be – as it should – normal to the transform and the cliff faces. What would then form the E-W trending, steeply south dipping cliffs? In some cases we found good evidence for exposed shear planes with, in one case striations on such a face with a 25° eastern pitch (several attempts to sample this rock failed) (Fig. 2.4.10.15). Assuming a dextral shear as derived

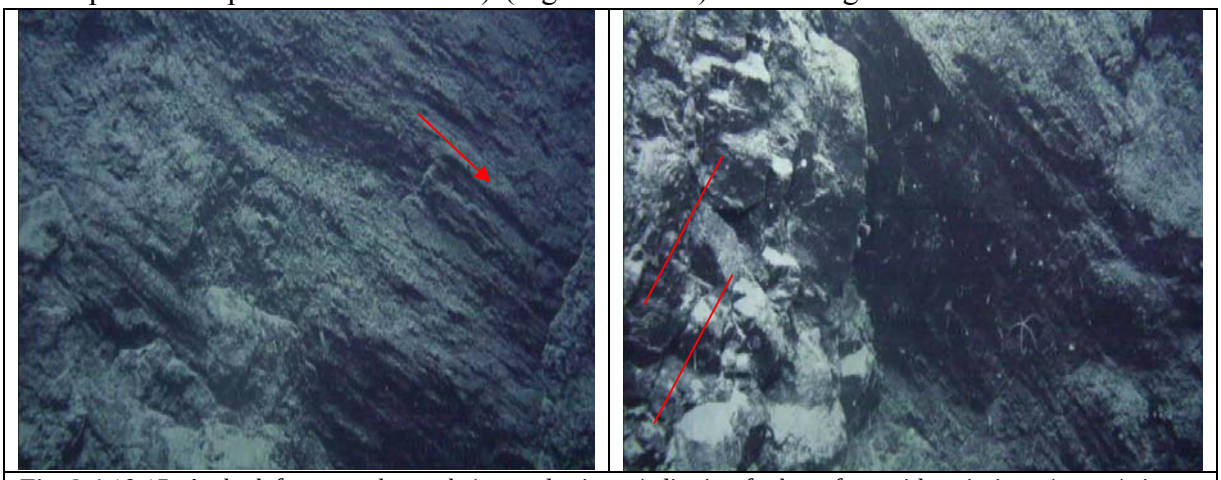

Fig. 2.4.10.15: At the left, a steeply south (towards viewer) dipping fault surface with striations (arrow) is shown (4350 mbsf.). Photo at right shows same feature in the geological context: the fault plane occurs as a wall behind a dyke complex which strikes at high angle to it and with contacts dipping steeply to the left (west, red lines)

from the overall transform movement, this would mean a thrust component on the transverse movement, i.e. the southern block appears to have moved obliquely up and west with respect to the northern block (moving obliquely down and east). Higher up in the profile, at 4000 mbsf, a fault plane dipping 40° to the south was observed. Note that in this upper part, the topography is also shallower. We speculate that most of the near-vertical cliff are the expression of a late, brittle transverse fault.

The highest section covered with the ROV has a markedly different appearance. The dominant jointing system is absent, the rocks show a small-scale, intensely fractured surface, and a dominant structural grain may represent flow planes (Fig. 2.4.10.16). A working model calls here for massive flows.

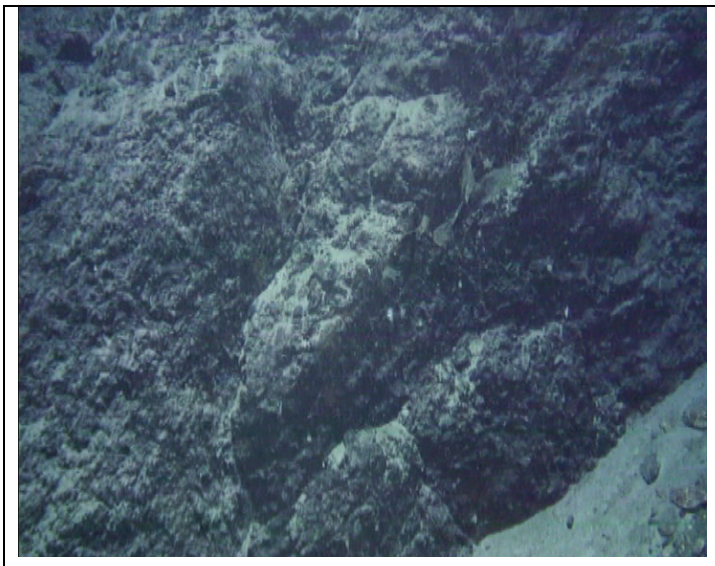

Fig. 2.4.10.16: Near the upper end of the profile, intensely jointed rocks with a locally visible structural grain (here from top right to bottom left) became dominant. Our working model calls for an origin as massive flows.

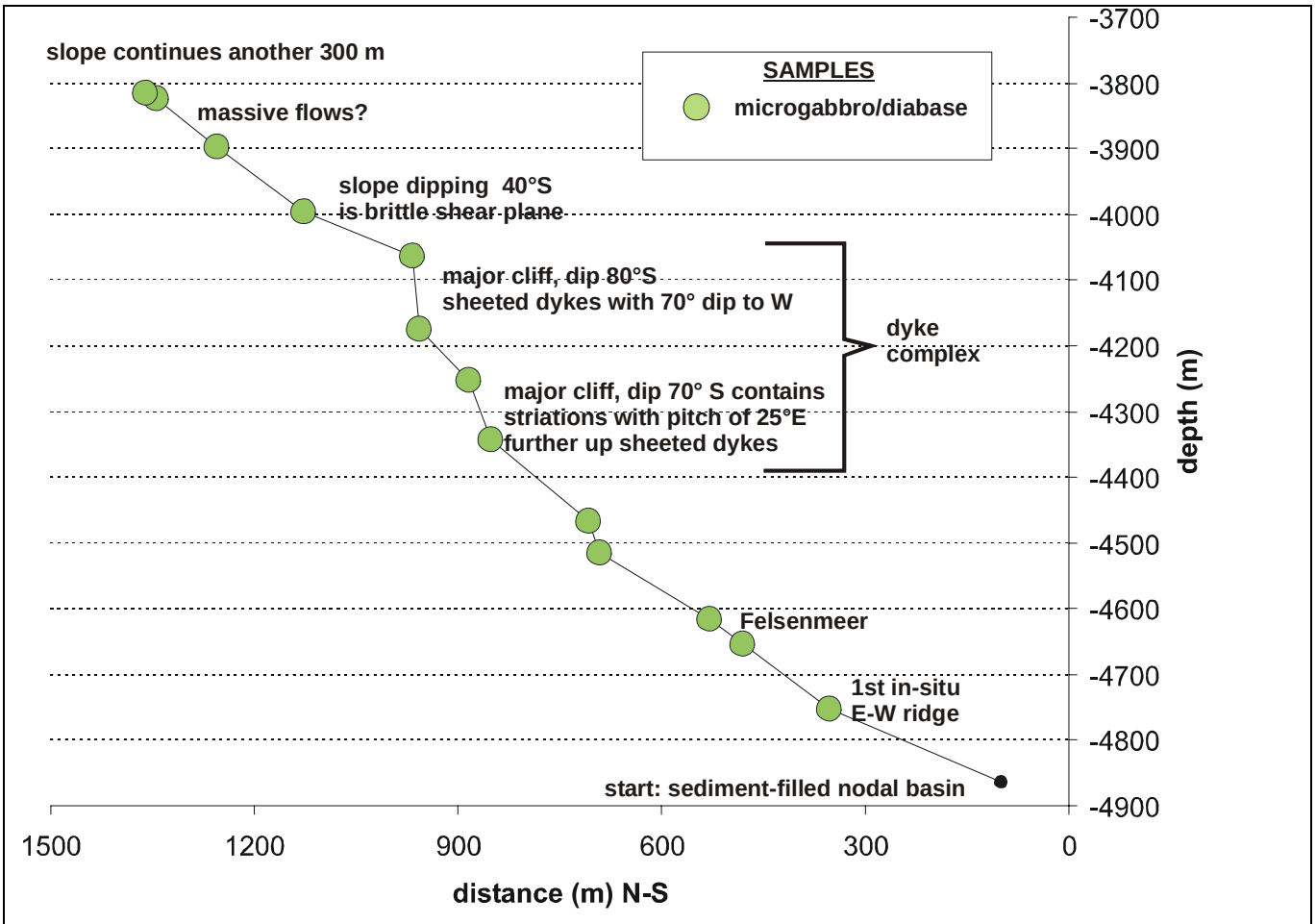

Fig. 2.4.10.17: Transform wall traverse projected onto a N-S plane. Sample locations in green.

2.4.11 ROV deployments during MAR SOUTH IV

(K. Lackschewitz, D. Comany, A. Foster, C. Hinz, E. Labahn, A. Meier, M. Pieper, J. Schneider)

Leg 2 of RV ATALANTE is the second scientific cruise of the Kiel ROV 6000 within the priority program 1144 „From mantle to ocean". A detailed technical description and operation of the entire system is given in the „chapter 1.4.10" of the Leg 1 cruise report „HYDROMAR V".

Table 2.4.11.1: Summary of ROV dives during MAR SOUTH IV

ATA-Leg 2 Station #	IFM-GEOMAR Dive #	Date	Site	Depth (m)	Time Launch	Time (UTC) Start (Bottom)	Time (UTC) End (Bottom)	Time (UTC) on Deck	Bottom Time	Total Dive Time
35ROV	13	14.01.08	Turtle Pits	2988	09:39	11:13	17:40	18:55	**06:27**	**09:16**
37ROV	14	15.01.08	Wideawake/	3000	09:39	11:12	16:50	18:15	**05:38**	**08:36**
42ROV	15	16.01.08	Comfortless Cove	3000	09:20	10:48	18:08	19:24	**07:20**	**10:04**
46ROV	16	18.01.08	Turtle Pits/ Wideawake	3000	09:25	11:10	17:58	19:15	**06:48**	**09:50**
50ROV	17	19.01.08	Inside Corner High 5°S	3095	09:40	11:29	17:32	18:43	**06:03**	**09:03**
52ROV	18	20.01.08	Comfortless Cove	2990	10:00	11:43	17:20	18:39	**05:37**	**8:39**
57ROV	19	21.01.08	Turtle Pits	2990	09:36	11:03	19:29	20:50	**08:26**	**11:14**
63ROV	20	23.01.08	Inside Corner High 5°S	2000	08:50	10:34	17:32	18:29	**06:58**	**9:39**
67ROV	21	24.01.08	Red Lion	2960	09:20	11:42	15:19	16:26	**03:37**	**7:06**
68ROV	22	24.01.08	400m NW of Comfortless Cove	3000	17:17	18:33	21:36	22:45	**03:03**	**5:28**
70ROV	23	25.01.08	Ascension Fracture Zone	4890	10:45	13:04	22:32	00:06	**09:28**	**13:21**

The technical innovations of the ROV provided a flexible and highly adaptable platform for scientific sampling and observation tasks and therefore played a major role for the scientific success aboard RV ATALANTE. Since the previous leg we have additionally installed a rotary sampler with a slurp gun.

In total 11 dives were carried out on 13 working days on the southern Mid Atlantic Ridge at 5°S. A summary about the statistics of the ROV dives are presented in Tab. 2.4.11.1. Launch and recovery has been done at sea states < 2m and winds < 4 bft.

Total dive times of 102 h including almost 70 h bottom time could be achieved at depths of 3000m. During our last dive ROV Kiel 6000 was deployed for the first time to a depth of 4890 m which is also the deepest dive for a ROV manufactured by Schilling Robotics.

The following scientific tools and devices were used on "KIEL ROV 6000m" during the above mentioned dives for obtaining biological, petrological and fluid-geochemical samples:

- KIPS fluid sampling system (incl. high-temperature sensor)
- Ti-Majors fluid sampler
- Isobaric gas sampler
- He tube
- 8-channel low-temperature lance
- SMONI (1-channel high temperature logger)
- Nets for biological sampling
- Slurp gun with rotary sampler

Three colour video cameras (1 HDTV and 2 Standard PAL cameras) have produced a large amount of video data. Videos from the standard cameras were permanently and synchronously recorded as mpeg2 files to a video server. HDTV videos were recorded only at scientific request. They are stored in HD format on a MacintoshPro and as mpeg2 files on the same video server as the standard videos. Approximately one hour of HDTV video was stored per dive. The video data stored on the video server is available to all scientists in SD converted format via the vessel's intranet using a web browser. The so-called Proxsys™ software on the server enables video previews (as mpeg4), cut and download of selected video sequences (as mpeg2).

Unfortunately, the digital still camera did not work after we had changed the defect controller board with a new board provided by the manufacturer.

After some problems during Leg 1, the Posodonia USBL navigation worked well. However, due to a malfunction of the Posidonia system it could not be used for dive 18 (station ATA-52ROV). In addition, at the beginning of our station work two homer beacons were set on the seafloor at Turtle Pits and Wideawake as reference positioning stations. Both were collected at the end of our dive operation in these areas.

2.5 Acknowledgements

The scientists of Atalante Leg 2 would like to thank Capt. Glehen and his crew for superb support at sea. The flexibility of the Senatskommission für Ozeanographie, the Deutsche Forschungsgemeinschaft and the Leitstelle Meteor/Merian in making these cruises possible in the short time available is gratefully acknowledged.

2.6 References

Baines, A.G., Cheadle, M. J. et al. (2003). Mechanism for generating the anomalous uplift of oceanic clore complexes: Atlantis Bank, southwest Indian Ridge. Geology 31, 1105-1108

Caldeira, K. and Wickett, M.E. (2003). Anthropogenic carbon and ocean pH. Nature, 425:365

Cann, J.R.; Blackman, D.K.; Smith, D.K.; McAllister, E.; Janssen, B.J.R.; Mello, S.; Avgerinos, E.; Pascoe, A.R.; Escartin, J. (1997). Corrugated slip surfaces formed at ridge-transform intersections on the Mid-Atlantic Ridge, Nature, 385, 329-332.

Cannat, M. (1996). How thick is the magmatic crust at slow spreading oceanic ridges? Journal of Geophysical Research 101, 2847-2857.

Cannat et al. (1995). An ultramafic lift at the Mid-Atlantic Ridge: successive stages of magmatism in serpentinized peridotites from the 15°N region, in: R.L.M. Vissers, A. Nicolas (Eds.), Mantle and lower crust exposed in oceanic ridges and in ophiolites, Kluwer, Dordrecht, 5-34.

Cannat et al. (1992). Serpentinized peridotites and gabbros in the Mid Atlantic Ridge axial valley at 15°37′N and 16°52′N. Earth Planet. Sci. Lett. 109 (1992), 87–106.

Damm et al. (1985). Chemistry of submarine hydrothermal solutions at 21°N, East Pacific Rise. Geochimica et Cosmochimica Acta 49 (11), 2197-2220.

Dick, H. J. B., J. H. Natland, et al. (2000). A long in-situ section of the Lower Ocean Crust: results of ODP Leg 176 Drilling at the Southwest Indian Ridge. Earth and Planetary Sciences Letters 179, 31-51.

Douville et al. (2002). The Rainbow vent fluids (36° 14'N, MAR): the influence of ultramafic rocks and phase separation on trace metal content in Mid-Atlantic Ridge hydrothermal fluids. Chemical Geology 184, 37-48.

Escartin, J., C. Mével, et al. (2003). Constraints on deformation conditions and the origin of oceanic detachments: The Mid-Atlantic Ridge core complex at 15_45°N. Geochemistry, Geophysics, Geosystems 4 (1067, doi:10.1029/2002GC000472).

Fahey, R.C. and Newton, G.L. (1987). Determination of low-molecular-weight thiols using monobromobimane fluorescent labeling and high-performance liquid chromatography. Methods Enzymol, 143, 85-96.

Garbe-Schönberg et al. (2006). KIPS – A new multiport valve-based all-teflon fluid sampling system for ROVs. EGU General Assembly, Vienna, April 2006.

Grasshoff (1999). Methods of Seawater Analysis. 3rd edition, 600 p., Wiley-VCH

Haase et al. (2007). Young volcanism and related hydrothermal activity at 5°S on the slow-spreading southern Mid-Atlantic Ridge. G^3, 8 (11).

Ildefonse, B., D. K. Blackman, et al. (2007). Oceanic core complexes and crustal accretion at slow spreding ridges. Geology 35, 623-626.

Kelley, D.S., Karson, J.A., Blackman, D.K., Fruh-Green, G.L., Butterfield, D.A., Lilley, M.D., Olson, E.J., Schrenk, M.O., Roe, K.K., Lebon, G.T.the AT3–60 Shipboard Party and Rivizzigno, P. (2001). An off-axis hydrothermal vent field near the Mid-Atlantic Ridge at 30°N. Nature 412, 145–149.

Klein, E. M., & Langmuir, C. H. (1987). Global correlations of ocean ridge basalt chemistry with axial depth and crustal thickness, J. Geophys. Res., 92, 8089-8115.

Koepke J, Christie DM, et al. (2007 submitted). Petrography of the Dike/Gabbro Transition at IODP Site 1256D (Equatorial Pacific): The evolution of the Granoblastic Dikes. Geochem Geophys Geosyst.

Koepke, J., Feig, S.T., Snow, J. (2005). Hydrous partial melting within the lower oceanic crust. Terra Nova 17, 286-291.

Koepke, J., Feig, S.T., Snow, J. (2005). Late-stage magmatic evolution of oceanic gabbros as a result of hydrous partial melting: Evidence from the ODP Leg 153 drilling at the Mid-Atlantic Ridge. Geochem. Geophys. Geosyst. 6, no. 2004GC000805.

Koepke, J., Feig, S.T., Snow, J., Freise, M. (2004). Petrogenesis of oceanic plagiogranites by partial melting of gabbros: An experimental study. Contrib. Mineral. Petrol. 146, 414–432.

Lavier, L. L., W. R. Buck, et al. (1999). Self-consistent rolling-hinge model for the evolution of large-offset low-angle normal faults. Geology 27 (12), 1127-1130.

Macdonald, K. C., P. J. Fox, et al. (1988). A new view of the mid-ocean ridge from the behaviour of ridge-axis discontinuities. Nature 335, 217-225.

Mitchell, J. (Ed.), 2005. The greenhouse effect and climate change – A briefing from the Hadley Centre, 77 pp.; Hadley Centre, Exeter.

Parmentier, E. M. and J.P. Morgant (1990). Spreading rate dependence of three-dimensional structure in oceanic spreading centers. Nature, 348, 325-328.

Rehder et al. (1999). Methane in the northern Atlantic controlled by microbial oxidation and atmospheric history. Geophysical Research Letters, 26 (5), 587-590.

Reston, T. J., W. Weinrebe, et al. (2002). A rifted inside corner massif on the Mid-Atlantic Ridge at 5°S. Earth and Planetary Science Letters 200, 255-269.

Rethmeier, J., Rabenstein, A., Langer M., Fischer U.(1997). Detection of traces of oxidized and reduced sulfur compounds in small samples by combination of different high-performance liquid chromatography methods. Journal of Chromatography A, 760, 295-302.

Tucholke, B.E., Lin, J. et al. (1998). Megamullions and mullion structure defining oceanic metamorphic core complexes on the Mid-Atlantic Ridge. J. Geophys. Res. 103, 9857-9866